NASA TN D-1461

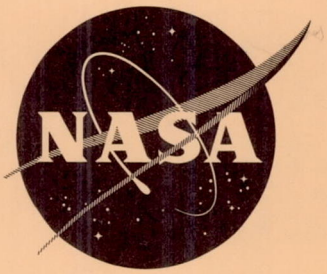

TECHNICAL NOTE

D-1461

SPACE-CHARGE-FLOW THEORY AND ELECTRODE DESIGN

FOR ELECTROSTATIC ROCKET ENGINES

By David L. Lockwood and Vladimir Hamza

Lewis Research Center
Cleveland, Ohio

NATIONAL AERONAUTICS AND SPACE ADMINISTRATION

WASHINGTON

December 1962

NATIONAL AERONAUTICS AND SPACE ADMINISTRATION

TECHNICAL NOTE D-1461

SPACE-CHARGE-FLOW THEORY AND ELECTRODE DESIGN FOR ELECTROSTATIC ROCKET ENGINES

By David L. Lockwood and Vladimir Hamza

SUMMARY

The basic theory of space-charge flow is described, and three general methods of solution are discussed. Specific space-charge-flow geometries are described in detail; these include flow between coaxial cylinders, concentric spheres, coaxial cones, hyperbolic flow, flow between inclined planes, and circular flow. Since all the solutions discussed are for space-charge-limited flow, a discussion of partial space-charge flow is presented. The Pierce method of electrode design is described, and some practical limitations of this method are discussed. Electrode shapes for various space-charge flows are shown.

INTRODUCTION

The performance and design requirements of electrostatic rocket engines have brought a new emphasis to the theory of space-charge flow. Considerable reductions in engine size and substantial improvement in engine efficiency may be gained by the use of ion and charged-particle accelerators operating with current densities at or near the space-charge limit. Such high current densities bring about definite space-charge effects, so that Poisson's equation must be used to describe the potential distribution in the engine accelerator. In addition to the requirement of high current density, the electrostatic rocket engine must be capable of operating for very long times, of the order of years for interplanetary space missions. Such long-duration operation requires near-perfect "ion optics" to keep electrode sputtering erosion to reasonable limits. Since the ions, or charged particles, are accelerated to kinetic energies in the range from a few thousand to hundreds of thousands of electron volts, each ion striking an electrode may sputter away several electrode atoms. For these reasons, some estimates of the degree of perfection of ion optics place an upper limit of ion impingement of less than 0.01 to 0.1 percent of the total ion beam to keep erosion to a reasonable level.

The space-charge-flow problem in electrostatic rocket engines is characterized by the necessity for the ions, or charged particles, to leave the engine permanently through an open exhaust aperture, as shown in sketch (a):

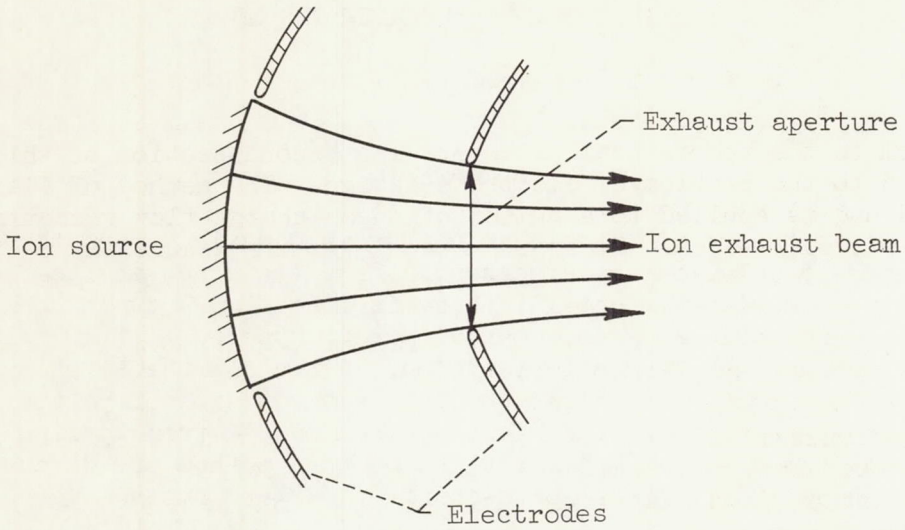

(a)

Since the ion source is at a potential considerably higher (or lower, for negative ions) than the potential of free space, the equipotential lines in the accelerator will tend to bow, or bulge, out of the exhaust aperture. This aperture effect not only reduces the current carrying capacity of the accelerator, but also introduces another complicating boundary condition on the space-charge-flow equations.

The complexities of the space-charge flow in electrostatic rocket engines indicate that complete analytical design of space-charge-flow accelerators will be very difficult. For this reason, recourse has been made to analog or empirical methods (i.e., experimental "cut-and-try"). Not only are these methods inadequate for extrapolation or scaling of engine designs, but in addition they do not offer sufficient basic understanding of space-charge flow to allow positive prediction and evaluation of the effects of configuration changes in design optimization studies.

It is evident that a convenient, universal method for the analytic solution of the space-charge-flow problem would be of great value in the design of electrostatic rocket engines. The survey of existing literature on space-charge flow reported herein has yielded no completely universal analytic method, but some progress has been made in that direction.

The first section of this report is devoted to a discussion of the three methods of solution that have been used to date for space-charge-flow problems. The remainder of the section on space-charge-flow theory is a compilation of analytic solutions for specific space-charge-flow geometries found in the literature and also includes a calculation of the flow between coaxial cones that was not previously available.

Since the analytic solutions to space-charge flow usually assume that the flow fills all space, it is necessary to take a segment of this flow and to provide electrodes external to the ion beam to force the flow to conform to the theoretical pattern. The second section of this report is devoted to the problem of electrode design. The method of Pierce is described and is applied to a number of space-charge-flow geometries to obtain electrode shapes. Some of these shapes are accurately recomputed using techniques found in the literature, and others appear not to have been computed previously. Some practical limitations to the application of space-charge flow theory and the Pierce method of electrode design are discussed.

The parameters of the various space-charge flows examined in this report may be used to determine the theoretical performance of electrostatic rocket engines. An analysis is made in reference 1 in which the various space-charge flows are compared in terms of relative engine performance.

The work described in this report was carried out as part of the electrostatic propulsion research program of the NASA Lewis Research Center.

SPACE-CHARGE-FLOW THEORY

In the study of the performance of ion engines the analysis of space-charge flow is very important. Since the early studies of Child (1911, ref. 2) and Langmuir (1913, ref. 3), who solved the problem of space-charge-limited flow between parallel plates more than half a century ago, there have appeared extensive publications on space-charge effects in certain new geometries. Most of the early analyses (refs. 2 to 5) have been concerned with one-dimensional cases, and it has been only in recent years that two- and three-dimensional cases were solved or solutions were suggested (refs. 6 to 13).

In most ion engines, ions move as a very nearly continuous fluid in an electrostatic field in which the magnetic force is negligible. The flow of ions is assumed to form a system of curves (streamlines) filling a portion of space such that the velocity is a single-valued function of position.

The fundamental differential equations governing steady-state space-charge flow are:

Poisson's equation:

$$\nabla^2\Phi = \frac{\rho}{\epsilon_o} \tag{1}$$

Equation of motion:

$$\dot{\vec{mv}} = q\nabla\Phi \tag{2}$$

Conservation of charge:

$$\nabla \cdot \vec{j} = 0 \tag{3}$$

(Note that $\Phi = \varphi_o - \varphi$.)

It is mathematically convenient to assume that the flow is space-charge limited. In this case the velocity and electric field will both be zero on the emitting surface. Under these conditions it can readily be shown (ref. 9) that the flow will be irrotational; that is,

$$\nabla \times \vec{v} = 0 \tag{4}$$

In this case, the velocity can be expressed as the gradient of a scalar action function:

$$\vec{v} = \nabla W \tag{5}$$

Combining equation (5) with the vector identity $\dot{\vec{v}} = (\vec{v} \cdot \nabla)\vec{v}$ yields

$$\dot{\vec{v}} = (\nabla W \cdot \nabla)\nabla W \tag{6}$$

Application of equation (4) to the identity

$$(\nabla W \cdot \nabla)\nabla W = \frac{1}{2}\nabla(\nabla W)^2 - \nabla W \times (\nabla \times \nabla W)$$

gives

$$\dot{\vec{v}} = \frac{1}{2}\nabla(\nabla W)^2 \tag{7}$$

Substitution for $\vec{v}$ from equation (2) yields

$$\nabla(\nabla W)^2 = \left(\frac{2q}{m}\right)\nabla\Phi \tag{8}$$

Hence,

$$(\nabla W)^2 = \left(\frac{2q}{m}\right)\Phi \tag{9}$$

where the constant of integration is included by letting $\Phi = \varphi_o - \varphi$.

The five equations used to formulate space-charge-flow problems are:

Hamilton-Jacobi equation:

$$(\nabla W)^2 = \left(\frac{2q}{m}\right)\Phi \tag{9}$$

Poisson's equation:

$$\nabla^2\Phi = \frac{\rho}{\epsilon_o} \tag{1}$$

Total ion energy:

$$\frac{1}{2}mv^2 - q\Phi = 0 \tag{10}$$

Conservation of charge:

$$\nabla \cdot \vec{j} = 0 \tag{3}$$

Vector current density:

$$\vec{j} = \rho\vec{v} \tag{11}$$

Analytical Methods

Historically the first analytical solutions of the space-charge-flow problem were for particular cases of rectilinear flow between specified equipotential surfaces. These are flow between infinite planes (refs. 2 and 3), flow between coaxial cylinders (refs. 3 and 4), and flow between concentric spheres (ref. 5). One of the first attempts at a general solution of the space-charge-flow equations was made by Spangenberg (ref. 6) following his formulation of the general equations in terms of the action

function. His multidimensional analysis yields a partial differential equation in terms of the action function, which is much too unwieldy for exact solution.

In 1949 Meltzer (ref. 7) introduced a unique approach to the solution of space-charge-flow problems. By his method the space-charge-flow parameters are expressed in terms of the acceleration and velocity. Meltzer shows that there are two conditions necessary for a space-charge solution to exist; namely,

$$\nabla \times \dot{\vec{v}} = 0 \tag{12}$$

$$\nabla \cdot (\vec{v}\nabla \cdot \dot{\vec{v}}) = 0 \tag{13}$$

Using the relation $\dot{\vec{v}} = (\vec{v} \cdot \nabla)\vec{v}$ to obtain the acceleration from a previously assumed velocity, v and $\dot{v}$ are tested in equations (12) and (13). If they satisfy (12) and (13), they define a type of space-charge flow whose parameters are as follows:

$$\rho = \left(\frac{m}{q}\right)\epsilon_o(\nabla \cdot \dot{\vec{v}}) \tag{14}$$

$$\nabla\Phi = \left(\frac{m}{q}\right)\dot{\vec{v}} \tag{15}$$

$$\Phi = \left(\frac{m}{q}\right)\oint \dot{\vec{v}} \cdot d\vec{s} \tag{16}$$

$$\vec{j} = \left(\frac{m}{q}\right)\epsilon_o\vec{v}(\nabla \cdot \dot{\vec{v}}) \tag{17}$$

This method leaves one big equation unanswered. How may a velocity function be found that will satisfy equations (12) and (13)? The search for an answer to this question led Meltzer (ref. 11) and later Rosenblatt (ref. 12) to develop the trajectory action function method, which is more readily applicable to space-charge-flow problems than any previous method.

In the action function method of Meltzer and Rosenblatt it is assumed that the flow of charged particles is laminar, and that an orthogonal curvilinear coordinate system

$$\xi(x,y,z) \tag{18a}$$

$$\eta(x,y,z) \tag{18b}$$

$$\zeta(x,y,z) \tag{18c}$$

can be found such that the ion trajectories are completely described by variation of the parameters η and ζ (i.e., η = const. and ζ = const. specify a particular trajectory). Then the orthogonal surfaces ξ = constant will be surfaces of constant action, and the Hamilton-Jacobi equation (9) becomes

$$\frac{1}{h_1^2}\left(\frac{dW}{d\xi}\right)^2 = \left(\frac{2q}{m}\right)\Phi \tag{19}$$

where h_1 is the scale factor corresponding to the coordinate ξ. Rosenblatt shows that if a function Γ is defined such that

$$\Gamma = h_1^2\Phi \tag{20}$$

the general differential equation for space-charge flow can be written

$$\Gamma^{1/2}\left[\frac{\partial}{\partial\xi}\left(C\,\frac{d\Gamma}{d\xi}\right) + B\Gamma\right] = K(\eta,\zeta) \tag{21}$$

where

$$C = \frac{h_2h_3}{h_1^5} \tag{22}$$

$$B = \left(\frac{h_2h_3}{h_1}\right)\nabla^2\left(\frac{1}{h_1^2}\right) \tag{23}$$

$$K(\eta,\zeta) = \frac{h_2h_3}{\epsilon_o}\,j\sqrt{\frac{m}{2q}} \tag{24}$$

The differential equations for several known space-charge-flow cases are derivable from equations (21), (22), (23), and (24). The variables ξ, η, and ζ, the scale factors, and equations (21) to (24) are tabulated for certain of these cases in table I. It is still necessary, however, to apply the classical techniques to obtain final solutions.

Particular Solutions of Space-Charge Flow

It is of interest here to discuss particular solutions of the differential equations listed in table I and to express these solutions in nomographic form. In addition to these previously listed space-charge-flow solutions, there are two other known analytic space-charge flows included in the following sections.

Rectilinear flow between infinite plane electrodes. - Sketch (b) illustrates rectilinear flow between plane electrodes.

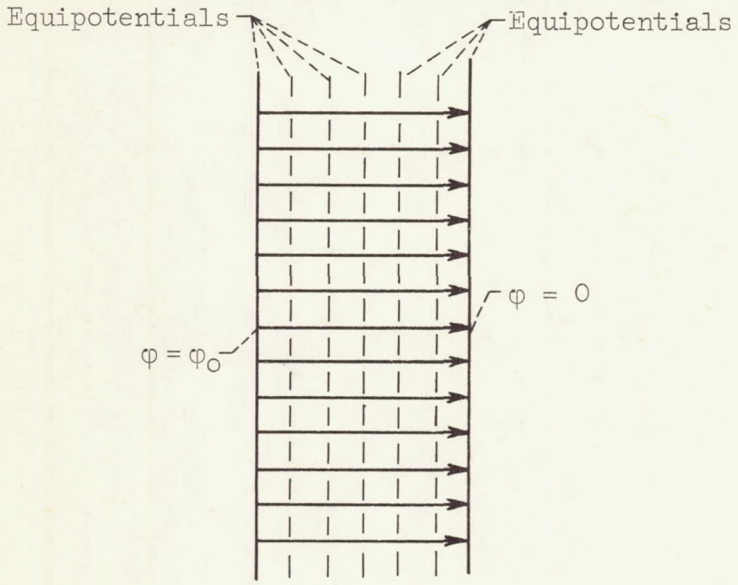

(b)

In 1911, Child (ref. 2) published the solution to this case. From his analysis he obtained what is now known as the Child-Langmuir space-charge law:

$$j = \frac{4}{9} \epsilon_o \sqrt{\frac{2q}{m}} \frac{(\varphi_o - \varphi)^{3/2}}{x^2} \tag{25}$$

where φ_o is the potential at $x = 0$. When the constants are written:

$$\frac{4}{9} \epsilon_o \sqrt{\frac{2q}{m}} = 5.467 \times 10^{-8} \ A^{-1/2}$$

where A is the molecular weight per ionic charge, equation (25) becomes

$$j = 5.467\times10^{-8}\ A^{-1/2}(\varphi_o - \varphi)^{3/2}x^{-2} \tag{26}$$

A nomogram relating j, $(\varphi_o - \varphi)$, A, and x is shown in figure 1. The velocity v as shown in equation (10) is obtained for this and each subsequent case from the nomogram in figure 2.

Rectilinear flow between coaxial cylinders is shown in sketch (c).

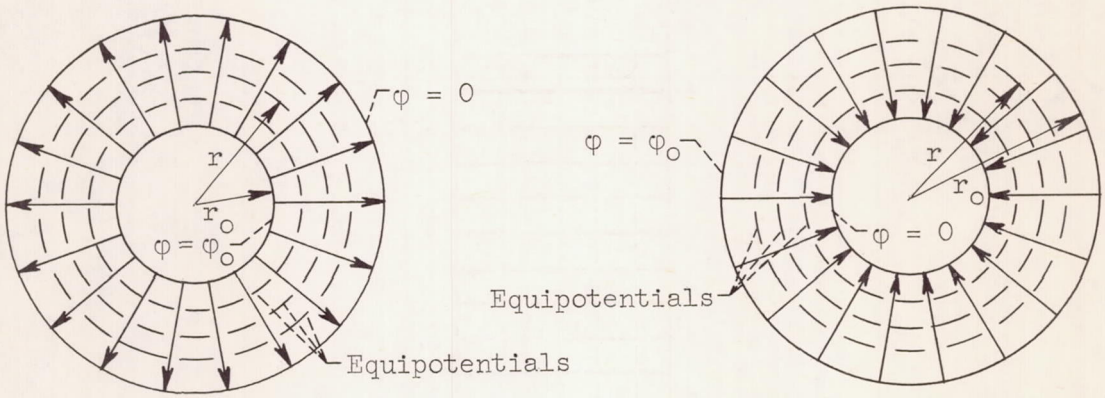

Diverging flow

Converging flow

(c)

In 1913 a paper by Langmuir (ref. 3) was published that contained an approximate solution for this type of flow. The current density and current per unit length may be written

$$j = 5.467\times10^{-8}\ A^{-1/2}(\varphi_o - \varphi)^{3/2}r^{-2}\beta^{-2} \tag{27}$$

$$\frac{J}{l} = 2\pi rj = 3.43\times10^{-7}\ A^{-1/2}(\varphi_o - \varphi)^{3/2}(r\beta^2)^{-1} \tag{28}$$

where φ_o is the potential at r_o and β is a nondimensional function of r expressed as a power series in $\ln(r/r_o)$.

In 1923 an improved solution by Langmuir and Blodgett (ref. 4) was published. Two series representations for β were given. One of these most useful for electrode design is:

$$\beta = \left(\frac{r}{r_o}\right)^{-1/2}\left[\left(\ln \frac{r}{r_o}\right) + 0.1\left(\ln \frac{r}{r_o}\right)^2 + 0.0167\left(\ln \frac{r}{r_o}\right)^3 + \ldots\right] \quad (29)$$

The Langmuir function β^2 is plotted as a function of r/r_o in figure 3 and is tabulated in table II. Note that β^2 for $r/r_o > 1$ is for divergent flow (from the inner to the outer cylinder), and β^2 for $r/r_o < 1$ is for convergent flow. The numbers in table II were computed from equation (29) using all 14 coefficients given by Langmuir in reference 4. These numbers agree well with those shown by Langmuir. Nomograms relating J/l, $(\varphi_o - \varphi)$, A, r, r/r_o, and v are shown in figures 2, 4, and 5.

Rectilinear flow between concentric spheres. - Sketch C also depicts rectilinear flow between concentric spheres. The solution for this case, due to Langmuir and Blodgett (ref. 5), was published in 1924. The current density and total current may be written

$$j = 5.467\times10^{-8}\, A^{-1/2}(\varphi_o - \varphi)^{3/2} r^{-2} \alpha^{-2} \quad (30)$$

$$J = 4\pi r^2 j = 6.87\times10^{-7}\, A^{-1/2}(\varphi_o - \varphi)^{3/2} \alpha^{-2} \quad (31)$$

where α is a nondimensional function of r expressed as the power series

$$\alpha = \left[\left(\ln \frac{r}{r_o}\right) - 0.3\left(\ln \frac{r}{r_o}\right)^2 + 0.075\left(\ln \frac{r}{r_o}\right)^3 - 0.014\left(\ln \frac{r}{r_o}\right)^4 + \ldots\right] \quad (32)$$

The Langmuir function α^2 is plotted as a function of r/r_o in figure 6 and is tabulated in table III. As in the cylindrical flow case, α^2 for $r/r_o > 1$ corresponds to diverging flow and α^2 for $r/r_o < 1$ to converging flow. The numbers in table III were computed from equation (32) and agree well with Langmuir's data.

Nomograms relating J, $(\varphi_o - \varphi)$, A, r/r_o, and v are shown in figures 2, 7, and 8.

Circular flow. - Circular flow is depicted in sketch (d).

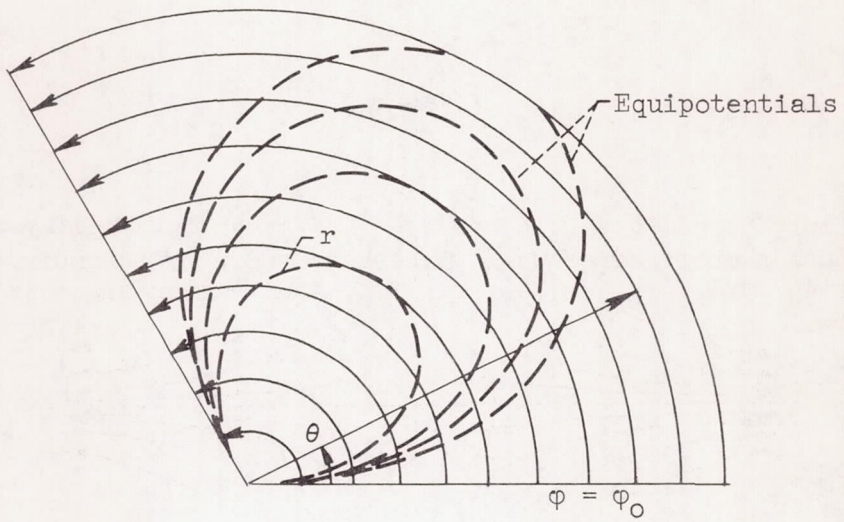

(d)

The solution to this case is given by Meltzer in reference 11. The current density may be written

$$j = 1.23\times10^{-7}\, A^{-1/2}(\varphi_o - \varphi)^{3/2}\left(r \sin\frac{3\theta}{2}\right)^{-2} \qquad (33)$$

where φ is the potential at (r,θ) and j is the current density in the current sheet r. Figure 9 is a nomogram relating j, $(\varphi_o - \varphi)$, A, r, and θ. The velocity can be obtained from figure 2. This flow has several peculiarities that are not evident from equation (33). Since these are discussed in reference 11, they will only be mentioned here. First of all, the ions accelerate through an angle of 60^o and then decelerate, reaching zero velocity at 120^o. Since the equipotentials do not lie along a radial plane except at $\theta = 0^o$ and $\theta = 120^o$, the velocity varies along any radial plane in the flow. Finally, along any radial plane the current density j is proportional to $1/r^5$. This poses a very difficult problem in ionizer design.

If a beam is considered that is bounded by an inner trajectory of radius a and an outer trajectory of radius b, the current per unit length may be written

$$\frac{J}{l} = 3.08\times10^{-8}\, A^{-1/2}\left(\frac{1}{a}\right)\left(1 - \frac{a^4}{b^4}\right)(\varphi_o - \varphi)^{3/2}\left(\sin\frac{3\theta}{2}\right)^{-2} \qquad (34)$$

This equation is used in the electrode design section.

Hyperbolic flow. - Hyperbolic flow is shown in the following sketch:

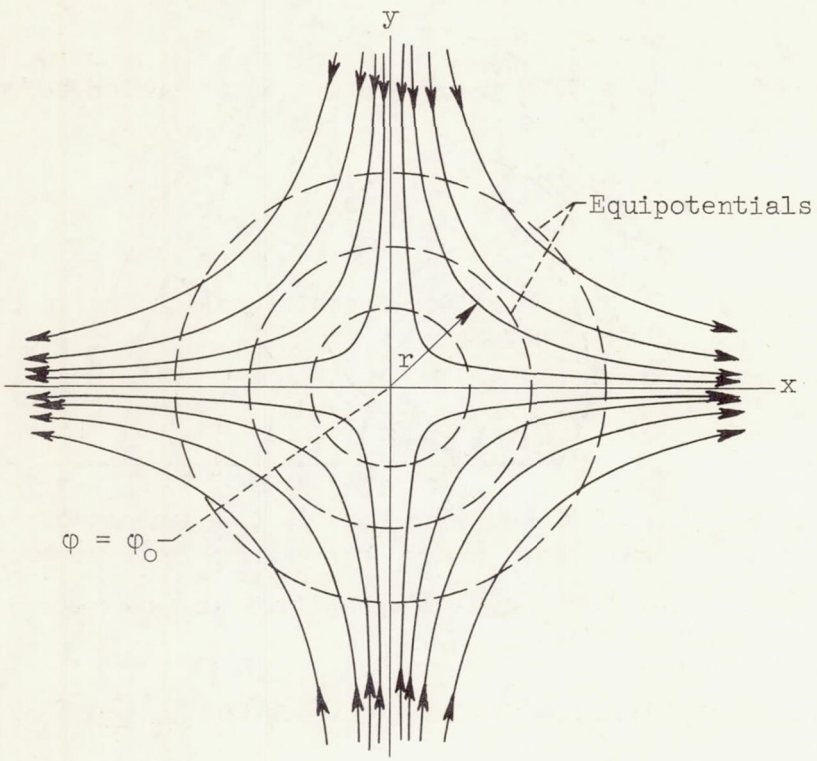

(e)

The solution to this case was obtained by Meltzer (ref. 7) and later by Rosenblatt (ref. 12). The space-charge-limited current density may be written:

$$j = 4.92 \times 10^{-7} A^{-1/2} (\varphi_o - \varphi)^{3/2} r^{-2} \tag{35}$$

where φ is the potential at radius r. This equation is expressed in terms of a nomogram in figure 10. It is interesting to note that J along any given trajectory is a function only of the radial component of the trajectory. If the bounding trajectory is defined by the equation $y = (\lambda/x)$, the current per unit length for one quadrant may be written

$$\frac{J}{l} = 4.92 \times 10^{-7} A^{-1/2} \lambda (\varphi_o - \varphi)^{3/2} \left(x^2 + \frac{\lambda^2}{x^2} \right)^{-3/2} \tag{36}$$

where Z is measured normal to the (x,y) plane.

Flow between two inclined planar electrodes. - The configuration of two inclined planar electrodes presents a very interesting problem of space-charge flow applicable to ion engine design.

Walker (ref. 9) solved this problem by first assuming negligible space charge. In this case the potential distribution between two inclined planar electrodes is known and can be written:

$$\Phi = \frac{\varphi_o}{\alpha}\theta \tag{37}$$

By substituting (37) into Hamilton-Jacobi equation (9) in polar coordinates, equation (9) then becomes

$$\left(\frac{\partial W}{\partial r}\right)^2 + \left(\frac{1}{r}\frac{\partial W}{\partial \theta}\right)^2 = \frac{2q}{m}\frac{\varphi_o}{\alpha}\theta \tag{38}$$

Because the right side of equation (38) is independent of r, so must be also the left side of (38). Therefore, Walker (ref. 9) sought a solution of the action function in the form

$$W = rz(\theta) \tag{39}$$

By substituting (39) into (38) the Hamilton-Jacobi equation becomes

$$z^2 + z'^2 = \left(\frac{2q}{m}\frac{\varphi_o}{\alpha}\right)\theta \tag{40}$$

where $z = \frac{\partial W}{\partial r}$ and $z' = \frac{1}{r}\frac{\partial W}{\partial \theta}$. Equation (40) was solved by Walker in the form of a power series.

The components of velocity are then given by

$$v_r = \frac{\partial W}{\partial r} = z$$

$$v_\theta = \frac{1}{r}\frac{\partial W}{\partial \theta} = z'$$

Hence,

$$\frac{dr}{r} = \frac{z}{z'}\,d\theta$$

and after integration the trajectory equation is obtained:

$$\frac{r}{r_o} = \exp\left(\int_0^\theta \frac{z}{z'}\, d\theta\right) \tag{41}$$

where $(r_o,0)$ is the initial point of a particular trajectory, and (r,θ) are the coordinates of the remainder of that particular trajectory (sketch (f)).

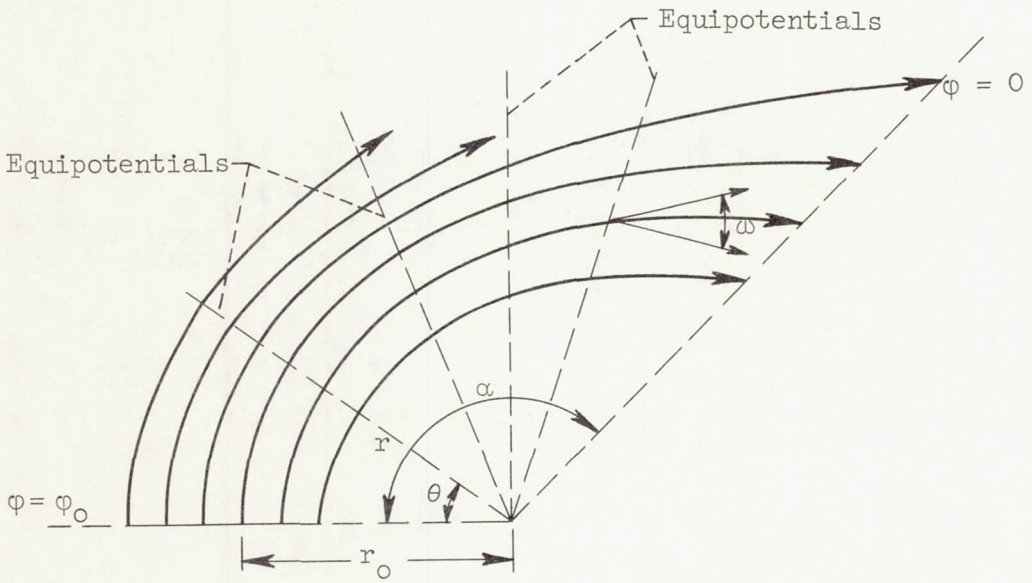

(f)

The angle between the trajectory and the normal to equipotential is given by

$$\tan \omega = \frac{dr}{r\, d\theta} = \frac{z}{z'} \tag{42}$$

In the case of space-charge flow between two inclined planar electrodes, Walker assumed an action function in the form

$$W = rg(\theta) \tag{43}$$

By substituting (43) into Hamilton-Jacobi equation (9), equation (9) becomes

$$g^2 + g'^2 = \left(\frac{2q}{m}\right)\Phi \tag{44}$$

Now the left side of equation (44) is a function of θ only; and, hence, Φ must be a function of θ only.

By expressing Poisson's equation (1) in polar coordinates, it follows that

$$\rho = \frac{\epsilon_o \Phi''}{r^2} \tag{45}$$

The components of vector current density are

$$j_r = \frac{\epsilon_o \Phi'' g}{r^2}$$

and

$$j_\theta = \frac{\epsilon_o \Phi'' g'}{r^2}$$

By substituting these components into the equation of conservation of charge (eq. (3))

$$\nabla \cdot \vec{j} = \frac{\partial j_r}{\partial r} + \frac{1}{r} j_r + \frac{1}{r} \frac{\partial j_\theta}{\partial \theta} = 0$$

Walker obtained

$$\frac{d}{d\theta} (\Phi'' g') - \Phi'' g = 0 \tag{46}$$

By eliminating Φ from equations (44) and (46) an ordinary fourth-order differential equation in g is obtained in the form

$$g'''' + g'' \left[4\left(\frac{g'''}{g'} + 1 \right) + \frac{g''^2 - g^2}{g'^2} \right] - g = 0 \tag{47}$$

Any solution of this equation defines a possible motion. In a fashion similar to that in the space-charge-free case the trajectory equation is given by

$$\frac{r}{r_o} = \exp\left(\int_0^\theta \frac{g}{g'} \, d\theta \right) \tag{48}$$

and the angle between the trajectory and the normal to the equipotential is given by

$$\tan \omega = \frac{dr}{r\, d\theta} = \frac{g}{g'} \tag{49}$$

Ivey (ref. 10) made a detailed calculation of this problem and his results of equations (41), (42), (48), and (49) are presented in figures 11 and 12.

The space-charge-limited current density of the emitter as calculated in reference 10 is

$$j = \frac{4}{9} \epsilon_o \left(\frac{2q}{m}\right)^{1/2} \frac{\Phi^{3/2}}{r_o^2} F(\alpha) \tag{50}$$

where $F(\alpha)$ could be defined as a perveance function depending on the magnitude of the angle α shown in sketch (f). At any place in the flow the current density may be written

$$j = \frac{j_o(\theta)}{r/r_o}$$

Substitution into equation (50) yields

$$j = \frac{4}{9} \epsilon_o \left(\frac{2q}{m}\right)^{1/2} \frac{\Phi^{3/2}}{r^2} \left[\left(\frac{r}{r_o}\right) F(\theta)\right] \tag{51}$$

where Φ is the potential difference between $\theta = 0$ and θ, and the range of θ is $0 \leq \theta \leq \alpha$. A nomogram of equation (51) is shown in figure 13 where $\frac{4}{9} \epsilon_o \sqrt{\frac{2q}{m}} = 5.467 \times 10^{-8}\ A^{-1/2}$ for singly charged ions. The normalized potential distribution for space-charge-limited flow as a function of normalized angle θ/α is shown in figure 14 for several values of α. It is interesting to note that for $\alpha = 0$ the potential distribution is that for two parallel planes and, further, that the potential distribution for $\alpha < \pi/2$ is not greatly different from that for $\alpha = 0$.

Flow between two coaxial right circular conical electrodes whose vertexes coincide. - In this configuration it is also assumed, as in the case of the flow between two inclined planar electrodes, that the end effects can be taken care of in all directions. Walker has outlined the

procedure for the solution of this problem for the space-charge flow (see sketch (g)). The authors of this paper assumed an action function in the form

$$W = r \cdot s(\theta) \tag{52}$$

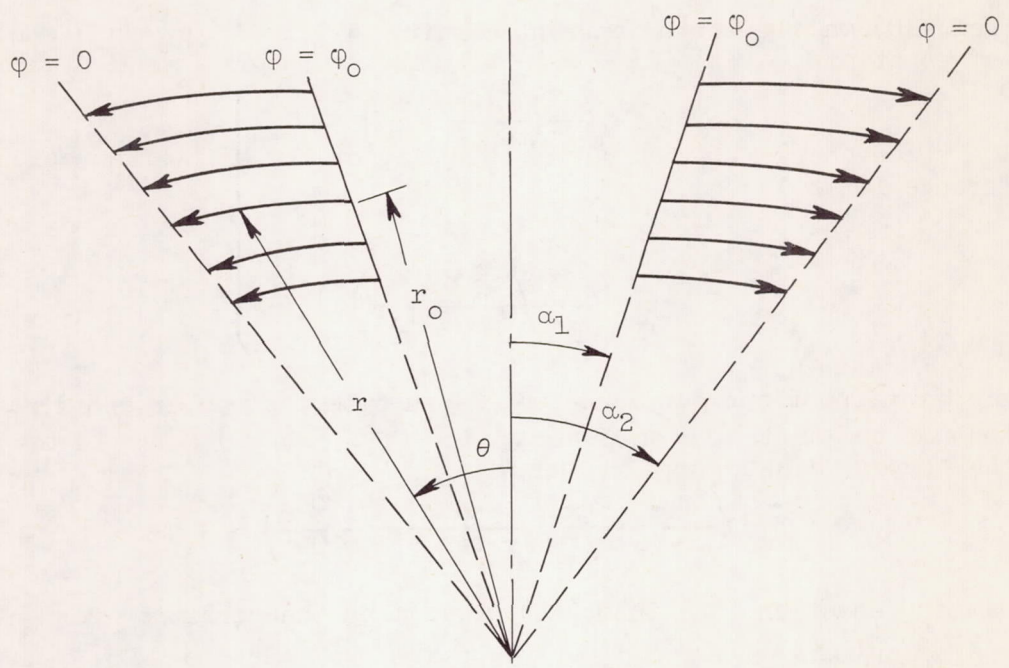

(g)

Kino and Harker (ref. 13) in their analysis used a similar form of action function $W = r^n \cdot s(\theta)$ and investigated cases for $n < 1$. Some of the cases investigated in their paper show beam trajectories that pass through potential minimums (accelerate-decelerate system). In the case of $W = r \cdot s(\theta)$, investigated herein, the beam trajectories are continuously accelerated (accelerate system).

By substituting (52) into Hamilton-Jacobi equation (9) this equation becomes

$$s^2 + s'^2 = \left(\frac{2q}{m}\right)\varphi \tag{53}$$

As in the case of the flow between two inclined planes, it was deduced that φ has to be a function of θ only.

By expressing Poisson's equation (1) in spherical polar coordinates, it follows that

$$\rho = \frac{\epsilon_o}{r^2}\left(\frac{\varphi'}{\tan\theta} + \varphi''\right) \tag{54}$$

The components of the vector current density are

$$\left.\begin{aligned} j_r &= \frac{\epsilon_o s}{r^2}\left(\frac{\varphi'}{\tan\theta} + \varphi''\right) \\ \text{and} \\ j_\theta &= \frac{\epsilon_o s'}{r^2}\left(\frac{\varphi'}{\tan\theta} + \varphi''\right) \end{aligned}\right\} \tag{55}$$

The conservation of current equation (3) in spherical polar coordinates is

$$\nabla \cdot \vec{j} = \left(\frac{2j_r}{r} + \frac{\partial j_r}{\partial r} + \frac{j_\theta}{r\tan\theta} + \frac{1}{r}\frac{\partial j_\theta}{\partial\theta}\right) = 0 \tag{56}$$

Substituting equation (55) into (56) gives then the condition for which div j is zero, namely, when

$$\cot\theta(2\varphi''s' + \varphi's'') + \varphi'''s' + \varphi''s'' - \varphi's' = 0 \tag{57}$$

By eliminating φ from equations (53) and (57) a fourth-order nonlinear ordinary differential equation in s is obtained in the form

$$s'''' = -\cot\theta\left[2(s''' + s') + 3\frac{s''}{s'}(s'' + s)\right] - \frac{2s''}{s'}\left[2s''' + \frac{s''(s'' + s)}{2s'}\right] + s\left(1 - \frac{s'''}{s'}\right) - 3s'' \tag{58}$$

Equation (58) was solved numerically for $s(\theta)$ and $s'(\theta)$, which were then used for determination of ion trajectories.

The components of velocity are

$$v_r = \frac{\partial W}{\partial r} = s$$

and

$$v_\theta = \frac{1}{r}\frac{\partial W}{\partial \theta} = s'$$

and

$$\frac{dr}{r} = \frac{s}{s'}\,d\theta$$

and by integration

$$\frac{r}{r_o} = \exp\left(\int_0^\theta \frac{s}{s'}\,d\theta\right) \tag{59}$$

The angle between the trajectories and the normals to the equipotentials is given by

$$\tan \gamma = \frac{dr}{r\,d\theta} = \frac{s}{s'} \tag{60}$$

The current density is given by

$$|j| = \sqrt{j_r^2 + j_\theta^2} \tag{61}$$

To obtain more accurate values of j_o, the current density at the emitter, the current density j_a at the collector was first calculated from equation (61). The current density at the emitter was then calculated from

$$j_o = j_a\left(\frac{r}{r_o}\right) = \frac{4}{9}\,\epsilon_o\sqrt{\frac{2q}{m}}\,\frac{\Phi^{3/2}}{r_o^2}\,s(\alpha_2 - \alpha_1) \tag{62}$$

The solutions of ion trajectories and the angle between the trajectories and the normals to the equipotentials are presented in figures 15 and 16, respectively. A nomogram of equation (62) is given in figure 17. The normalized potential distribution as a function of normalized angle $(\theta - \alpha_1)/(\alpha_2 - \alpha_1)$ for several angles $(\alpha_2 - \alpha_1)$ is shown in figure 18.

Partial Space-Charge Flow

As early as 1920, Jaffe considered the plane diode under partial space-charge conditions where the current is less than space-charge limited, sometimes called temperature or flow-rate-limited condition, (ref. 14). Since that time there have been several papers on this subject, two of which will be noted here. Brubaker (ref. 15) and Ivey (ref. 16) derived the equations governing the flow of electrons or ions under partial space-charge conditions independently at about the same time. Brubaker made use of normalized variables representing current density, voltage, distance, and emitter field, so that these variables range between zero and unity as the current density varies from zero to the space-charge-limited value. He defined the normalized variables as

$$\bar{j} = \frac{\text{Current density}}{\text{Space-charge-limited current density}} = \frac{j}{j_s}$$

$$\bar{V} = \frac{\text{Voltage at distance } X \text{ from emitter}}{\text{Voltage at collector, at distance } X_a \text{ from emitter}} = \frac{V_x}{V_a}.$$

$$\bar{X} = \frac{\text{Distance from emitter}}{\text{Emitter-collector spacing}} = \frac{X}{X_a}$$

$$\bar{\gamma} = \frac{\text{Gradient at emitter under influence of space charge}}{\text{Gradient at emitter in absence of space charge}} = \left(\frac{X_a}{V_a}\right)\left(\frac{dV}{dX}\right)_{X=0}$$

The previously mentioned assumption still holds, namely, zero velocity of the particles at the emitter.

The potential distribution and electric field are fully defined by equations (63) and (64):

$$16(\bar{j}\bar{V}^{3/2} - \bar{j}^2\bar{X}^2) = 27(\bar{V}\bar{\gamma}^2 - \bar{X}\bar{\gamma}^3) \tag{63}$$

$$\frac{d\bar{V}}{dx} = \frac{27\bar{\gamma}^3 - 32\bar{j}\bar{X}}{27\bar{\gamma}^2 - 24\bar{j}\bar{V}^{1/2}} \tag{64}$$

The relation between the current density $\bar{j}$ and the electric field at the emitter is given by equation (63). By setting $\bar{V} = \bar{X} = 1$ the condition at the collector is given by

$$\bar{j} = \frac{1}{2} + \left(\frac{1}{2} - \frac{3}{4}\bar{\gamma}\right)(3\bar{\gamma} + 1)^{1/2} \tag{65}$$

Equation (65) is plotted in figure 19. It is interesting to see that the emitter field rises rapidly as the current is decreased from space-charge-limited values. Decreasing the current 10 percent from the space-charge-limited value causes the field to increase from zero to more than 25 percent of its value in the absence of space charge.

If equation (63) is solved for specific values of the electric field $\bar{\gamma}$ and the current density $\bar{j}$ or, in other words, if $\bar{\gamma} = \bar{\gamma}_o$ and $\bar{j} = \bar{j}_o$ are held constant, equation (63) gives a relation between $\bar{V}$ and $\bar{X}$. By substituting $\bar{\gamma}_o$ and $\bar{j}_o$ into (63) and rearranging terms, equation (63) becomes

$$\bar{X} = \frac{27\bar{\gamma}_o^3}{32\bar{j}_o^2}\left[1 + \left(\frac{8\bar{j}_o\bar{V}^{1/2}}{9\bar{\gamma}_o^2} - 1\right)\left(\frac{16\bar{j}_o\bar{V}^{1/2}}{9\bar{\gamma}_o^2} + 1\right)^{1/2}\right] \qquad (66)$$

Equation (66) is plotted in figure 20. It is seen that the maximum depression of the space potential for space-charge-limited conditions ($\bar{j}_o = 1$) occurs at $\bar{x} = 27/64$ where the normalized slope is unity. By using the data obtained in figures 19 and 20 in equation (64) the electric field is obtained as a function of position. This is presented in figure 21. The normalized gradient is equal to unity in the plane $\bar{x} = 27/64$ independent of the current density $\bar{j}$. As Brubaker points out, this is only an approximation. However, the maximum deviation from unity is only 0.6 percent as the current density is varied from zero to space-charge-limited values.

Ivey investigated the case of a cylindrical diode under partial space-charge conditions (ref. 16). In this case Poisson's equation cannot be integrated directly so a differential analyzer was used to obtain a numerical solution. Without a rigorous proof, Ivey then states that it appears that the emitter field characteristic as shown in figure 19 is "universal" and applies also to other geometries, including those with external emitters. He points out also that this seems to be a direct consequence of Poisson's equation, and the only restrictions on the applicability of figure 19 are those of negligible initial velocities and an equipotential emitter (the same conditions imposed on the generalized space-charge law).

THEORY OF PIERCE ELECTRODE DESIGN

The problem of design of electrode systems that will constrain an accelerating ion beam to travel in a desired region has confronted scientists and engineers for many years. Before 1940 most electrode systems

were designed using assumptions of either zero space charge or paraxial flow. Since then much progress has been made toward the development of general methods for the design of electrodes for high-charge-density ion beams. These methods can be divided into two categories:

(1) Analog methods such as the resistance network and electrolytic tank

(2) Analytic solution of the space-charge equations and of Laplace's equation in the region surrounding the ion beam

The most widely used analytic approach to accelerator design was proposed by Pierce (ref. 17) in 1940. Although the Pierce method was originally intended for rectilinear flow, it has since been generalized to include any type of curvilinear flow provided the boundary conditions are regular (ref. 18). When the solution to a particular type of space-charge flow (such as those described in the first section of this report) is found, it generally will fill all space. To form a beam it is necessary to take a segment of this flow and replace the missing portion with an electric field that will exactly match the conditions along the streamlines bounding the ion beam. This is done by arranging suitably shaped electrodes around the ion beam. The electrode shapes are found by solving Laplace's equation in the charge-free space surrounding the ion beam subject to the conditions of continuity of potential and normal gradient across the beam edge.

When the space-charge flow can be expressed in terms of some type of cylindrical coordinate system, as is frequently the case, application of complex variable theory becomes quite useful. This is demonstrated in sketch (h). Curve C represents the boundary of a general curvilinear ion beam that extends to infinity normal to the paper. If an analytic function can be found which transforms C into the u-axis, then the potential distribution along C and the gradient normal to C will be transformed as shown.

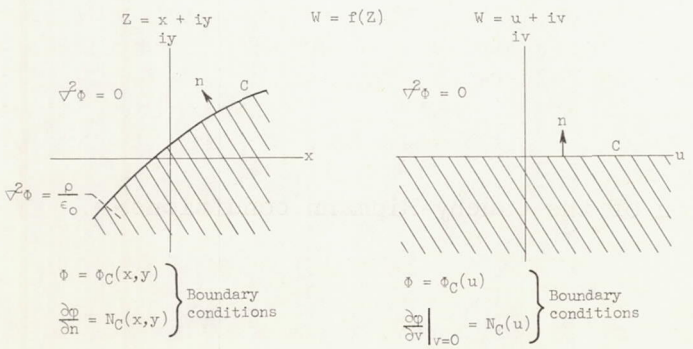

(h)

Since harmonic functions remain harmonic under conformal transformation, a solution of Laplace's equation for the upper half of the W-plane can be converted to the desired solution in the Z-plane by application of the inverse transformation. A general solution of Laplace's equation in the upper-half plane subject to Cauchy boundary conditions is given in reference 19:

$$\Phi(u,v) = \mathrm{Re}\Phi_C(W) + \mathrm{Im}\int_0^W N_C(\zeta)d\zeta \tag{67}$$

where

Re real part

Im imaginary part

Φ_C potential distribution along $v = 0$

N_C potential gradient normal to $v = 0\left(\frac{d\varphi}{dv}\right)_{v=0}$

In the event that N_C cannot be integrated explicitly as an analytic function of W, another technique described by Lomax (ref. 18) may be used to obtain $\Phi(u,v)$.

It can be seen from equation (67) that $\Phi(u,v)$ can be written as the real part of a complex function:

$$\Lambda = \Phi + i\Psi = \Phi_C(W) - i\int_0^W N_C(\zeta)d\zeta \tag{68}$$

Hence,

$$\frac{d\Lambda}{dW} = \frac{d\Phi_C}{dW} - iN_C(W) \tag{69}$$

By application of the Cauchy-Riemann conditions

$$\frac{d\Lambda}{dW} = \frac{\partial\Phi}{\partial u} - \frac{\partial\Phi}{\partial v} = -E_u + iE_v$$

where E_u and E_v are the electric field components in the u and v directions transformed from the Z-plane by the mapping function $W = f(Z)$.

Specifically, E_u corresponds to the electric field tangent to the beam edge and E_v corresponds to the field normal to the beam edge.

Since E_u and E_v are derivable from an analytic function, they are differentiable; and the differential equation of a line of electric flux can be written:

$$\frac{dv}{du} = \frac{E_v}{E_u} \qquad E_u \neq 0 \tag{70}$$

The equipotentials are orthogonal to the lines of force and are therefore determined by the equation

$$\frac{dv}{du} = \frac{E_u}{E_v} \qquad E_v \neq 0 \tag{71}$$

The condition $E_v \neq 0$ is always satisfied in cases of interest since $E_v = -N_C(u)$. By taking the real and imaginary parts of equation (69), equation (71) can be written:

$$\frac{dv}{du} = \frac{\left[\mathrm{Re}\,\frac{d\Phi_C}{dW} + \mathrm{Im}N_C(W)\right]}{\left[\mathrm{Im}\,\frac{d\Phi_C}{dW} - \mathrm{Re}N_C(W)\right]} = \cot\left(\arg\frac{d\Lambda}{dW}\right) \tag{72}$$

This is the differential equation specifying the equipotential surfaces.

While this technique is applicable to a large number of geometries, there are some configurations of interest that cannot be handled in this way. An example of one of these is rectilinear flow with circular cross section. The solution of this particular problem will be discussed later.

Electrodes for Rectilinear Flow ($N_C = 0$)

Rectilinear slab beam. - This is an application of the solution of flow between infinite parallel planes to the formation of a finite slab ion beam as shown in sketch (i).

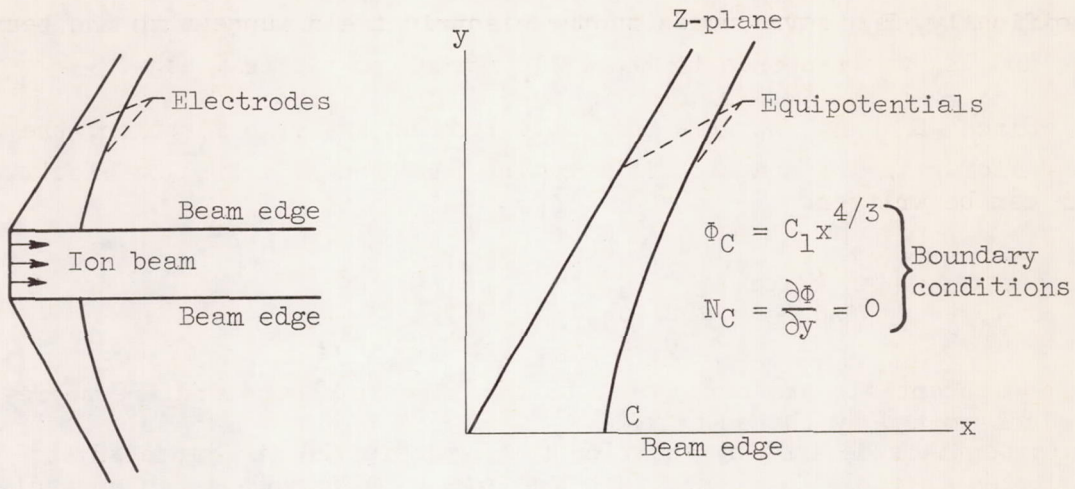

Electrode configuration Mathematical model

(i)

From equation (25) the potential distribution along the beam edge is

$$\Phi_C = C_1 x^{4/3} \tag{73}$$

$$C_1 = 6.942 \times 10^4 \, A^{1/3} j^{2/3}$$

There is no need for conformal mapping since the beam edge already coincides with the real axis. The boundary conditions to be satisfied are shown in sketch (i). The potential gradient normal to the beam edge N_C is zero. Therefore, equation (67) has the particularly simple form:

$$\Phi = \mathrm{Re}\Phi_C(Z) = C_1 \mathrm{Re} Z^{4/3}$$

$$= C_1 (x^2 + y^2)^{2/3} \cos\left(\frac{4}{3} \tan^{-1} \frac{y}{x}\right) \tag{74}$$

Equation (74) is developed in dimensional form for clarity. It is much more convenient, however, to nondimensionalize from the start. This may be done by letting $X = x/l$, $Y = y/l$, and $\chi = \Phi_C/(C_1 l^{4/3})$ where l is the unit of length. Then equation (73) becomes

$$\chi = X^{4/3} \tag{75}$$

Sketch (i) remains the same except that now the boundary conditions are:

$$\chi_C = X^{4/3} \tag{75}$$

$$N_C = \left.\frac{\partial \chi}{\partial Y}\right|_{y=0} = 0$$

and equation (74) becomes

$$\chi = \mathrm{Re}(X + iY)^{4/3} = (X^2 + Y^2)^{2/3} \cos\left(\frac{4}{3} \tan^{-1} \frac{Y}{X}\right) \tag{76}$$

Equipotentials defined by equation (76) are plotted in figure 22 and tabulated in table IV. Note that the $\chi = 0$ electrode makes an angle of 67.5° with the beam edge. This is called the Pierce angle, and it occurs in every geometry because, as the ion emitter is approached closer and closer, the potential distribution approaches that of a plane diode. The function $X^{4/3}$ is multiple-valued and hence can give rise to solutions that do not satisfy the boundary conditions. While it is a simple matter to choose the proper solution in this case, it is not so simple in some of the cases that follow where the complex potential function is a power series. The coordinates listed in table IV agree with the curves shown by Pierce in reference 17.

Beams of circular cross section. - The potential distribution has the same form as equation (73), but in this case polar coordinates are used and x is replaced by z:

$$\Phi_C = C_1 z^{4/3}$$

$$C_1 = 6.942 \times 10^4 \, A^{1/3} j^{2/3} \tag{77}$$

In 1955 a paper by Daykin (ref. 20) appeared in which a solution to this problem was described. A sketch of the problem is shown as follows:

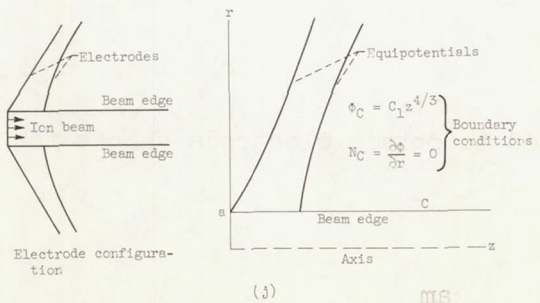

(j)

Equation (77) can be nondimensionalized by writing

$$\chi_C = \frac{\Phi_C}{C_1 a^{4/3}} = \left(\frac{z}{a}\right)^{4/3} \tag{78}$$

where a is the radius of the ion beam. Daykin showed that the potential distribution near the beam edge can be expressed by an infinite series of the form

$$\chi = \left(\frac{z}{a}\right)^{4/3}\left[1 + \left(\frac{a}{z}\right)^2 F_2\left(\frac{r}{a}\right) + \left(\frac{a}{z}\right)^4 F_4\left(\frac{r}{a}\right) + \cdots\right] \tag{79}$$

The functions F_2 and F_4 are plotted in figure 23. Because of its rapid convergence near the beam edge, this series may be truncated at three terms without introducing serious error. In order to extend the solution away from the beam edge the asymptotic forms of the equipotentials are computed. For this purpose it is convenient to define a new coordinate system in terms of r and z. This is shown in sketch (k).

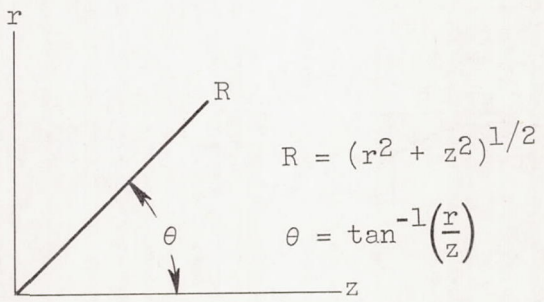

(k)

The equipotentials are then written in terms of Legendre functions $P_{4/3}$ of order 4/3 as

$$\chi = \left(\frac{R}{a}\right)^{4/3} P_{4/3}(\cos\theta) \tag{80}$$

Equation (80) is used to obtain electrode shapes far from the beam edge. Equipotentials from equations (79) and (80) are plotted in figure 24(a) and tabulated in tables V and VI. The transition region is shown by dotted lines.

For a hollow ion beam another set of electrodes is required inside the beam. Daykin derived an expression for these equipotentials for

small r/b where b is the inner radius of the beam. This equation may be written

$$\frac{r}{b} = \exp - \left\{ \frac{9}{2}\left(\frac{z}{b}\right)^2 \left[1 - \left(\frac{b}{z}\right)^{4/3} \chi \right] + \frac{1}{2} \right\} \qquad (81)$$

As in the previous case it is necessary to fair in part of the equipotentials. Some of these are shown in figure 24(b) and tabulated in table VII. The dotted portion joins the equipotentials from equation (81) to the proper intercept on the inner beam edge defined by equation (78). Until recently this was the only analytic solution of the Pierce electrode problem for axisymmetric ion beams. Harker (ref. 21) has recently developed a very general method whereby any axisymmetric electrode design problem can be solved with the aid of a digital computer.

Cylindrical flow. - The application of converging and diverging flow between coaxial cylinders is considered in this section. The two configurations are shown in sketches (l) and (m).

Converging flow

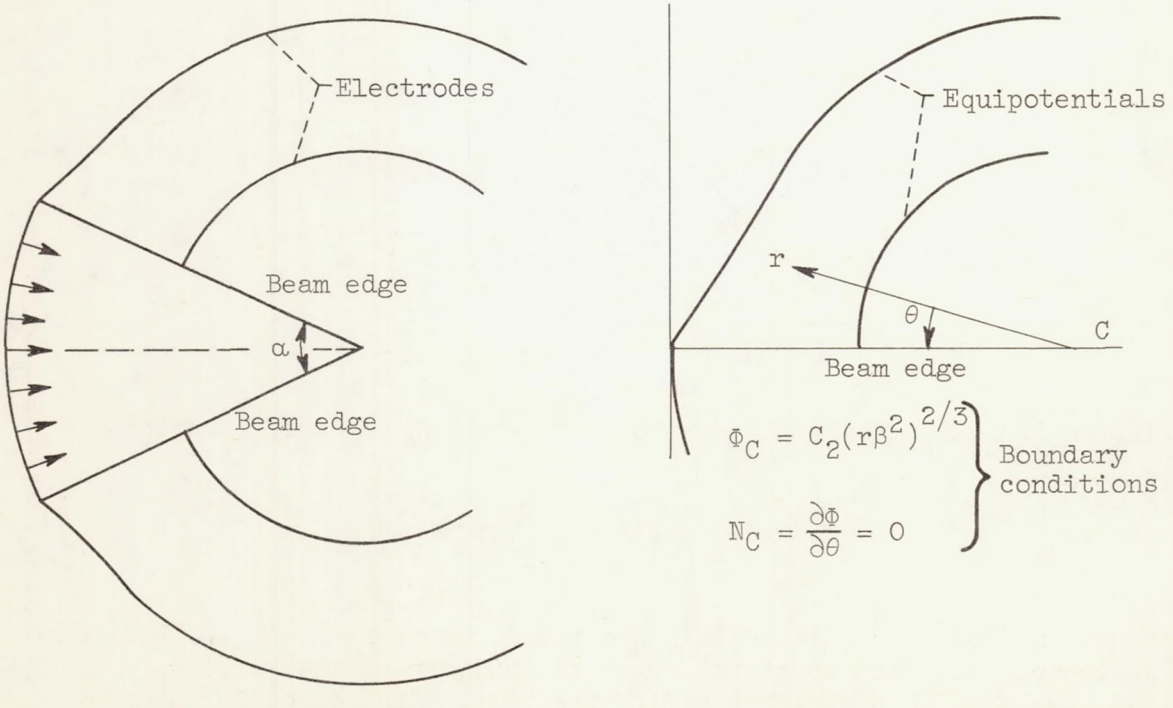

Electrode shapes

(l)

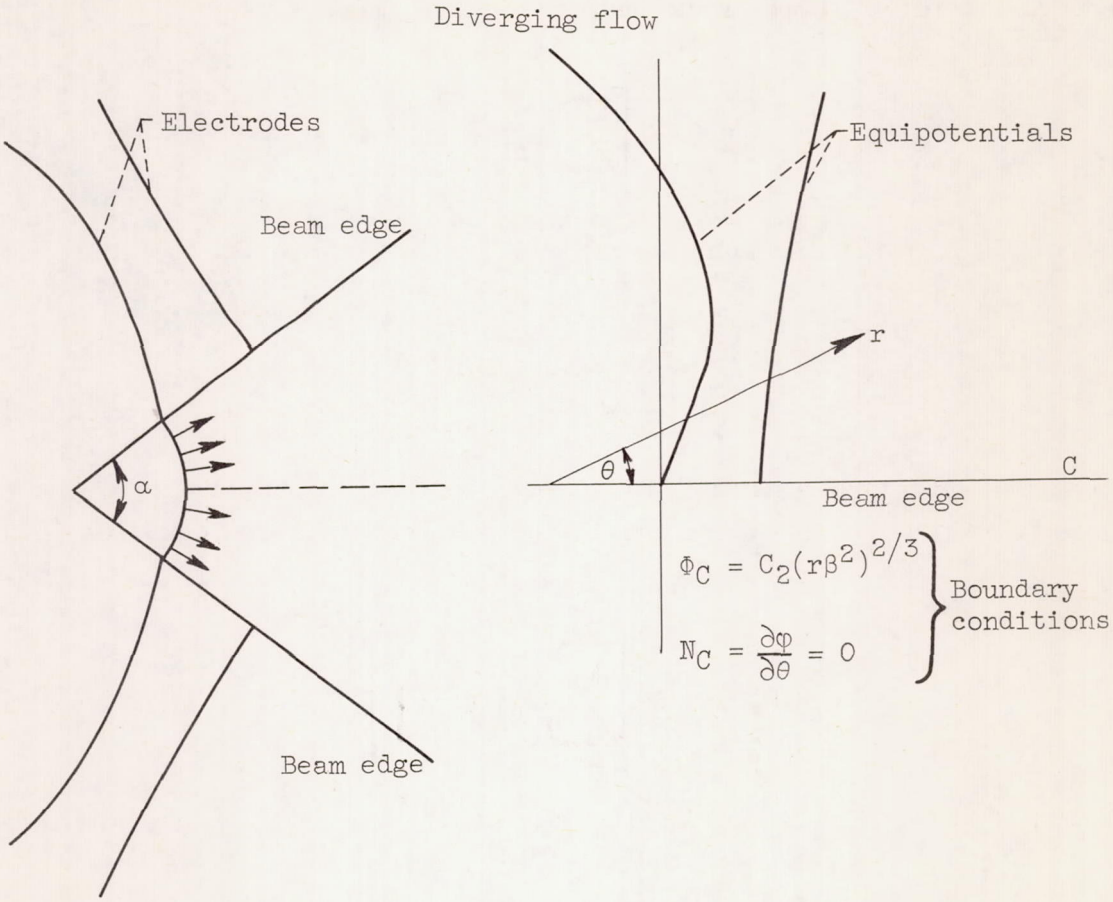

(m)

Since the included angle of the wedge is α, the current per unit length from equation (28) will be multiplied by the factor $\alpha/2\pi$. The potential distribution becomes

$$\left.\begin{aligned} \Phi_C &= C_2(r\beta^2)^{2/3} \\ C_2 &= 6.942\times10^4\, A^{1/3}\left(\frac{J}{\alpha l}\right)^{2/3} \end{aligned}\right\} \qquad (82)$$

This is nondimensionalized by letting $R = r/r_o$ and $\chi_C = \Phi_C/(C_2 r_o^{2/3})$. The nondimensional potential distribution becomes

$$\chi = (R\beta^2)^{2/3} \qquad (83)$$

From equation (29) it follows that

$$(R\beta^2) = \left[\sum_{n=1}^{\infty} B_n(\ln R)^n\right]^2$$

and

$$\chi = \left[\sum_{n=1}^{\infty} B_n(\ln R)^n\right]^{4/3} \tag{84}$$

Since the potential gradient N_C normal to the ion beam is zero, the expression for the potential outside of the beam is, from equation (67),

$$\chi(R,\theta) = \mathrm{Re}\left[\sum_{n=1}^{\infty} B_n\left(\ln \frac{Z}{r_o}\right)^n\right]^{4/3} \tag{85}$$

where

$$\frac{Z}{r_o} = \frac{r}{r_o} e^{i\theta} = Re^{i\theta} = R(\cos\theta + i \sin\theta)$$

Equation (85) can be rewritten

$$\chi = (P^2 + Q^2)^{2/3} \cos\left(\frac{4}{3} \tan^{-1} \frac{Q}{P}\right) \tag{86}$$

where

$$P = \left[\ln R + 0.1(\ln^2 R - \theta^2) + 0.0167(\ln R^3 - 3\theta^2 \ln R) + 0.00242(\ln^4 R - 6\theta^2 \ln R + \theta^4) + \ldots\right]$$

and

$$Q = \left[\theta + 0.2\,\theta \ln R + 0.0167(3\theta \ln^2 R - \theta^3) + 0.00242(4\theta \ln^3 R - 4\theta^3 \ln R) + \ldots\right]$$

Equation (86) was solved for several values of X on a digital computer. Equipotentials for both converging and diverging flow are shown in figures 26 and 27 and are tabulated in tables VIII and IX, respectively. This case was also solved by Radley (ref. 22) for convergent flow, and the results shown in table VII agree with those shown in reference 22.

Electrodes for Curvilinear Flow ($N_C \neq 0$)

Circular flow. - The space-charge-limited-flow equations for which the ion trajectories are concentric circular arcs are used here in the design of a curved ion beam. This solution was obtained by Lomax in reference 18. The potential distribution obtained from equation (34) is:

$$\Phi_C = C_3 r^{-2} \left(\sin \frac{3\theta}{2}\right)^{4/3} \tag{87}$$

where

$$C_3 = 1.02 \times 10^5 \, A^{1/3} \left(\frac{a^4 b^4}{b^4 - a^4}\right)^{2/3} \left(\frac{J}{\epsilon_0 l}\right)^{2/3}$$

The potential gradient normal to the beam is

$$\frac{\partial \varphi}{\partial r} = - \frac{\partial \Phi_C}{\partial r} = \frac{2C_3}{r^3} \left(\sin \frac{3\theta}{2}\right)^{4/3} \tag{88}$$

A sketch of the electrode structure is shown as follows:

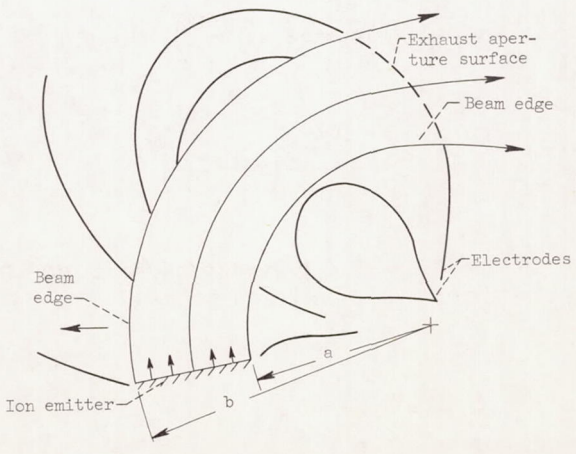

(n)

From the sketch it is seen that the problem can be divided in two parts: $r \geq b$ and $r \leq a$. Sketches for these two problems together with the corresponding boundary conditions are shown as follows: (The shaded region is the region of interest in each case.)

$$\Phi_a = \frac{C_3}{a^2}\left(\sin\frac{3\theta}{2}\right)^{4/3}$$

$$N_a = -\frac{2C_3}{a^3}\left(\sin\frac{3\theta}{2}\right)^{4/3}$$

$r \leq a$

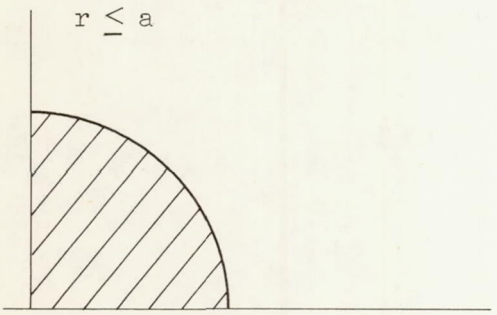

$$\Phi_b = \frac{C_3}{b^2}\left(\sin\frac{3\theta}{2}\right)^{4/3}$$

$$N_b = -\frac{2C_3}{b^3}\left(\sin\frac{3\theta}{2}\right)^{4/3}$$

$r \geq b$

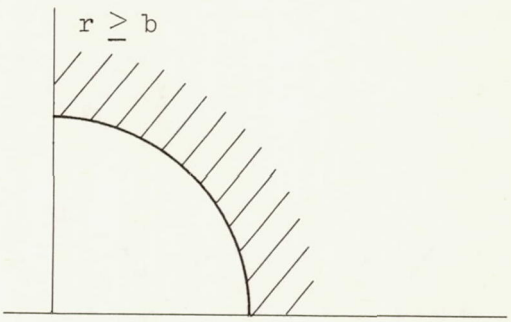

(o)

In this case it is necessary to map the beam edge onto the real axis. Lomax shows that a mapping function that will do this is (for $r = b$)

$$Z = be^{iW} \tag{89}$$

The boundary conditions become, on $v = 0$,

$$\Phi_C(u) = \frac{C_3}{b^2}\left(\sin\frac{3u}{2}\right)^{4/3}$$

$$N_C(u) = \frac{2C_3}{b^2}\left(\sin\frac{3u}{2}\right)^{4/3}$$

The formal solution of Laplace's equation in the upper half of the W-plane is given by equation (67), which becomes

$$\Phi(u,v) = \mathrm{Re}\,\frac{C_3}{b^2}\left(\sin\frac{3W}{2}\right)^{4/3} + \mathrm{Im}\int_0^W \frac{2C_3}{b^2}\left(\sin\frac{3\zeta}{2}\right)^{4/3} d\zeta \qquad (90)$$

Explicit integration of the second term is not readily carried out; therefore, the differential equation representing the equipotentials must be solved. By combining equations (69), (72), and (90), the differential equation becomes

$$\frac{dv}{du} = \cot\left[\frac{1}{3}\tan^{-1}\left(\frac{\tanh\frac{3}{2}v}{\tan\frac{3}{2}u}\right) - \frac{3}{2}u\right] \qquad (91)$$

From the transformation equation (89) it follows that

$$R = \frac{r}{b} = e^{-v}$$

and

$$\theta = u$$

Equation (91) becomes in the Z-plane

$$R\frac{d\theta}{dR} = \tan\left[\frac{3}{2}\theta - \frac{1}{3}\tan^{-1}\left(\frac{1 - R^3}{1 + R^3}\right)\cot\frac{3\theta}{2}\right] \qquad (92)$$

Equation (92) was integrated using the Runge-Kutta method, and some typical equipotentials are shown for $a/b = 0.7$ in figure 27 and are tabulated in tables X and XI. The inside equipotentials were found by simply replacing b by a in equations (89) and (92). In figure 27 $\chi_b = \Phi(b^2/C_3)$ and $\chi_a = \Phi(a^2/C_3)$. These results agree with those obtained by Lomax in reference 18.

Electrodes for hyperbolic flow. Sketch (p) shows a segment of hyperbolic flow bounded by the curves $y = 1/x$ and $10/x$. This solution was obtained by Rosenblatt in reference 12.

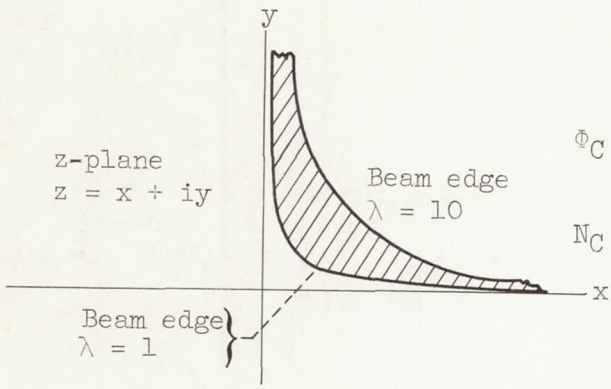

$$\Phi_C = -C_4\left[x^2 + \left(\frac{\lambda}{x}\right)^2\right]$$

$$N_C = -4C_4\lambda\left[x^2 + \left(\frac{\lambda}{x}\right)^2\right]^{-1}$$

(p)

The potential distribution along the beam edge as given in the space-charge-flow section is

$$\Phi_C = -C_4\left[x^2 + \left(\frac{\lambda}{x}\right)^2\right]$$

where

$$C_4 = 1.60\times10^4\ A^{1/3}\left(\frac{J}{\lambda\bar{l}}\right)^{2/3}$$

and

$$\lambda = 1,10$$

The solution of Laplace's equation outside the ion beam in the upper part of the first quadrant (i.e., outside the boundary $\lambda = 10$) will be obtained first. It is shown in reference 12 that a transformation that will map the beam boundary onto the real axis is:

$$\left.\begin{aligned} W &= \frac{1}{2}\left(Z^2 - 2i\lambda\right) = u + iv \\ u &= \frac{1}{2}\left(x^2 - y^2\right) \\ v &= xy - \lambda \end{aligned}\right\} \qquad (93)$$

A sketch of the transformed boundary is shown as follows:

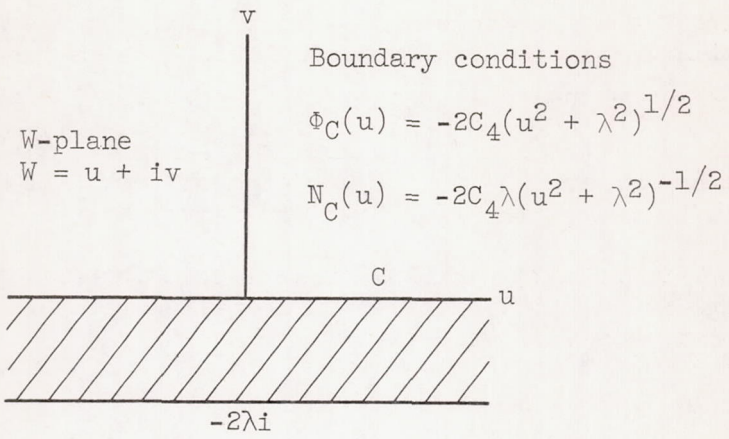

(q)

The transformed boundary conditions are also shown. Equation (67) may now be used:

$$\varphi(u,v) = \mathrm{Re}\left[-2\lambda(W^2 + \lambda^2)^{1/2}\right] + \mathrm{Im}\int_0^W \left[-2C_4\lambda(\zeta^2 + \lambda^2)^{-1/2}\right]d\zeta \qquad (94)$$

After integration and separation of the real and imaginary parts the equipotentials in the W-plane are expressed by:

$$\Phi(u,v) = -2C_4\left(\frac{1}{\sqrt{2}}\left\{\left[(u^2 + \lambda^2 - v^2)^2 + 4u^2v^2\right]^{1/2} + (u^2 + \lambda^2 - v^2)\right\}^{1/2}\right.$$

$$\left. + \lambda \tan^{-1}\frac{v + \frac{1}{\sqrt{2}}\left\{\left[(u^2 + \lambda^2 - v^2)^2 + 4u^2v^2\right]^{1/2} - (u^2 + \lambda^2 - v^2)\right\}^{1/2}}{u + \frac{1}{\sqrt{2}}\left\{\left[(u^2 + \lambda^2 - v^2)^2 + 4u^2v^2\right]^{1/2} + (u^2 + \lambda^2 - v^2)\right\}^{1/2}}\right) \qquad (95)$$

This equation may be nondimensionalized by dividing equation (95) by $-C_4\lambda$. Substitution of the values of u and v from equation (93) yields the expression for the electrode shapes in the (x,y) plane. Some of these are plotted in figure 28. Equipotentials outside the beam edge $\lambda = 1$ may be obtained by the mapping $W = \frac{1}{2}(2i\lambda - Z^2)$. The potential function is identical to equation (95) except for minus signs in front of the nonsquared u and v in the arc tangent term. Some electrode shapes for this boundary are also shown in figure 28.

Since there is no zero velocity surface in this configuration, it may not have any practical application. It may possibly be used to deflect an ion beam, however.

Limitations of the Pierce Technique

The departure of analytically derived ion accelerators from physical fact lies mainly in two areas. The first of these is that practical requirements dictate modifications in the calculated electrode shapes. These modifications manifest themselves in the curtailment of electrode size and the insertion of apertures in the electrodes to pass the ion beam. The inherent instability in the solution of elliptic differential equations with Cauchy boundary conditions on open boundaries works in reverse to minimize the error caused by curtailment or modification of electrode shapes away from the boundary. This means that, while small variations of potential along the boundary will cause increasingly larger variations the farther away from the boundary, conversely, large variations far away from the boundary cause only small variations along the boundary. This is readily observed in an electrolytic tank where a tremendously wide variety of electrode shapes will give the proper potential distribution along the beam edge to within the accuracy of the measuring equipment. It is difficult to give exact numbers for the magnitude of this effect other than to say that the error propagates away from the boundary approximately as e^{Ky}, where y is the distance measured from the boundary and K is a constant.

Aperture effect. - Insertion of apertures in the electrodes has two deleterious effects on ion accelerator performance. The first is that the aperture acts as an electrostatic lens which will tend to diverge an accelerating ion beam. If multiple electrodes are being used, this results in impingement of ions on the electrodes. Even if only one accelerating electrode is used, the formation of a diverging ion beam will result and may cause some impingement on this electrode. It is shown in reference 23 that the focal length of an aperture is

$$f = \frac{-2g\Phi}{E_b} \tag{96}$$

where $g = 1$ for slits, $g = 2$ for circular apertures, and E_b is the negative potential gradient on the upstream (or source) side of the aperture. The meaning of this is demonstrated in sketch (r).

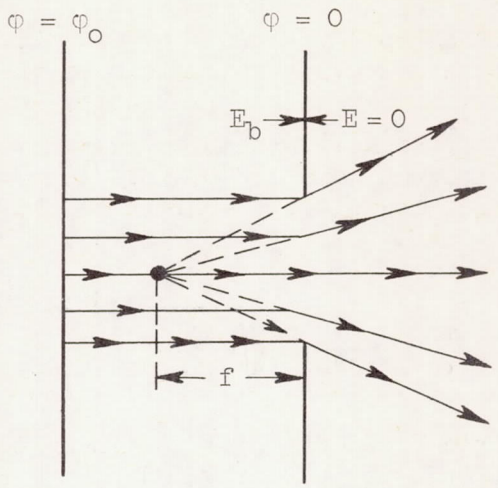

(r)

The second effect is to reduce the ion current by increasing the effective accelerating distance. Depending on the ratio of aperture width to accelerating distance, experimentally observed current densities can be a small fraction of the theoretically expected values.

Emitting surface irregularities. - The second area of departure of the Pierce theory from physical fact lies in the assumptions regarding initial conditions at the ion emitter. The usually assumed condition of zero initial velocity along a perfectly smooth equipotential surface is not met in practice, and it will be shown that considerable error can arise as a result of this. Rather than treat these effects separately, the nature of the ion trajectories in the neighborhood of a rough emitter will be investigated, and dispersion due to transverse electric fields will be compared directly with thermal spreading. In order to do this it is first necessary to examine the potential distribution near a surface irregularity. A sketch of the mathematical model is shown as follows:

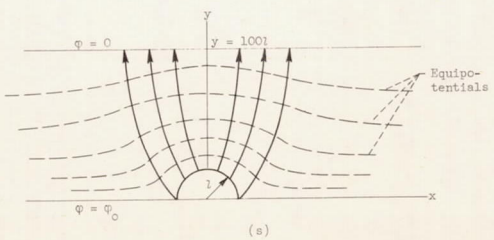

(s)

The surface irregularity is a cylindrical hump of radius l, and it is assumed that at 100 units above the hump the equipotentials are essentially plane. An approximate expression for a flux line as computed in appendix B is $(u/l) = (x/l)\left\{1 + 1/\left[(x/l)^2 + (y/l)^2\right]\right\}$. The bounding flux line, which originates at the point $x = l$, $y = 0$, is $(u/l) = 2$. This line intersects the line $y = 100l$ at $x \approx 2l$. Hence, the flux line spreading due to the electrostatic field of the hump is $\Delta x \approx l$. It is shown in appendix B that thermal spreading Δx_T at $y = 100l$, which is the product of the most probable thermal velocity and the ion transit time, can be written $\Delta x_T = 200l\sqrt{0.1/\varphi_o}$ where the effective thermal potential is assumed to be 0.1 volt. The ratio of electrostatic to thermal spreading is

$$\frac{\Delta x}{\Delta x_T} = \sqrt{\frac{\varphi_o}{4 \times 10^3}} \tag{97}$$

The macroscopic electric field strength E in an ion rocket is defined as the applied accelerating voltage divided by the accelerator spacing. For emission-limited flow E usually has a value of between 10^5 and 10^7 volts per meter. From sketch (s) it can be seen that the voltage across the model φ_o can be written $\varphi_o = E(100l)$, and the spreading ratio becomes

$$\frac{\Delta x}{\Delta x_T} = \sqrt{\frac{El}{40}} \tag{98}$$

Equation (98) is shown plotted in figure 29. It is seen from figure 29 that spreading due to the electrostatic field of a surface irregularity can be of the same order of magnitude as thermal spreading. It should be noted that this analysis is based on zero space charge and therefore is only approximate.

Analysis of accidental misalinement of parallel planar electrodes. - As pointed out by Ivey (ref. 10), an accidental misalinement of parallel planar electrodes can be analyzed as an application of the motion between two inclined planar electrodes. Consider the electrode arrangement as shown in sketch (t):

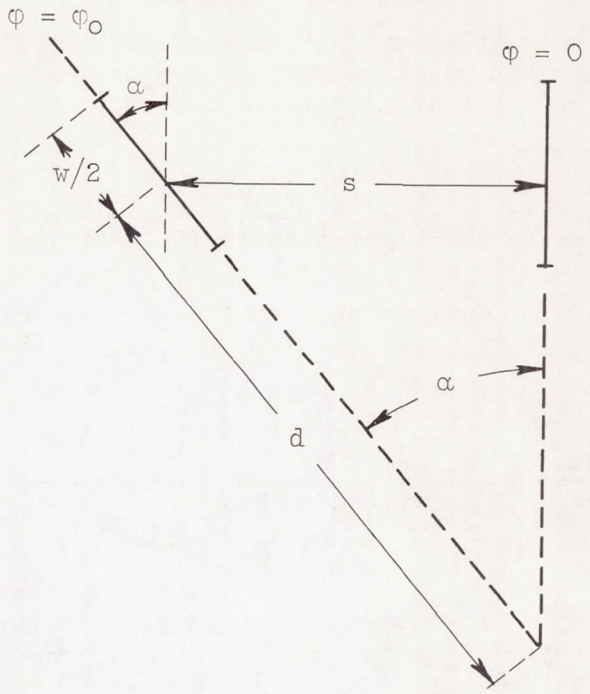

(t)

One electrode is tilted about its center by an angle α from the parallel condition and

$$d = \frac{s}{\sin \alpha}$$

The current per unit length when $\alpha = 0$ may be written

$$\frac{J_{\alpha=0}}{l} = \frac{4}{9} \epsilon_o \left(\frac{2q}{m}\right)^{1/2} \frac{\Phi^{3/2}_w}{s^2} \tag{99}$$

and thus the ratio $J/J_{\alpha=0}$, which gives the effect of the tilt, is

$$\frac{J}{J_{\alpha=0}} = \frac{H(\alpha)}{\left(\frac{1}{\sin \alpha}\right)^2 - \left(\frac{w}{2s}\right)^2} \tag{100}$$

Values from equation (100) were calculated by Ivey for small angles of α and are presented in figure 30. For a rectangular emitter with an aspect ratio of $w/s = 1.24$, the current per unit length is insensitive to the angle of tilt about a line passing through its center and parallel

to its side. Ivey also showed the independence of angular misalinement in an arbitrary direction by the use of a disk-shaped emitter. The total current for $\alpha = 0$ in this case is

$$J_{\alpha=0} = \frac{4}{9} \epsilon_0 \left(\frac{2q}{m}\right)^{1/2} \frac{\Phi^{3/2} \pi D^2}{4s^2} \tag{101}$$

where D is now the diameter of the disk, and the effect of electrode tilt becomes

$$\frac{J}{J_{\alpha=0}} = 8G(\alpha)\left(\frac{s}{D}\right)^2 \left\{ \frac{1}{\left[1 - \left(\frac{D \sin \alpha}{2s}\right)^2\right]^{1/2}} - 1 \right\} \tag{102}$$

Values from equation (102) were also calculated by Ivey and are presented in figure 31. It is seen that the variation of current for the aspect ratio $D/s = 1.42$ is zero. For this optimum geometry (aspect ratio $D/s = 1.42$) equation (101) becomes

$$J_{\alpha=0} = 6.233 \times 10^{-12} \left(\frac{2q}{m}\right)^{1/2} \Phi^{3/2} \tag{103}$$

and the behavior of $J/J_{\alpha=0}$ for the above optimum geometry is shown in figure 31. It is seen that even a large angle of tilt does not change the total current appreciably. This, of course, does not mean that the ion optics will not be affected, and in an ion rocket the ion impingement on the electrodes must be reduced to nearly zero for long-duration operation. Therefore, electrode alinement is still quite critical.

CONCLUDING REMARKS

Three methods for the analytic solution of the space-charge-flow problem appear in the literature, in which certain properties of the flow are prescribed. These are (1) initial and final equipotentials, (2) velocity and acceleration, and (3) trajectories and action function. None of these methods is generally applicable at present. Of the three methods, the trajectory-action function method appears the most versatile for the design of electrostatic rocket engine accelerators.

The existing solutions of space-charge flow have been described, and the parameters pertinent to the design of electrostatic rocket engine accelerators have been given for the following geometries: (1) paraxial

flow, (2) flow between coaxial cylinders, (3) flow between concentric spheres, (4) circular flow, (5) hyperbolic flow, (6) flow between inclined planes, and (7) flow between coaxial cones.

Electrode shapes determined by the method of Pierce have been given for the following geometries: (1) rectilinear flow with rectangular cross section, (2) paraxial flow with circular cross section, (3) convergent flow between coaxial cylinders, (4) divergent flow between coaxial cylinders, (5) circular flow, and (6) hyperbolic flow.

Limitations of the space-charge-flow and electrode design theories have been discussed. One is the aperture effect and another is the effect of irregularities on the ion emitting surface. Surface irregularities have been demonstrated to cause lateral ion velocity components of the same order of magnitude as thermal ion velocities.

Lewis Research Center
National Aeronautics and Space Administration
Cleveland, Ohio, August 20, 1962

APPENDIX A

SYMBOLS

(mks units used throughout.)

A	molecular weight/ionic charge (ionic charge may be greater than one in multiply charged ions)
a	inner radius of circular ion beam; outer radius of ion beam with circular cross section
B	$(h_2h_3/h_1)\nabla^2(1/h_1^2)$
b	outer radius of circular ion beam; inner radius of ion beam with circular cross section
C	h_2h_3/h_1^5; also ion beam edge
C_1, C_2, C_3, C_4	constants identified in text
D	diameter of disk emitter
d	$S/\sin\alpha$, for electrode tilt analysis
E	electric field strength, volts/meter
e	unit electronic charge, 1.602×10^{-19} coulomb
F_2, F_4	dimensionless functions of r/a defined in ref. 16
$F(\alpha)$	function defined in eq. (50)
$g(\theta)$	function defined in eq. (43)
g_c	gravitational conversion factor, 9.806 meters/sec^2
$H(\alpha)$	function defined in eq. (100)
h_1, h_2, h_3	scale factors in curvilinear coordinates, $ds^2 = h_1^2\, d\xi^2 + h_2^2\, d\eta^2 + h_3^2\, d\zeta^2$
Im	imaginary part
J	total current, amp

J/l	current per unit length, amp/meter
j	current density, amp/meter^2
$K(\eta,\zeta)$	$(h_2h_3/\epsilon_o)j\sqrt{m/2q}$
l	accelerator height, meters; also unit of length
m	particle mass, kg
N_C	potential gradient normal to boundary C
q	charge, coulombs
R	r/r_o, r/r_a, r/r_b
Re	real part
r	radius as in spherical and cylindrical polar coordinates
r_o	emitter radius; also initial radius of trajectory in flow between inclined planes; also inner radius in circular flow engine
S	accelerating distance for electrode tilt analysis
$s(\theta)$	function defined in eq. (52)
$\vec{ds}$	differential displacement along a trajectory
u,v	coordinates in W-plane ($W = u + iv$)
$\vec{v}$	ion velocity
v_x, v_y, v_z	velocity components in Cartesian coordinates
v_r, v_θ	velocity components in polar coordinates
$\dot{\vec{v}}$	acceleration vector
$\bar{v}$	most probable thermal velocity
W	action function, meter^3/sec; also complex number $u + iv$
w	tilt analysis
X,Y	nondimensional Cartesian coordinates

x,y,z	Cartesian coordinates
$y(\theta)$	function defined in eq. (39)
Z	$x + iy$
$\overline{Z}$	$x - iy$
α	Langmuir function for spheres; angle between inclined planes; arbitrary fixed angle
α_1,α_2	conical half-angles
β	Langmuir function for cylinders
Γ	$h_1^2\Phi$
γ	angle between ion trajectory and flux line in flow between coaxial cones
ϵ_o	permittivity of free space, 8.855×10^{-12} coulomb/(newton)(meter^2)
ζ,η	curvilinear coordinate defining trajectories
θ	angular displacement, deg
Λ	complex potential function, $\Phi + i\Psi$
λ	hyperbolic trajectory parameter
ξ	curvilinear coordinate defining action function
ρ	charge density, coulomb/meter^3
Φ	$\varphi_o - \varphi$
Φ_C	potential distribution along beam boundary
φ	angular displacement in spherical coordinates; also potential, volts
φ_o	emitter potential, volts
χ	nondimensional potential distribution

Ψ flux line

ω angle between ion trajectory and flux line for flow between coaxial cones

Superscripts:

$'$, $''$, $'''$, $''''$ differentiation with respect to variable θ

APPENDIX B

APPROXIMATE ION BEAM DISPERSION DUE TO SURFACE ROUGHNESS

In this appendix the electric field in the neighborhood of a cylindrical hump will be obtained. Following that the transit time of an ion through the diode will be calculated, and an expression for thermal spreading, which is the product of the most probable thermal velocity and the ion transit time, will be shown.

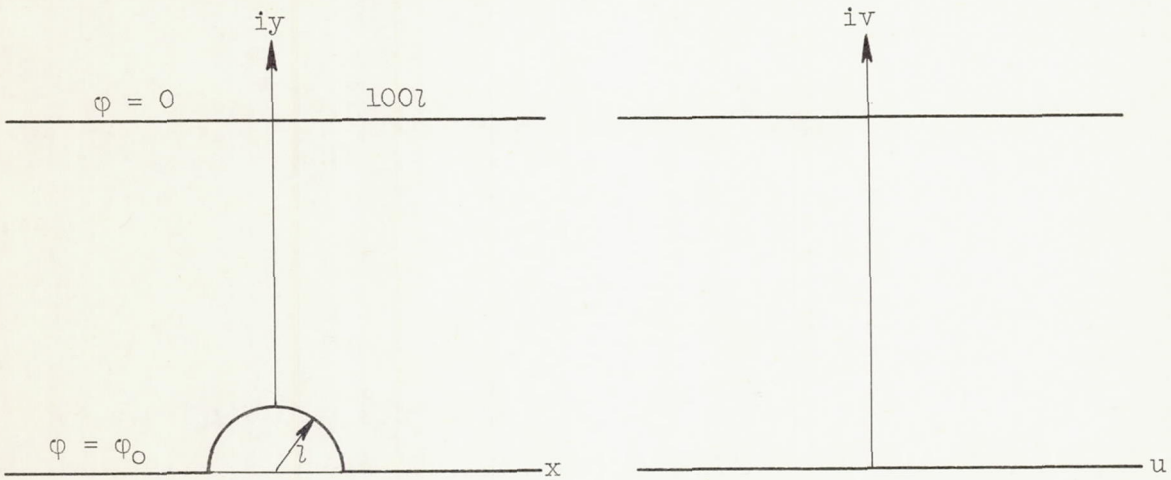

(u)

The surface is an infinite plane containing a cylindrical hump of radius l. It is assumed that at a distance $y = 100l$ the equipotential surfaces are plane. By the conformal transformation $w = z + 1/z$ the system is converted into two plane electrodes separated by a distance of $99.99\ l$. This is shown on the right side of sketch (u). The space-charge-free potential distribution in the W-plane is

$$\varphi(u,v) = \varphi_o\left(1 - \frac{v}{99.99\ l}\right) \tag{B1}$$

The electric field is obtained by differentiation of equation (B1) with respect to v:

$$E = -\frac{d\varphi}{dv} = \frac{\varphi_o}{99.99\ l} \tag{B2}$$

Returning to the right side of sketch (u) the flux lines are given by u/l = constant. From the transformation equation the expression for u/l is

$$\frac{u}{l} = \frac{x}{l}\left[1 + \frac{1}{\left(\frac{x}{l}\right)^2 + \left(\frac{y}{l}\right)^2}\right] \tag{B3}$$

This equation is used in the computation of spreading due to the electric field of a surface irregularity.

In the computation of transit time through the diode in sketch (u) (left side), it is assumed that the electric field is constant; that is,

$$E = \frac{\varphi_o}{100l} \tag{B4}$$

The equation of motion of an ion is

$$m\frac{d^2y}{dt^2} = qE = \frac{q\varphi_o}{100l} \tag{B5}$$

Integration of equation (B5) subject to the initial conditions of

$$\frac{dy}{dt} \cong 0 \qquad \text{at} \qquad t = 0$$

and

$$y = 0 \qquad \text{at} \qquad t = 0$$

yields

$$y = \frac{q\varphi_o}{200ml} t^2 \tag{B6}$$

At $y = 100l$ the transit time is

$$t = 100l\sqrt{\frac{2m}{q\varphi_o}} \tag{B7}$$

From reference 24 it is seen that the most probable thermal velocity is

$$\bar{v} = \sqrt{\frac{2q\bar{\varphi}}{m}} \tag{B8}$$

where $\bar{\varphi}$ is the mean thermal potential (usually taken to be about 0.1 volt). Thermal spreading is then the product of equations (B7) and (B8):

$$\Delta x_T = 200l\sqrt{\frac{\bar{\varphi}}{\varphi_o}} = 200l\sqrt{\frac{0.1}{\varphi_o}} \tag{B9}$$

APPENDIX C

RESCALING OF NOMOGRAMS

The nomograms shown in this report may be easily rescaled to allow computations beyond the range of one or more of the variables. Consider, for example, the nomogram in figure 1, which represents the space-charge-flow equation for a plane diode. The equation is

$$j = 5.467\times10^{-8}\, A^{-1/2}(\varphi_o - \varphi)^{3/2}x^{-2} \qquad (26)$$

The ranges of the various scales are

$$10 \leq A \leq 10^3$$

$$2 \times 10 \leq J \leq 10^3$$

$$10^{-4} \leq x \leq 10^{-2}$$

$$10^2 \leq (\varphi_o - \varphi) \leq 10^4$$

Suppose that it is desired to calculate the current density for heavier particles, say up to 10^5 amu. This means that the new range of the A scale will be from 10^3 to 10^5 amu. It is seen from equation (26) that, if $(\varphi_o - \varphi)$ and x are held constant and if A is multiplied by 10^2, then J will be divided by 10. That is, there exists a scale factor associated with A which, when multiplied by the range of J, will give the new range. In this case, $K_A = 10^{-1}$ and the new range of J will be

$$2 \leq J \leq 10^2$$

Usually it is necessary to rescale several variables simultaneously. This may be done in a similar manner. Suppose, for instance, that the desired ranges are to be changed in accordance with the following list:

$$10 \leq A \leq 10^3 \rightarrow 10^3 \leq A \leq 10^5$$

$$2 \times 10 \leq J \leq 10^3 \rightarrow \ ? \leq J \leq \ ?$$

$$10^{-4} \leq x \leq 10^{-2} \rightarrow 10^{-2} \leq x \leq 10^{0}$$

$$10^{2} \leq (\varphi_{o} - \varphi) \leq 10^{4} \rightarrow 10^{4} \leq (\varphi_{o} - \varphi) \leq 10^{6}$$

Referring again to equation (26) it is seen that scaling factors may be assigned to each variable. For instance, it was shown that the scaling factor K_A due to a hundredfold increase in A is 10^{-1}. The net scaling factor applied to J will be the products of the individual factors. These are

$$K_A = 10^{-1}$$

$$K_\chi = 10^{-4}$$

$$K_\varphi = 10^{3}$$

and finally

$$K_J = K_A K_\chi K_\varphi = 10^{-2}$$

Therefore, the new range of the J scale will be

$$2 \times 10^{-1} \leq J \leq 10$$

REFERENCES

1. Lockwood, David L., Mickelsen, William, and Hamza, Vladimir: Analytic Space-Charge Flow and Theoretical Electrostatic Rocket Engine Performance. Paper 4300-62, Am. Rocket Soc., Inc., 1962.

2. Child, C. D.: Discharge from Hot CaO. Phys. Rev., vol. 32, May 1911, pp. 492-511.

3. Langmuir, I.: The Effect of Space Charge and Residual Gases on Thermionic Currents in High Vacuum. Phys. Rev., ser. 2, vol. 2, no. 6, Dec. 1913, pp. 450-486.

4. Langmuir, I., and Blodgett, K.: Currents Limited by Space Charge Between Coaxial Cylinders. Phys. Rev., ser. 2, vol. 22, no. 4, Oct. 1923, pp. 347-356.

5. Langmuir, I., and Blodgett, K.: Currents Limited by Space Charge Between Concentric Spheres. Phys. Rev., ser. 2, vol. 24, no. 1, July 1924, pp. 49-59.

6. Spangenberg, K.: Use of the Action Function to Obtain the General Differential Equations of Space Charge Flow in More than One Dimension. Jour. Franklin Inst., vol. 232, no. 4, Oct. 1941, pp. 365-372.

7. Meltzer, B.: Electron Flow in Curved Paths Under Space-Charge Conditions. Phys. Soc. Proc., sec. B, vol. 62, no. 355, July 1949, pp. 431-437.

8. Meltzer, B.: Electron Flow in Curved Paths Under Space-Charge Conditions. Phys. Soc. Proc., sec. B, vol. 62, no. 360, Dec. 1949, pp. 813-817.

9. Walker, G. B.: Congruent Space Charge Flow. Phys. Soc. Proc., sec. B, vol. 63, 1950, pp. 1017-1027.

10. Ivey, Henry F.: Space-Charge-Limited Currents Between Inclined Plane Electrodes. Jour. Appl. Phys., vol. 23, no. 2, Feb. 1952, pp. 240-249.

11. Meltzer, B.: Single-Component Stationary Electron Flow Under Space-Charge Conditions. Jour. Electronics, vol. 2, no. 2, Sept. 1956, pp. 118-127.

12. Rosenblatt, Jorge: Three-Dimensional Space Charge Flow. Jour. Appl. Phys., vol. 31, no. 8, Aug. 1960, pp. 1371-1377.

13. Kino, G. S., and Harker, K. J.: Space-Charge Theory for Ion Beams. Paper 1382-60, Am. Rocket Soc., Inc., 1960.

14. Jaffe, G.: Zur Theorie der Hochvakummentladung. Ann. Phys., bd. 63, no. 18, 1920, pp. 145-174.

15. Brubaker, W. M.: Potential and Gradient Distributions in Parallel Plane Diodes at Currents Below Space-Charge-Limited Values. Phys. Rev., vol. 83, no. 2, July 1951, pp. 268-270.

16. Ivey, Henry F.: Cathode Field in Diodes Under Partial Space-Charge Conditions. Phys. Rev., vol. 76, no. 4, Aug. 1949, pp. 554-558.

17. Pierce, J. R.: Rectilinear Electron Flow in Beams. Jour. Appl. Phys., vol. 11, no. 8, Aug. 1940, pp. 548-554.

18. Lomax, R. J.: Exact Electrode Systems for the Formation of a Curved Space-Charge Beam. Jour. Electronics and Controls, pt. 4, vol. 3, Oct. 1957, pp. 367-374.

19. Morse, P. M., and Feshbach, H.: Methods of Theoretical Physics. Vol. 1. McGraw-Hill Book Co., Inc., 1943.

20. Daykin, P. N.: Electrode Shapes for a Cylindrical Electron Beam. British Jour. Appl. Phys., vol. 6, July 1955, pp. 248-250.

21. Harker, Kenneth J.: Determination of Electrode Shapes for Axially Symmetric Electron Guns. Jour. Appl. Phys., vol. 31, no. 12, Dec. 1960, pp. 2165-2170.

22. Radley, D. E.: The Theory of the Pierce Type Electron Gun. Jour. of Electronics and Controls, vol. 4, no. 2, Feb. 1958, pp. 125-148.

23. Harnwell, G. P.: Principles of Electricity and Electromagnetism. McGraw-Hill Book Co., Inc., 1949, pp. 252-253.

24. Kaufman, Harold R.: One-Dimensional Analysis of Ion Rockets. NASA TN D-261, 1960.

TABLE I. - SPACE-CHARGE-FLOW EQUATIONS FOR SEVERAL GEOMETRIES

Type of flow	ξ	η	ζ	h_1	h_2	h_3	B	C	$K(\eta,\zeta)$	General equation (24)
Rectilinear between plane electrodes	x	y = const.	z = const.	1	1	1	0	1	$*\frac{j}{\epsilon_o}\sqrt{\frac{m}{2q}}$	$r^{1/2}\frac{d^2r}{dx^2} = K(\eta,\zeta)$
Rectilinear between concentric cylindrical electrodes	$r = (x^2 + y^2)^{1/2}$	$\theta = \cos^{-1}\frac{x}{r}$	z = const.	1	r	1	0	r	$\frac{rj}{\epsilon_o}\sqrt{\frac{m}{2q}}$	$r^{1/2}\left[\frac{\partial}{\partial r}\left(r\frac{dr}{dr}\right)\right] = K(\eta,\zeta)$
Rectilinear between concentric spherical electrodes	$r = (x^2 + y^2 + z^2)^{1/2}$	$\theta = \cos^{-1}\frac{z}{r}$	φ = const.	1	r	r sin θ	0	r^2 sin θ	$\frac{r^2(\sin\theta)j}{\epsilon_o}\sqrt{\frac{m}{2q}}$	$r^{1/2}\left[\frac{\partial}{\partial r}\left(r^2\sin\theta\frac{dr}{dr}\right)\right] = K(\eta,\zeta)$
Circular	$\theta = \cos^{-1}\frac{x}{r}$	$r = (x^2 + y^2)^{1/2}$	z = const.	r	1	1	$4r^{-5}$	r^{-5}	$\frac{j}{\epsilon_o}\sqrt{\frac{m}{2q}}$	$**r^{1/2}\left[\frac{d^2r}{d\theta^2} + 4r\right] = K(\eta,\zeta)$
Hyperbolic	$\frac{1}{2}(x^2 - y^2)$	xy	z = const.	$\frac{1/2}{(\xi^2 + \eta^2)^{1/2}}$	$\frac{1/2}{(\xi^2 + \eta^2)^{1/2}}$	1	4	$4(\xi^2 + \eta^2)$	$\frac{j\sqrt{m/2q}}{2\epsilon_o(\xi^2 + \eta^2)^{1/2}}$	$***4r^{1/2}\left[\frac{\partial}{\partial\xi}(\xi^2+\eta^2)\left(\frac{dr}{d\xi}\right)+r\right] = K(\eta,\zeta)$

*$\sqrt{\frac{m}{2q}} = 0.7199\times10^{-4}\sqrt{A}$.

**Identical to Meltzer's equation in ref. 10.

***This equation is treated in ref. 11 and in a different fashion in ref. 6.

TABLE II. - LANGMUIR FUNCTION FOR CONCENTRIC CYLINDRICAL FLOW

r/r_o	β^2	r/r_o	β^2	r/r_o	β^2	r/r_o	β^2
0.01000	1174.9000	0.2500	6.06010	1.00	0.00000	4.0	0.6671
.01111	1018.5000	.2632	5.37950	1.01	.00010	4.2	.6902
.01250	867.1100	.2778	4.72980	1.02	.00039	4.4	.7115
.01429	721.4300	.2941	4.11260	1.04	.00149	4.6	.7313
.01667	582.1400	.3125	3.52930	1.06	.00324	4.8	.7496
.02000	450.2300	.3333	2.98140	1.08	.00557	5.0	.7666
.02500	327.0100	.3448	2.72140	1.10	.00842	5.2	.7825
.03333	214.4200	.3571	2.47080	1.15	.01747	5.4	.7973
.05000	115.6400	.3704	2.23010	1.20	.02875	5.6	.8111
.05556	97.9970	.3846	1.99950	1.30	.05589	5.8	.8241
.06250	81.2030	.4000	1.77920	1.40	.08672	6.0	.8362
.07143	65.3520	.4167	1.56970	1.50	.11934	6.5	.8635
.08333	50.5590	.4348	1.37120	1.60	.15250	7.0	.8870
.10000	36.9760	.4545	1.18400	1.70	.18540	7.5	.9074
.10530	33.7910	.4762	1.00860	1.80	.21770	8.0	.9253
.11110	30.6980	.5000	.84540	1.90	.24910	8.5	.9410
.11760	27.7010	.5263	.69470	2.00	.27930	9.0	.9548
.12500	24.8050	.5556	.55720	2.10	.30830	9.5	.9672
.13330	22.0150	.5882	.43320	2.20	.33610	10.0	.9782
.14290	19.3370	.6250	.32330	2.30	.36260	12.0	1.0122
.15380	16.7770	.6667	.22820	2.40	.38790	14.0	1.0352
.16670	14.3430	.7143	.14856	2.50	.41210	16.0	1.0513
.17240	13.4070	.7692	.08504	2.60	.43510	18.0	1.0630
.17860	12.4930	.8333	.03849	2.70	.45710	20.0	1.0715
.18520	11.6010	.8696	.02186	2.80	.47800	30.0	1.0908
.19230	10.7330	.9091	.00980	2.90	.49800	40.0	1.0946
.20000	9.8887	.9259	.00630	3.00	.51700	50.0	1.0936
.20830	9.0696	.9434	.00356	3.20	.55260	60.0	1.0910
.21740	8.2763	.9615	.00159	3.40	.58510	70.0	1.0878
.22730	7.5096	.9804	.00040	3.60	.61480	80.0	1.0845
.23810	6.7705	.9901	.00010	3.80	.64200	90.0	1.0813
		1.0000	.00000			100.0	1.0782

TABLE III. - LANGMUIR FUNCTION FOR CONCENTRIC SPHERICAL FLOW

r/r_o	α^2	r/r_o	α^2	r/r_o	α^2	r/r_o	α^2
0.01000	1144.000	0.2500	4.9680	1.00	0.0000	4.2	0.979
.01111	974.100	.2632	4.4290	1.05	.0023	4.4	1.022
.01250	813.700	.2778	3.9130	1.10	.0086	4.6	1.063
.01429	663.300	.2941	3.4210	1.15	.0180	4.8	1.103
.01667	523.600	.3125	2.9540	1.20	.0299	5.0	1.141
.02000	395.300	.3333	2.5120	1.25	.0437	5.2	1.178
.02500	279.600	.3448	2.3020	1.30	.0591	5.4	1.213
.03333	178.200	.3571	2.0980	1.35	.0756	5.6	1.247
.05000	93.240	.3704	1.9010	1.40	.0931	5.8	1.280
.05556	78.560	.3846	1.7120	1.45	.1114	6.0	1.311
.06250	64.740	.4000	1.5310	1.50	.1302	6.5	1.385
.07143	51.860	.4167	1.3580	1.60	.1688	7.0	1.453
.08333	39.980	.4348	1.1930	1.70	.2080	7.5	1.516
.10000	29.190	.4545	1.1036	1.80	.2480	8.0	1.575
.10530	26.680	.4762	.8880	1.90	.2870	8.5	1.630
.11110	24.250	.5000	.7500	2.00	.3260	9.0	1.682
.11760	21.890	.5263	.6210	2.10	.3640	9.5	1.731
.12500	19.620	.5556	.5020	2.20	.4020	10.0	1.777
.13330	17.440	.5882	.3940	2.30	.4380	12.0	1.938
.14290	15.350	.6250	.2968	2.40	.4740	14.0	2.073
.15830	13.350	.6667	.2118	2.50	.5090	16.0	2.189
.16670	11.460	.6897	.1740	2.60	.5430	18.0	2.289
.17240	10.730	.7143	.1396	2.70	.5760	20.0	2.378
.17860	10.010	.7407	.1084	2.80	.6080	30.0	2.713
.18520	9.315	.7692	.0809	2.90	.6390	40.0	2.944
.19230	8.636	.8000	.0571	3.00	.6690	50.0	3.120
.20000	7.976	.8333	.0372	3.20	.7270	60.0	3.261
.20830	7.334	.8696	.0213	3.40	.7830	70.0	3.380
.21740	6.712	.9091	.0096	3.60	.8360	80.0	3.482
.22730	6.109	.9524	.0024	3.80	.8860	90.0	3.572
.23810	5.528	1.0000	.0000	4.00	.9340	100.0	3.652

TABLE IV. - ELECTRODE COORDINATES

FOR RECTILINEAR SLAB ION BEAM

Y	X	X	X
	X = 0	X = 0.4	X = 1.0
0	0	0	1.0000
.1	.04141	.50626	1.0017
.2	.08283	.51578	1.0066
.3	.12425	.53072	1.0147
.4	.16567	.55009	1.0258
.5	.20708	.57298	1.0395
.6	.24850	.59864	1.0558
.7	.28992	.62648	1.0743
.8	.33133	.65607	1.0947
.9	.37275	.68708	1.1169
1.0	.41416	.71924	1.1406
2.0	.82833	1.07580	1.4338
3.0	1.24250	1.46010	1.7793
4.0	1.65670	1.85490	2.1477
5.0	2.07080	2.25520	2.5285
6.0	2.48500	2.65870	2.9167
7.0	2.89920	3.06440	3.3100
8.0	3.31330	3.47150	3.7067
9.0	3.72750	3.87970	4.1061
10.0	4.14160	4.28870	4.5075

TABLE V. - ELECTRODE COORDINATES FOR RECTILINEAR ION BEAM WITH CIRCULAR CROSS SECTION NEAR BEAM EDGE

R	z/a			
	X = 0	X = 0.5	X = 1.0	X = 2.0
1.00	0	0.593	1.000	1.683
1.25		.611	1.009	1.687
1.50		.649	1.033	1.702
1.75		.699	1.072	1.727
2.00		.751	1.115	1.756
2.25		.804	1.161	1.791
2.50		.852	1.211	1.830
2.75		.898	1.259	1.872
3.00		.932	1.310	1.915
3.25		.951	1.355	1.959
3.50			1.400	2.007
3.75			1.441	2.052
4.00			1.482	2.099
4.25			1.512	2.146
4.50			1.540	2.189
4.75			1.551	2.237
5.00			1.540	2.278

TABLE VI. - ELECTRODE COORDINATES FOR RECTILINEAR ION BEAM WITH CIRCULAR CROSS SECTION AWAY FROM BEAM EDGE

z/a	r/a	z/a	r/a	z/a	r/a	z/a	r/a
X = 0		X = 0.5		X = 1.0		X = 2.0	
0.2728	0.962	0.659	0.751	1.000	0		
.5456	1.924	.870	1.801	1.173	1.619	1.730	0.994
.8184	2.886	1.108	2.788	1.384	2.667	1.904	2.314
1.0910	3.848	1.356	3.767	1.611	3.660	2.104	3.400
1.3640	4.810	1.609	4.733	1.849	4.644	2.317	4.429
1.6368	5.772	1.873	5.705	2.102	5.625	2.541	5.429
1.9096	6.734	2.131	6.666	2.347	6.590	2.777	6.425
2.1824	7.697	2.393	7.633	2.599	7.564	3.010	7.409
2.4550	8.659	2.660	8.599	2.857	8.536	3.251	8.391
2.7280	9.621	2.929	9.561	3.120	9.505	3.504	9.371

TABLE VII. - INNER ELECTRODE COORDINATES

FOR HOLLOW CYLINDRICAL ION BEAM

z/b	r/b			
	X = 0	X = 0.5	X = 1.0	X = 2.0
0	[a]1.00000	[b]1.00000	[c]1.00000	[d]1.00000
.1	.57984	.94153	1.52880	4.03090
.2	.50662	1.09360	2.36070	11.00100
.3	.40454	1.10880	3.03930	22.83400
.4	.29523	1.00150	3.39730	39.09300
.5	.19691	.81254	3.35290	57.09100
.6	.12003	.59487	2.94820	72.41500
.7	.06687	.39410	2.32260	80.67000
.8	.03405	.23669	1.64540	79.51700
.9	.01584	.12904	1.05100	69.72300
1.2	.00093	.01181	.14981	24.12400
1.4	.00009	.00150	.02501	6.98090
1.6	0	.00013	.00284	1.33890
1.8	0	.00001	.00022	.17162
0	.60653	.60653	.60653	.60653
1.0	.00674	.06393	.60653	.54598
2.0	0	0	.00001	.01480
3.0	0	0	0	0
4.0				0

[a]At beam edge z/b = 0 (see fig. 24(b)).

[b]At beam edge z/b = 0.5946 (see fig. 24(b)).

[c]At beam edge z/b = 1.000 (see fig. 24(b)).

[d]At beam edge z/b = 1.6818 (see fig. 24(b)).

TABLE VIII. - ELECTRODE COORDINATES FOR CONVERGING CYLINDRICAL FLOW ($r/r_o < 1$)

Y	X	Y	X	Y	X
X = 0		X = 0.05		X = 0.1	
0.	1.4901161E-08	0.	1.0134754E-01	0.	1.6557144E-01
1.7327307E-02	7.3193461E-03	1.5676782E-02	1.0187791E-01	1.4559204E-02	1.6590387E-01
3.4403409E-02	1.4815383E-02	3.1308669E-02	1.0343715E-01	2.9092681E-02	1.6689474E-01
5.1229439E-02	2.2484176E-02	4.6855480E-02	1.0594428E-01	4.3575742E-02	1.6852541E-01
6.7806510E-02	3.0321851E-02	6.2284440E-02	1.0929112E-01	5.7985585E-02	1.7076761E-01
8.4135733E-02	3.8324289E-02	7.7570459E-02	1.1336571E-01	7.2301837E-02	1.7358633E-01
1.0021819E-01	4.6487704E-02	9.2694856E-02	1.1806747E-01	8.6506767E-02	1.7694319E-01
1.1605496E-01	5.4808304E-02	1.0764398E-01	1.2331023E-01	1.0058527E-01	1.8079878E-01
1.3164710E-01	6.3282333E-02	1.2240783E-01	1.2902313E-01	1.1452462E-01	1.8511509E-01
1.4699567E-01	7.1905963E-02	1.3697898E-01	1.3514885E-01	1.2831423E-01	1.8985595E-01
1.6210168E-01	8.0675788E-02	1.5135194E-01	1.4164060E-01	1.4194529E-01	1.9498834E-01
2.3402917E-01	1.2659134E-01	2.2012883E-01	1.7846812E-01	2.0750718E-01	2.2557276E-01
3.0004260E-01	1.7563984E-01	2.8361744E-01	2.2076759E-01	2.6841175E-01	2.6254488E-01
3.6026066E-01	2.2741862E-01	3.4176071E-01	2.6709189E-01	3.2443286E-01	3.0425158E-01
4.1479772E-01	2.8154937E-01	3.9457661E-01	3.1657337E-01	3.7548927E-01	3.4963360E-01
4.6376501E-01	3.3767502E-01	4.4211587E-01	3.6859320E-01	4.2156789E-01	3.9793874E-01
5.0727155E-01	3.9545741E-01	4.8444563E-01	4.2266027E-01	4.6269212E-01	4.4858510E-01
5.4542555E-01	4.5457456E-01	5.2164348E-01	4.7835662E-01	4.9890723E-01	5.0109286E-01
5.7833529E-01	5.1471918E-01	5.5379397E-01	5.3531178E-01	5.3027326E-01	5.5504799E-01
6.0611091E-01	5.7559668E-01	5.8098834E-01	5.9318770E-01	5.5686167E-01	6.1008136E-01
6.2886524E-01	6.3692459E-01	6.0332389E-01	6.5167089E-01	5.7875361E-01	6.6585655E-01
6.4671565E-01	6.9843165E-01	6.2090467E-01	7.1046750E-01	5.9603973E-01	7.2206221E-01
6.5978537E-01	7.5985788E-01	6.3384263E-01	7.6930026E-01	6.0881998E-01	7.7840775E-01
6.6820469E-01	8.2095520E-01	6.4225804E-01	8.2790759E-01	6.1720467E-01	8.3462061E-01
6.7211226E-01	8.8148860E-01	6.4628109E-01	8.8604332E-01	6.2131492E-01	8.9044553E-01
6.7165611E-01	9.4123783E-01	6.4605217E-01	9.4347788E-01	6.2128334E-01	9.4564487E-01
6.6699437E-01	1.0000001E 00	6.4172279E-01	1.0000001E 00	6.1725439E-01	1.0000001E 00
6.5829513E-01	1.0575935E 00	6.3345532E-01	1.0554203E 00	6.0938472E-01	1.0533144E 00
6.4573593E-01	1.1138608E 00	6.2142304E-01	1.1095738E 00	5.9784291E-01	1.1054160E 00
6.2950262E-01	1.1686749E 00	6.0580840E-01	1.1623260E 00	5.8280764E-01	1.1561630E 00
6.0978640E-01	1.2219443E 00	5.8680097E-01	1.2135783E 00	5.6446637E-01	1.2054491E 00
5.8678002E-01	1.2736202E 00	5.6459342E-01	1.2632744E 00	5.4301158E-01	1.2532106E 00
5.6067187E-01	1.3237042E 00	5.3937621E-01	1.3114092E 00	5.1863534E-01	1.2994344E 00
5.3163729E-01	1.3722567E 00	5.1132942E-01	1.3580369E 00	4.9152240E-01	1.3441679E 00
4.9982693E-01	1.4194048E 00	4.8061167E-01	1.4032813E 00	4.6183891E-01	1.3875291E 00
4.6535114E-01	1.4653514E 00	4.4734451E-01	1.4473448E 00	4.2971812E-01	1.4297184E 00

TABLE VIII. - CONTINUED. ELECTRODE COORDINATES FOR CONVERGING CYLINDRICAL FLOW ($r/r_o < 1$)

Y	X	Y	X	Y	X
X = 0.2		X = 0.4		X = 0.6	
0.	2.6515514E-01	0.	4.1059425E-01	0.	5.1765506E-01
1.2823116E-02	2.6536427E-01	1.0285877E-02	4.1072260E-01	8.4177403E-03	5.1774804E-01
2.5632195E-02	2.6599005E-01	2.0564585E-02	4.1110741E-01	1.6830868E-02	5.1802705E-01
3.8413405E-02	2.6702865E-01	3.0828995E-02	4.1174780E-01	2.5234791E-02	5.1849155E-01
5.1153300E-02	2.6847383E-01	4.1072036E-02	4.1264259E-01	3.3624927E-02	5.1914120E-01
6.3838983E-02	2.7031718E-01	5.1286758E-02	4.1378975E-01	4.1996744E-02	5.1997507E-01
7.6458250E-02	2.7254844E-01	6.1466322E-02	4.1518709E-01	5.0345736E-02	5.2099238E-01
8.8999655E-02	2.7515606E-01	7.1604072E-02	4.1683171E-01	5.8667475E-02	5.2219181E-01
1.0145261E-01	2.7812724E-01	8.1693500E-02	4.1872061E-01	6.6957579E-02	5.2357213E-01
1.1380736E-01	2.8144868E-01	9.1728344E-02	4.2085011E-01	7.5211752E-02	5.2513174E-01
1.2605502E-01	2.8510652E-01	1.0170255E-01	4.2321626E-01	8.3425789E-02	5.2686889E-01
1.8543078E-01	3.0796298E-01	1.5046891E-01	4.3844246E-01	1.2375295E-01	5.3814775E-01
2.4121209E-01	3.3727531E-01	1.9695296E-01	4.5887626E-01	1.6250279E-01	5.5352730E-01
2.9296916E-01	3.7172569E-01	2.4067456E-01	4.8387180E-01	1.9927134E-01	5.7266129E-01
3.4046437E-01	4.1029850E-01	2.8128519E-01	5.1279983E-01	2.3372754E-01	5.9517208E-01
3.8357151E-01	4.5220320E-01	3.1853940E-01	5.4507865E-01	2.6560768E-01	6.2067297E-01
4.2223080E-01	4.9680501E-01	3.5226841E-01	5.8018293E-01	2.9470601E-01	6.4878311E-01
4.5642468E-01	5.4357539E-01	3.8236013E-01	6.1763994E-01	3.2086524E-01	6.7913482E-01
4.8616425E-01	5.9205984E-01	4.0874477E-01	6.5702249E-01	3.4396825E-01	7.1137643E-01
5.1148127E-01	6.4185706E-01	4.3138507E-01	6.9794099E-01	3.6393096E-01	7.4517286E-01
5.3242416E-01	6.9260486E-01	4.5026961E-01	7.4003679E-01	3.8069745E-01	7.8020428E-01
5.4905587E-01	7.4397113E-01	4.6540889E-01	7.8297635E-01	3.9423615E-01	8.1616473E-01
5.6145254E-01	7.9564809E-01	4.7683284E-01	8.2644712E-01	4.0453754E-01	8.5276045E-01
5.6970347E-01	8.4734851E-01	4.8458929E-01	8.7015477E-01	4.1161261E-01	8.8970881E-01
5.7391128E-01	8.9880406E-01	4.8874348E-01	9.1382142E-01	4.1549208E-01	9.2673761E-01
5.7419226E-01	9.4976479E-01	4.8937808E-01	9.5718505E-01	4.1622600E-01	9.6358502E-01
5.7067636E-01	1.0000001E 00	4.8659261E-01	1.0000001E 00	4.1388389E-01	1.0000001E 00
5.6350801E-01	1.0493007E 00	4.8050415E-01	1.0420388E 00	4.0855455E-01	1.0357440E 00
5.5284489E-01	1.0974816E 00	4.7124676E-01	1.0830936E 00	4.0034621E-01	1.0705919E 00
5.3885795E-01	1.1443867E 00	4.5897142E-01	1.1229811E 00	3.8938621E-01	1.1043358E 00
5.2172913E-01	1.1898940E 00	4.4384486E-01	1.1615464E 00	3.7582074E-01	1.1367877E 00
5.0164882E-01	1.2339228E 00	4.2604782E-01	1.1986695E 00	3.5981377E-01	1.1677840E 00
4.7881162E-01	1.2764422E 00	4.0577304E-01	1.2342733E 00	3.4154598E-01	1.1971918E 00
4.5340990E-01	1.3174812E 00	3.8322098E-01	1.2683344E 00	3.2121273E-01	1.2249157E 00
4.2562461E-01	1.3571417E 00	3.5859436E-01	1.3008966E 00	2.9902162E-01	1.2509091E 00
3.9561192E-01	1.3956122E 00	3.3208930E-01	1.3320895E 00	2.7518806E-01	1.2751882E 00

TABLE VIII. - CONCLUDED. ELECTRODE COORDINATES FOR CONVERGING CYLINDRICAL FLOW ($r/r_o < 1$)

Y	X	Y	X
X = 0.8		X = 1.0	
0.	6.0113725E-01	0.	6.6808197E-01
6.9609271E-03	6.0120879E-01	5.7926631E-03	6.6813859E-01
1.3918603E-02	6.0142340E-01	1.1582931E-02	6.6830828E-01
2.0869779E-02	6.0178094E-01	1.7368407E-02	6.6859109E-01
2.7811222E-02	6.0228104E-01	2.3146702E-02	6.6898677E-01
3.4739711E-02	6.0292333E-01	2.8915439E-02	6.6949506E-01
4.1652042E-02	6.0370734E-01	3.4672235E-02	6.7011576E-01
4.8545030E-02	6.0463250E-01	4.0414739E-02	6.7084841E-01
5.5415553E-02	6.0569791E-01	4.6140609E-02	6.7169255E-01
6.2260466E-02	6.0690294E-01	5.1847492E-02	6.7264785E-01
6.9076721E-02	6.0824649E-01	5.7533106E-02	6.7371358E-01
1.0262334E-01	6.1700452E-01	8.5562512E-02	6.8067639E-01
1.3501944E-01	6.2903718E-01	1.1272692E-01	6.9028537E-01
1.6594096E-01	6.4413850E-01	1.3876833E-01	7.0241039E-01
1.9510403E-01	6.6206996E-01	1.6345069E-01	7.1689513E-01
2.2226539E-01	6.8257217E-01	1.8656168E-01	7.3356234E-01
2.4722046E-01	7.0537417E-01	2.0791291E-01	7.5221908E-01
2.6979982E-01	7.3020023E-01	2.2733941E-01	7.7266063E-01
2.8986560E-01	7.5677392E-01	2.4469884E-01	7.9467334E-01
3.0730811E-01	7.8482060E-01	2.5987023E-01	8.1803695E-01
3.2204290E-01	8.1406850E-01	2.7275310E-01	8.4252597E-01
3.3400864E-01	8.4424926E-01	2.8326694E-01	8.6791050E-01
3.4316571E-01	8.7509794E-01	2.9135070E-01	8.9395707E-01
3.4949506E-01	9.0635314E-01	2.9696273E-01	9.2042912E-01
3.5299808E-01	9.3775697E-01	3.0008121E-01	9.4708763E-01
3.5369632E-01	9.6905564E-01	3.0070402E-01	9.7369186E-01
3.5163151E-01	1.0000001E 00	2.9884966E-01	1.0000001E 00
3.4686594E-01	1.0303469E 00	2.9455707E-01	1.0257705E 00
3.3948213E-01	1.0598599E 00	2.8788637E-01	1.0507622E 00
3.2958314E-01	1.0883116E 00	2.7891851E-01	1.0747361E 00
3.1729210E-01	1.1154850E 00	2.6775547E-01	1.0974551E 00
3.0275180E-01	1.1411756E 00	2.5451967E-01	1.1186845E 00
2.8612359E-01	1.1651936E 00	2.3935304E-01	1.1381906E 00
2.6758647E-01	1.1873662E 00	2.2241644E-01	1.1557378E 00
2.4733526E-01	1.2075390E 00	2.0388784E-01	1.1710823E 00
2.2557906E-01	1.2255792E 00	1.8396113E-01	1.1839612E 00

TABLE IX. - ELECTRODE COORDINATES FOR DIVERGING CYLINDRICAL FLOW ($r/r_o > 1$)

Y	X	Y	X	Y	X
X = 0		X = 0.2		X = 0.4	
0.	-7.4505806E-09	0.	3.3672364E-01	0.	6.1308981E-01
1.7579666E-02	7.1382374E-03	2.3334026E-02	3.3680530E-01	2.8156436E-02	6.1308096E-01
3.5412857E-02	1.4091402E-02	4.6690750E-02	3.3704796E-01	5.6329107E-02	6.1305435E-01
5.3500735E-02	2.0854697E-02	7.0092498E-02	3.3744437E-01	8.4534138E-02	6.1300728E-01
7.1844539E-02	2.7424648E-02	9.3560911E-02	3.3798319E-01	1.1278749E-01	6.1293600E-01
9.0445459E-02	3.3796206E-02	1.1711662E-01	3.3864893E-01	1.4110482E-01	6.1283527E-01
1.0930475E-01	3.9965063E-02	1.4077909E-01	3.3942334E-01	1.6950149E-01	6.1269876E-01
1.2842366E-01	4.5926630E-02	1.6456644E-01	3.4028590E-01	1.9799242E-01	6.1251867E-01
1.4780346E-01	5.1676139E-02	1.8849541E-01	3.4121434E-01	2.2659205E-01	6.1228603E-01
1.6744551E-01	5.7209179E-02	2.1258137E-01	3.4218574E-01	2.5531434E-01	6.1199106E-01
1.8735106E-01	6.2520504E-02	2.3683830E-01	3.4317659E-01	2.8417275E-01	6.1162354E-01
2.9088010E-01	8.5579171E-02	3.6109524E-01	3.4762563E-01	4.3093650E-01	6.0827674E-01
4.0121142E-01	1.0231915E-01	4.9112276E-01	3.4934852E-01	5.8280022E-01	6.0123022E-01
5.1854261E-01	1.1201806E-01	6.2773326E-01	3.4617814E-01	7.4087051E-01	5.8880171E-01
6.4309365E-01	1.1387070E-01	7.7152793E-01	3.3632539E-01	9.0604094E-01	5.6930873E-01
7.7511073E-01	1.0697266E-01	9.2301402E-01	3.1820042E-01	1.0790749E 00	5.4107837E-01
9.1486998E-01	9.0299398E-02	1.0826651E 00	2.9026981E-01	1.2606677E 00	5.0240499E-01
1.0626813E 00	6.2681124E-02	1.2509553E 00	2.5095502E-01	1.4514924E 00	4.5149205E-01
1.2188907E 00	2.2770494E-02	1.4283786E 00	1.9855171E-01	1.6522315E 00	3.8638656E-01
1.3838814E 00	-3.0996077E-02	1.6154616E 00	1.3115807E-01	1.8635987E 00	3.0490550E-01
1.5580718E 00	-1.0044712E-01	1.8127676E 00	4.6601564E-02	2.0863557E 00	2.0455766E-01
1.7419094E 00	-1.8773461E-01	2.0209011E 00	-5.7638660E-02	2.3213259E 00	8.2451626E-02
1.9358589E 00	-2.9540533E-01	2.2405012E 00	-1.8452465E-01	2.5694041E 00	-6.4813845E-02
2.1403832E 00	-4.2648645E-01	2.4722355E 00	-3.3756696E-01	2.8315707E 00	-2.4128343E-01
2.3559130E 00	-5.8458941E-01	2.7167856E 00	-5.2095791E-01	3.1089087E 00	-4.5181609E-01
2.5828076E 00	-7.7403412E-01	2.9748363E 00	-7.3973613E-01	3.4026390E 00	-7.0230833E-01
2.8213036E 00	-1.0000006E 00	3.2470645E 00	-1.0000007E 00	3.7141906E 00	-1.0000008E 00
3.0714571E 00	-1.2687183E 00	3.5341515E 00	-1.3091990E 00	4.0453506E 00	-1.3539232E 00
3.3330855E 00	-1.5877137E 00	3.8368448E 00	-1.6765402E 00	4.3985717E 00	-1.7755879E 00
3.6057347E 00	-1.9661546E 00	4.1561400E 00	-2.1136354E 00	4.7776297E 00	-2.2801633E 00
3.8887087E 00	-2.4153753E 00	4.4937255E 00	-2.6355836E 00	5.1890756E 00	-2.8886706E 00
4.1812666E 00	-2.9497579E 00	4.8530455E 00	-3.2630137E 00	5.6457168E 00	-3.6326426E 00
4.4832159E 00	-3.5883874E 00	5.2419587E 00	-4.0264481E 00	6.1762113E 00	-4.5658393E 00
4.7965171E 00	-4.3585593E 00	5.6802182E 00	-4.9773338E 00	6.8593919E 00	-5.8030006E 00
5.1298906E 00	-5.3044917E 00	6.2265034E 00	-6.2246597E 00		
5.5149460E 00	-6.5149492E 00				

TABLE IX. - CONTINUED. ELECTRODE COORDINATES FOR DIVERGING CYLINDRICAL FLOW ($r/r_o > 1$)

Y	X	Y	X	Y	X
X = 0.6		X = 0.67825		X = 0.8	
0.	8.8981370E-01	0.	1.0000058E 00	0.	1.1743571E 00
3.2985843E-02	8.8975743E-01	3.4908992E-02	9.9993455E-01	3.7951939E-02	1.1742649E 00
6.5985871E-02	8.8958788E-01	6.9831797E-02	9.9972075E-01	7.5917358E-02	1.1739884E 00
9.9014231E-02	8.8930384E-01	1.0478216E-01	9.9936248E-01	1.1390967E-01	1.1735258E 00
1.3208498E-01	8.8890299E-01	1.3977382E-01	9.9885848E-01	1.5194231E-01	1.1728760E 00
1.6521205E-01	8.8838217E-01	1.7482034E-01	9.9820534E-01	1.9002859E-01	1.1720365E 00
1.9840921E-01	8.8773733E-01	2.0993522E-01	9.9739990E-01	2.2818174E-01	1.1710039E 00
2.3169004E-01	8.8696369E-01	2.4513177E-01	9.9643780E-01	2.6641490E-01	1.1697749E 00
2.6506783E-01	8.8605536E-01	2.8042310E-01	9.9531379E-01	3.0474097E-01	1.1683443E 00
2.9855577E-01	8.8500668E-01	3.1582220E-01	9.9402261E-01	3.4317285E-01	1.1667078E 00
3.3216655E-01	8.8380989E-01	3.5134164E-01	9.9255724E-01	3.8172317E-01	1.1648594E 00
5.0249035E-01	8.7531930E-01	5.3117205E-01	9.8236085E-01	5.7668148E-01	1.1522043E 00
6.7762592E-01	8.6176167E-01	7.1576786E-01	9.6655575E-01	7.7638677E-01	1.1331048E 00
8.5882140E-01	8.4174818E-01	9.0642015E-01	9.4382402E-01	9.8219366E-01	1.1063208E 00
1.0471626E 00	8.1373854E-01	1.1042771E 00	9.1266372E-01	1.1953417E 00	1.0703923E 00
1.2436208E 00	7.7607423E-01	1.3103836E 00	8.7142142E-01	1.4169867E 00	1.0236664E 00
1.4491020E 00	7.2697217E-01	1.5257256E 00	8.1828870E-01	1.6482389E 00	9.6429423E-01
1.6644896E 00	6.6448924E-01	1.7512717E 00	7.5127129E-01	1.8902038E 00	8.9020342E-01
1.8906810E 00	5.8646935E-01	1.9880102E 00	6.6813828E-01	2.1440212E 00	7.9904696E-01
2.1286179E 00	4.9047390E-01	2.2369844E 00	5.6635293E-01	2.4109060E 00	6.8813410E-01
2.3793153E 00	3.7369794E-01	2.4993252E 00	4.4298564E-01	2.6921904E 00	5.5433637E-01
2.6438909E 00	2.3286609E-01	2.7762878E 00	2.9460378E-01	2.9893748E 00	3.9396785E-01
2.9235959E 00	6.4101368E-02	3.0692970E 00	1.1713217E-01	3.3041949E 00	2.0262799E-01
3.2198635E 00	-1.3724078E-01	3.3800088E 00	-9.4329997E-02	3.6387179E 00	-2.5009155E-02
3.5343781E 00	-3.7679445E-01	3.7104117E 00	-3.4575500E-01	3.9954974E 00	-2.9548675E-01
3.8691927E 00	-6.6149026E-01	4.0629897E 00	-6.4453526E-01	4.3778323E 00	-6.1699017E-01
4.2269456E 00	-1.0000009E 00	4.4410203E 00	-1.0000009E 00	4.7902319E 00	-1.0000010E 00
4.6112645E 00	-1.4034344E 00	4.8491306E 00	-1.4242450E 00	5.2392960E 00	-1.4583801E 00
5.0275726E 00	-1.8864979E 00	5.2944126E 00	-1.9335490E 00	5.7355018E 00	-2.0113251E 00
5.4847822E 00	-2.4696444E 00	5.7888023E 00	-2.5511064E 00	6.2971761E 00	-2.6873249E 00
5.9992197E 00	-3.1835391E 00	6.3547701E 00	-3.3129490E 00	6.9606043E 00	-3.5334548E 00
6.6050682E 00	-4.0799958E 00	7.0414249E 00	-4.2834724E 00	7.8122556E 00	-4.6429169E 00
7.3900613E 00	-5.2666563E 00	7.9866989E 00	-5.6111254E 00		
8.7077599E 00	-7.0972426E 00				

TABLE IX. - CONCLUDED. ELECTRODE COORDINATES FOR DIVERGING CYLINDRICAL FLOW ($r/r_o > 1$)

Y	X	Y	X	Y	X
X = 1.0		X = 1.5		X = 2.0	
0.	1.4695159E 00	0.	2.2609916E 00	0.	3.1333990E 00
4.3103422E-02	1.4693931E 00	5.6917496E-02	2.2608008E 00	7.2144340E-02	3.1331460E 00
8.6220226E-02	1.4690239E 00	1.1384969E-01	2.2602280E 00	1.4430612E-01	3.1323860E 00
1.2936380E-01	1.4684080E 00	1.7081126E-01	2.2592726E 00	2.1650280E-01	3.1311191E 00
1.7254747E-01	1.4675435E 00	2.2781690E-01	2.2579330E 00	2.8875186E-01	3.1293434E 00
2.1578455E-01	1.4664284E 00	2.8488127E-01	2.2562073E 00	3.6107073E-01	3.1270568E 00
2.5908829E-01	1.4650601E 00	3.4201905E-01	2.2540934E 00	4.3347694E-01	3.1242570E 00
3.0247179E-01	1.4634347E 00	3.9924485E-01	2.2515879E 00	5.0598798E-01	3.1209409E 00
3.4594821E-01	1.4615491E 00	4.5657336E-01	2.2486878E 00	5.7862142E-01	3.1171048E 00
3.8953051E-01	1.4593985E 00	5.1401907E-01	2.2453883E 00	6.5139486E-01	3.1127447E 00
4.3323155E-01	1.4569779E 00	5.7159666E-01	2.2416853E 00	7.2432590E-01	3.1078557E 00
6.5396060E-01	1.4406139E 00	8.6197140E-01	2.2169207E 00	1.0919652E 00	3.0752689E 00
8.7951779E-01	1.4164550E 00	1.1578182E 00	2.1810791E 00	1.4662235E 00	3.0284154E 00
1.1113659E 00	1.3833315E 00	1.4609435E 00	2.1330031E 00	1.8493993E 00	2.9660491E 00
1.3508922E 00	1.3398136E 00	1.7731655E 00	2.0712122E 00	2.2438950E 00	2.8865396E 00
1.5994346E 00	1.2842290E 00	2.0963447E 00	1.9938900E 00	2.6522758E 00	2.7878418E 00
1.8583150E 00	1.2146531E 00	2.4324308E 00	1.8988577E 00	3.0773492E 00	2.6674413E 00
2.1288799E 00	1.1288795E 00	2.7835219E 00	1.7835213E 00	3.5222776E 00	2.5222769E 00
2.4125475E 00	1.0243673E 00	3.1519463E 00	1.6447964E 00	3.9907363E 00	2.3486246E 00
2.7108584E 00	8.9816294E-01	3.5403725E 00	1.4789948E 00	4.4871411E 00	2.1419291E 00
3.0255391E 00	7.4679531E-01	3.9519627E 00	1.2816660E 00	5.0169928E 00	1.8965613E 00
3.3585833E 00	5.6613253E-01	4.3906007E 00	1.0473700E 00	5.5874133E 00	1.6054527E 00
3.7123697E 00	3.5119139E-01	4.8612435E 00	7.6934704E-01	6.2080304E 00	1.2595371E 00
4.0898345E 00	9.5867082E-02	5.3704993E 00	4.3901993E-01	6.8925108E 00	8.4684141E-01
4.4947588E 00	-2.0745360E-01	5.9276203E 00	4.5198262E-02	7.6614143E 00	3.5091260E-01
4.9322571E 00	-5.6848438E-01	6.5463442E 00	-4.2727039E-01	8.5479789E 00	-2.5215045E-01
5.4096707E 00	-1.0000011E 00	7.2485798E 00	-1.0000015E 00	9.6113002E 00	-1.0000020E 00
5.9383136E 00	-1.5195364E 00	8.0726312E 00	-1.7062655E 00	1.0971956E 01	-1.9599242E 00
6.5371969E 00	-2.1526857E 00	9.0947183E 00	-2.6036464E 00		
7.2420303E 00	-2.9404981E 00	1.0501963E 01	-3.8139954E 00		
8.1316562E 00	-3.9596832E 00				
9.4393312E 00	-5.4016352E 00				

TABLE X. - OUTER ELECTRODE COORDINATES FOR CIRCULAR FLOW ION BEAM

θ	R	θ	R	θ	R	θ	R	θ	R	θ	R	θ	R	θ	R
χ = 0				χ = 0.16494				χ = 0.39685		χ = 0.62996		χ = 0.82549		χ = 0.95483	
0	1.4286	29.794	2.7774	10.000	1.4286	35.783	2.3843	20.000	1.4286	30.000	1.4286	40.000	1.4286	50.000	1.4286
.57296	1.4629	30.940	2.8126	10.573	1.4758	36.929	2.4089	20.573	1.4527	30.573	1.4426	41.146	1.4445	51.146	1.4358
1.14590	1.4967	32.086	2.8464	11.719	1.5508	38.075	2.4323	21.719	1.4978	31.146	1.4563	42.292	1.4594	52.292	1.4421
1.71890	1.5302	33.232	2.8790	12.865	1.6141	39.221	2.4546	22.865	1.5395	32.292	1.4825	44.011	1.4799	53.438	1.4475
2.29180	1.5633	34.377	2.9103	14.011	1.6712	40.367	2.4756	24.011	1.5785	33.438	1.5072	45.730	1.4981	55.157	1.4540
3.43770	1.6284	35.523	2.9403	15.157	1.7243	41.513	2.4955	25.157	1.6153	34.584	1.5306	47.448	1.5142	56.875	1.4585
4.58370	1.6921	36.669	2.9689	16.303	1.7744	42.659	2.5142	26.303	1.6500	35.730	1.5527	49.167	1.5281	58.594	1.4611
5.72960	1.7544	37.815	2.9963	17.448	1.8221	43.805	2.5318	27.448	1.6830	36.875	1.5735	50.886	1.5400	59.740	1.4618
6.87550	1.8154	38.961	3.0223	18.594	1.8678	44.950	2.5481	28.594	1.7144	38.021	1.5932	52.605	1.5497		
8.02140	1.8751	40.107	3.0470	19.740	1.9118	46.096	2.5632	29.740	1.7443	39.167	1.6118	54.324	1.5574		
9.16730	1.9335	41.253	3.0703	20.886	1.9541	47.242	2.5772	30.886	1.7728	40.313	1.6293	56.043	1.5631		
10.31300	1.9907	42.399	3.0923	22.032	1.9949	48.388	2.5900	32.032	1.7999	41.459	1.6456	57.762	1.5667		
11.45900	2.0467	43.545	3.1129	23.178	2.0343	49.534	2.6015	33.178	1.8258	42.605	1.6610	59.481	1.5684		
12.60500	2.1014	44.691	3.1322	24.324	2.0723	50.680	2.6119	34.324	1.8505	43.751	1.6752				
13.75100	2.1550	45.837	3.1501	25.470	2.1091	51.826	2.6211	35.470	1.8740	44.897	1.6885				
14.89700	2.2073	46.983	3.1666	26.616	2.1445	52.972	2.6290	36.616	1.8963	46.043	1.7008				
16.04300	2.2585	48.128	3.1818	27.762	2.1787	54.118	2.6358	37.762	1.9175	47.189	1.7120				
17.18900	2.3084	49.274	3.1956	28.908	2.2117	55.264	2.6414	38.908	1.9376	48.335	1.7223				
18.33500	2.3572	50.420	3.2080	30.054	2.2434	56.410	2.6458	40.054	1.9565	49.481	1.7316				
19.48100	2.4047	51.566	3.2190	31.199	2.2740	57.555	2.6489	41.199	1.9744	50.626	1.7399				
20.62600	2.4510	52.712	3.2286	32.345	2.3033	58.701	2.6509	42.345	1.9912	51.772	1.7473				
21.77200	2.4962	53.858	3.2368	33.491	2.3315	59.847	2.6517	43.491	2.0068	52.918	1.7537				
22.91800	2.5400	55.004	3.2436	34.637	2.3585			44.637	2.0215	54.064	1.7591				
24.06400	2.5827	56.150	3.2490					45.783	2.0350	55.210	1.7636				
25.21000	2.6242	57.296	3.2530					46.929	2.0475	56.356	1.7671				
26.35600	2.6643	58.442	3.2556					48.075	2.0590	57.502	1.7696				
27.50200	2.7033	59.588	3.2569					49.221	2.0693	58.648	1.7712				
28.64800	2.7410							50.367	2.0787	59.794	1.7719				
								51.513	2.0869						
								52.659	2.0942						
								53.805	2.1003						
								54.950	2.1055						
								56.096	2.1096						
								57.242	2.1126						
								58.388	2.1146						
								59.534	2.1155						

TABLE XI. - INNER ELECTRODE COORDINATES FOR CIRCULAR FLOW ION BEAM

R	θ								
	$\chi = 0$	$\chi = 0.16494$	$\chi = 0.39685$	$\chi = 0.62996$	$\chi = 0.82549$	$\chi = 0.95483$	$\chi = 1.0$	$\chi = 1.2856$	$\chi = 2.0408$
0	15.00000	15.0000	15.000	15.000	15.000	15.000	15.000	15.000	15.000
.02	14.99000	14.9910	14.993	14.994	14.996	14.997	14.997	14.999	15.004
.05	14.93800	14.9460	14.956	14.966	14.975	14.981	14.983	14.995	15.028
.10	14.76000	14.7900	14.831	14.872	14.906	14.929	14.937	14.988	15.120
.15	14.47600	14.5410	14.634	14.727	14.805	14.856	14.874	14.988	15.285
.20	14.09400	14.2110	14.375	14.541	14.679	14.771	14.803	15.005	15.534
.25	13.62400	13.8070	14.065	14.324	14.541	14.684	14.734	15.051	15.878
.30	13.07400	13.3390	13.711	14.085	14.398	14.606	14.678	15.136	16.330
.35	12.45200	12.8150	13.324	13.835	14.263	14.546	14.645	15.270	16.903
.40	11.76500	12.2420	12.911	13.582	14.145	14.517	14.646	15.467	17.612
.45	11.01800	11.6280	12.482	13.339	14.056	14.529	14.695	15.740	18.475
.50	10.21700	10.9800	12.047	13.115	14.008	14.597	14.803	16.104	19.513
.52	9.88320	10.7130	11.874	13.034	14.003	14.643	14.867	16.279	19.983
.55	9.36760	10.3060	11.616	12.923	14.015	14.736	14.987	16.577	20.752
.57	9.01480	10.0310	11.447	12.859	14.037	14.815	15.086	16.801	21.311
.60	8.47260	9.6135	11.200	12.779	14.094	14.962	15.265	17.179	22.224
.62	8.10270	9.3331	11.041	12.738	14.151	15.082	15.407	17.462	22.886
.65	7.53590	8.9108	10.813	12.698	14.266	15.298	15.658	17.935	23.967
.67	7.15020	8.6292	10.670	12.689	14.365	15.469	15.853	18.287	24.750
.70	6.56040	8.2087	10.473	12.704	14.552	15.768	16.192	18.872	26.027
.72	6.15990	7.9311	10.355	12.736	14.705	16.000	16.451	19.304	26.954
.75	5.54860	7.5213	10.203	12.822	14.982	16.400	16.894	20.021	28.466
.77	5.13420	7.2548	10.121	12.908	15.201	16.706	17.230	20.547	29.564
.80	4.50240	6.8692	10.034	13.087	15.588	17.226	17.797	21.413	31.364
.82	4.07470	6.6251	10.004	13.242	15.887	17.618	18.221	22.044	32.678
.85	3.42350	6.2858	10.009	13.536	16.402	18.277	18.930	23.078	34.851
.87	2.98300	6.0837	10.052	13.776	16.793	18.766	19.453	23.826	36.459
.90	2.31290	5.8311	10.185	14.208	17.454	19.576	20.316	25.043	39.176
.92	1.86010	5.7081	10.325	14.546	17.945	20.169	20.945	25.920	41.254
.95	1.17160	5.6178	10.621	15.131	18.758	21.138	21.970	27.338	44.981
.97	.70657	5.6381	10.878	15.572	19.352	21.837	22.709	28.356	48.159
1.00	0	5.8124	11.352	16.310	20.318	22.968	23.900	30.000	58.000

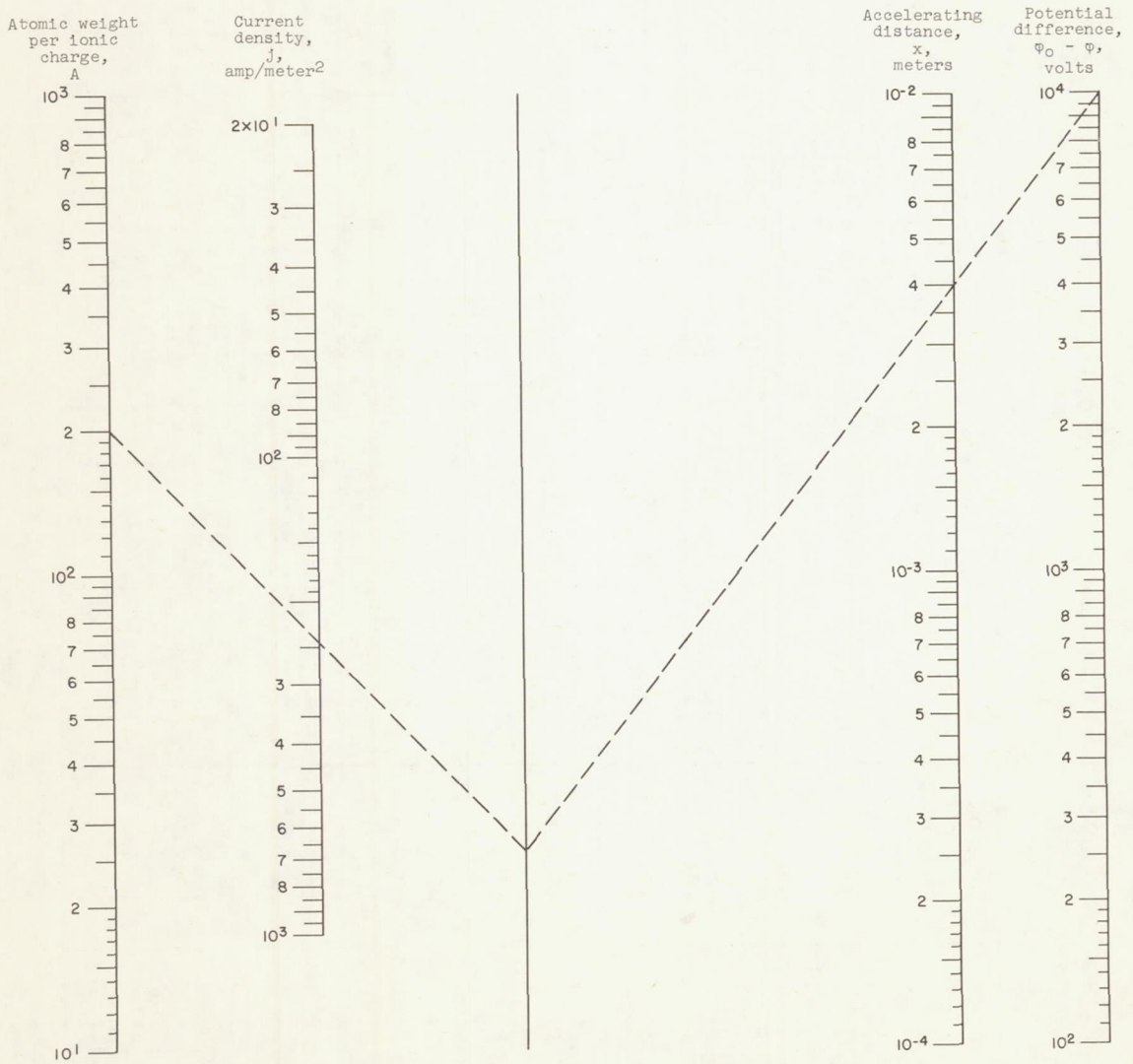

Figure 1. - Space-charge-limited flow between infinite plane electrodes. $j = 5.467\times10^{-8}A^{-1/2}(\varphi_o - \varphi)^{3/2}x^{-2}$. (See appendix C for rescaling.)

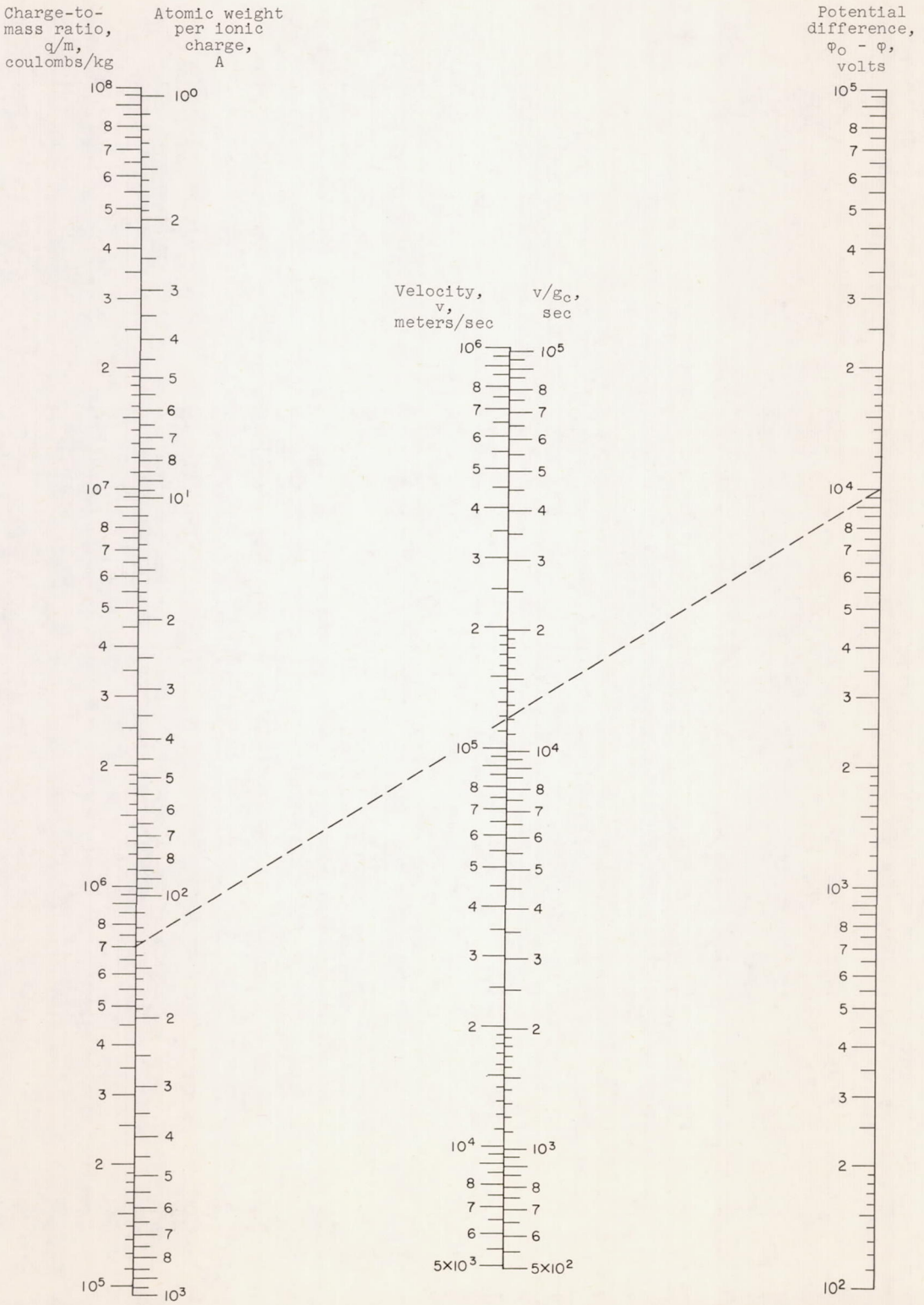

Figure 2. - Nomographic solution of $\frac{1}{2} mv^2 = q(\varphi_o - \varphi)$. (See appendix C for rescaling.)

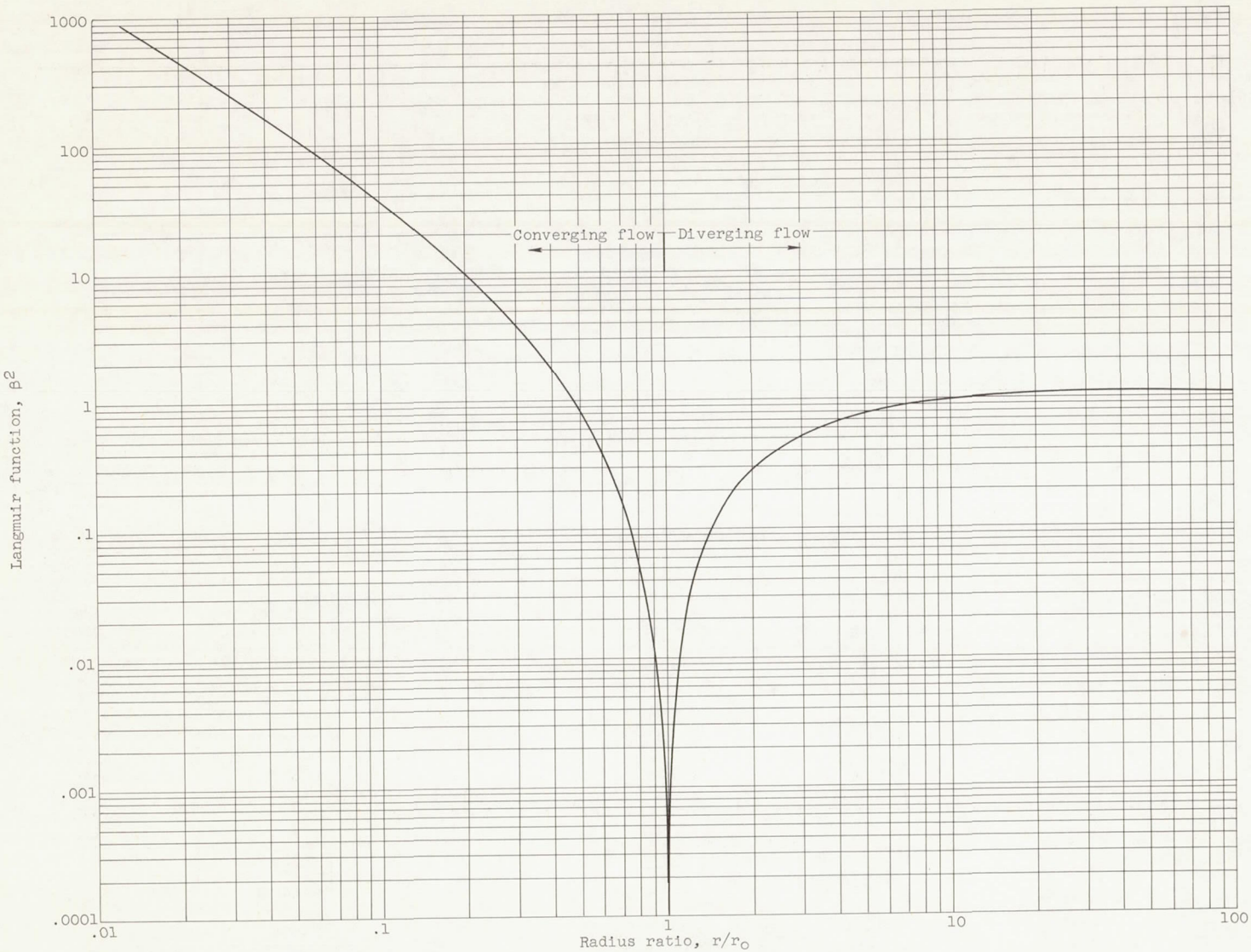

Figure 3. - Langmuir function for flow between coaxial cylinders.

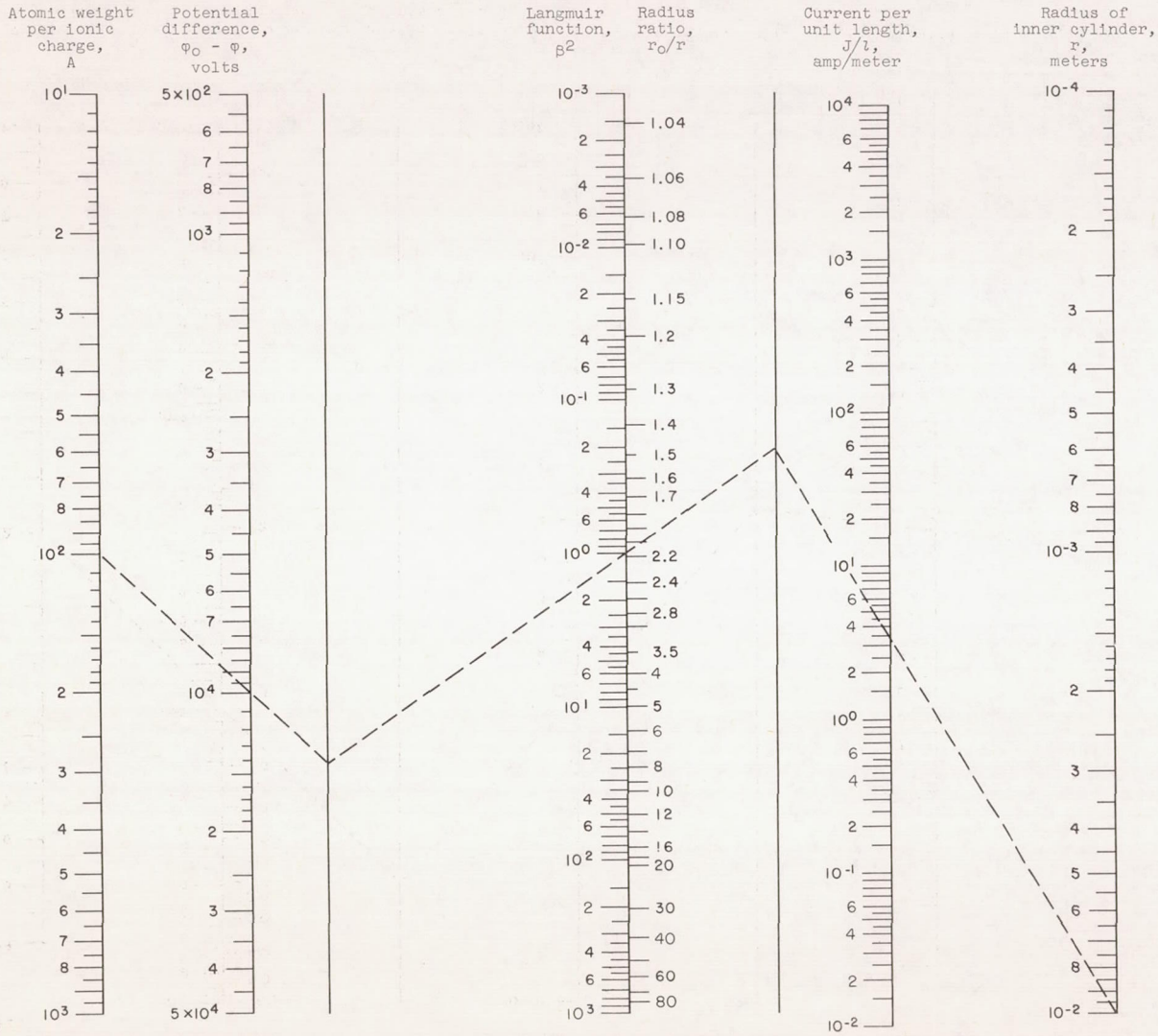

Figure 4. - Converging flow between coaxial cylinders. $J/l = 3.43 \times 10^{-7} A^{-1/2} (\varphi_o - \varphi)^{3/2} (r\beta^2)^{-1}$ for $r < r_o$; note that $j = (J/l)/2\pi r$. (See appendix C for rescaling.)

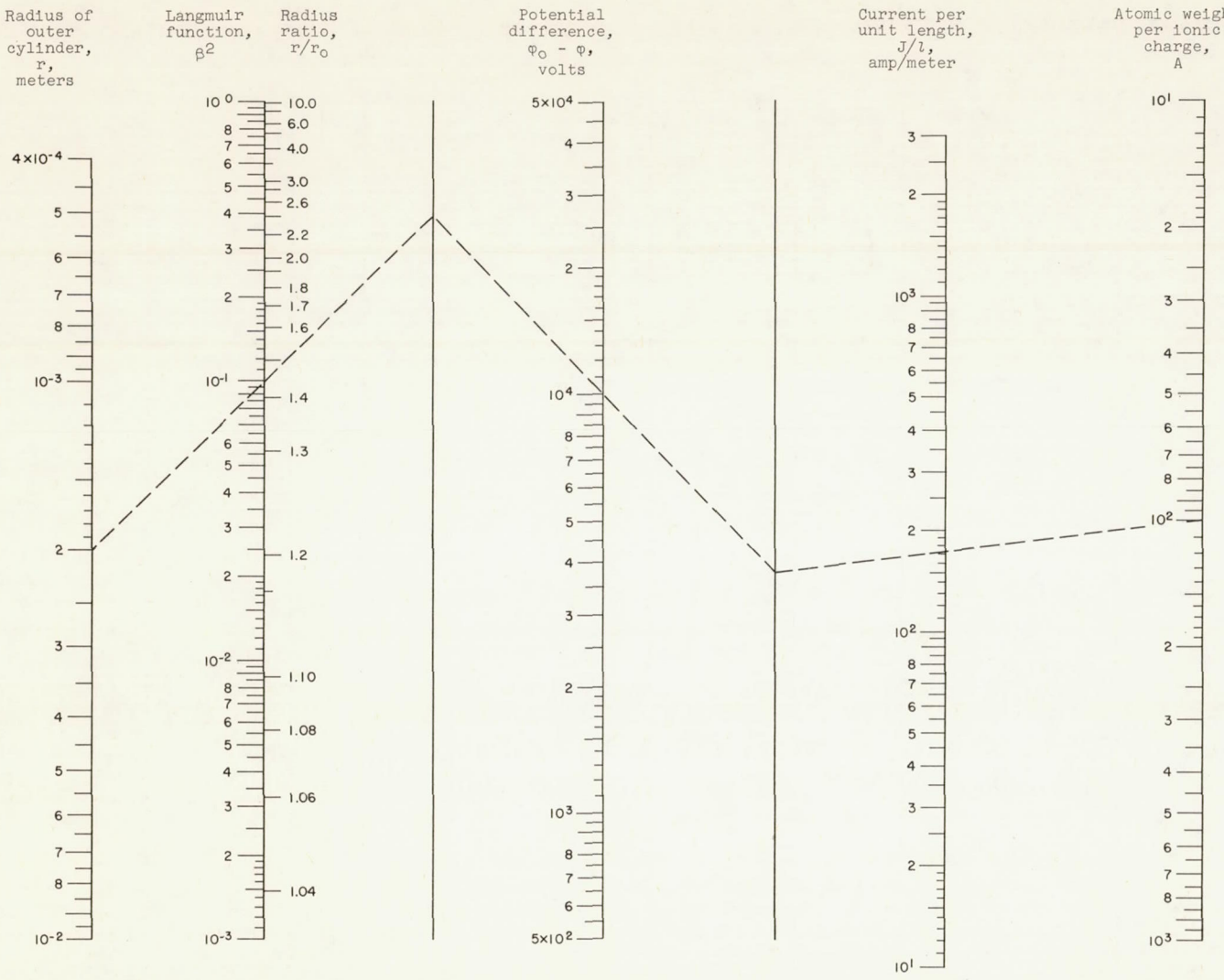

Figure 5. - Diverging flow between coaxial cylinders. $J/l = 3.43\times10^{-7}A^{-1/2}(\varphi_o - \varphi)^{3/2}(r\beta^2)^{-1}$ for $r > r_o$; note that $j = (J/l)/2\pi r$. (See appendix C for rescaling.)

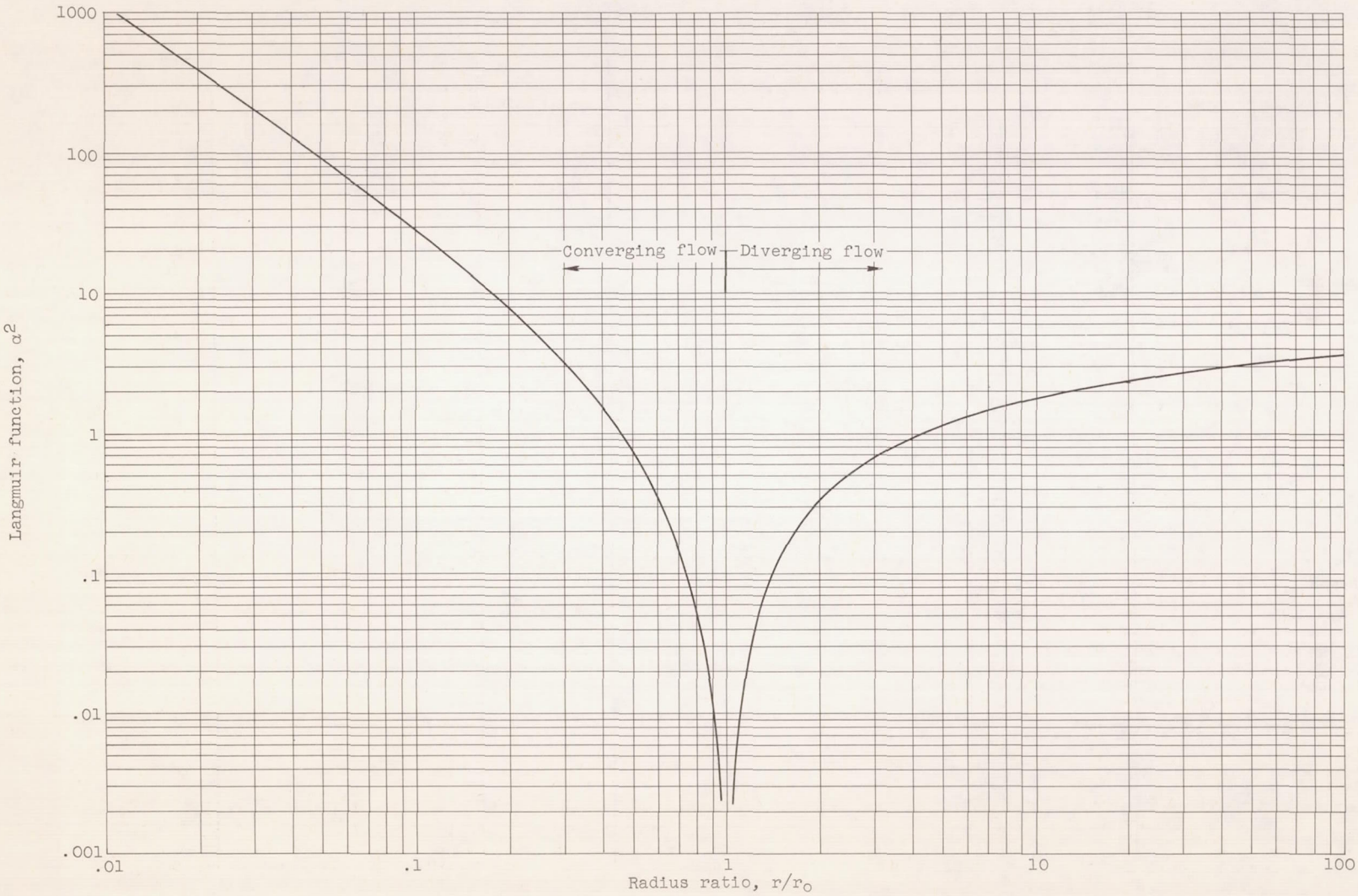

Figure 6. - Langmuir function for flow between concentric spheres.

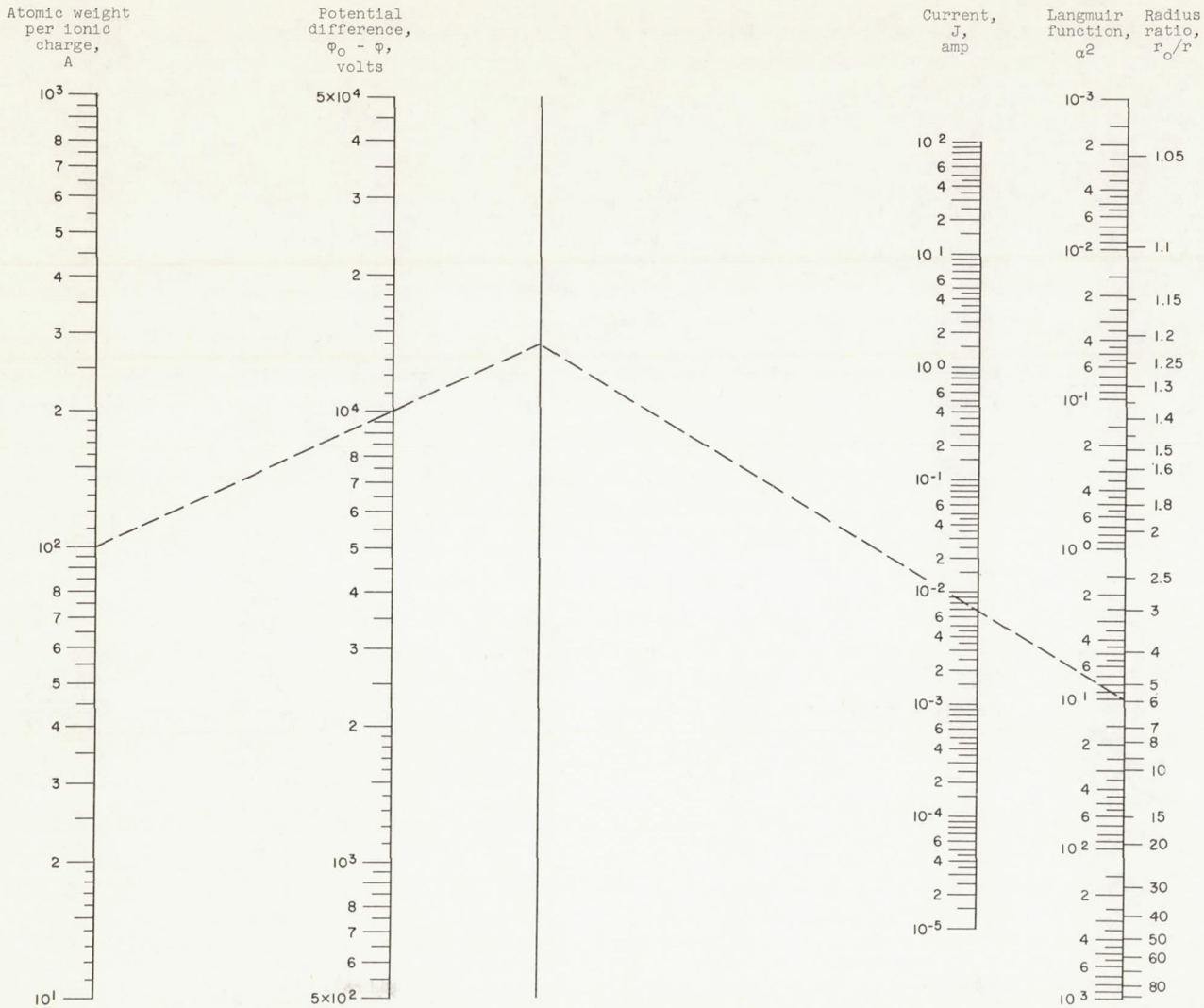

Figure 7. - Converging flow between concentric spheres. $J = 6.87\times10^{-7}A^{-1/2}(\varphi_o - \varphi)^{3/2}\alpha^{-2}$ for $r < r_o$; note that $j = J/4\pi r^2$. (See appendix C for rescaling.)

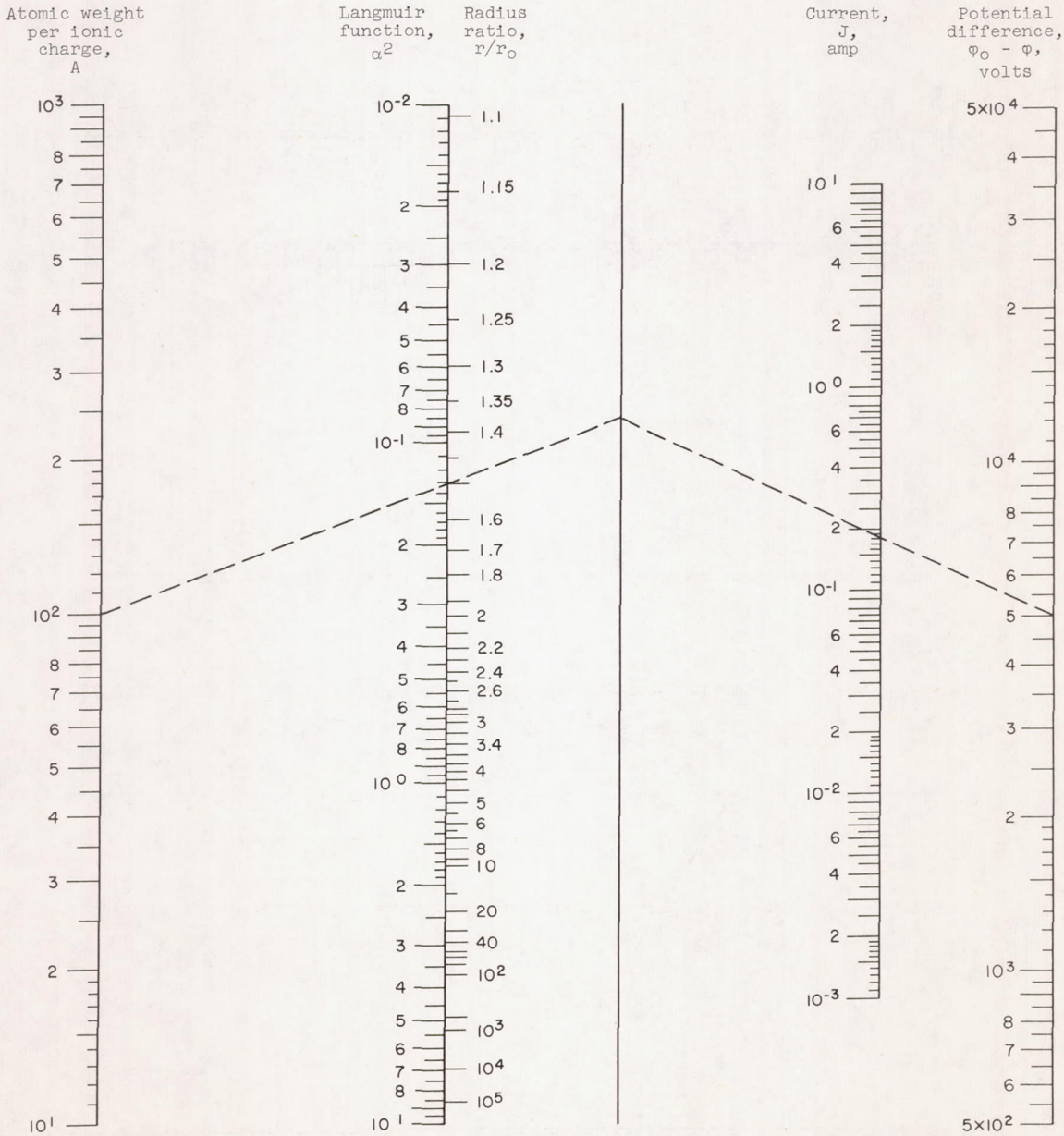

Figure 8. - Diverging flow between concentric spheres. $J = 6.87\times10^{-7}A^{-1/2}(\varphi_o - \varphi)^{3/2}\alpha^{-2}$ for $r > r_o$; note that $j = J/4\pi r^2$. (See appendix C for rescaling.)

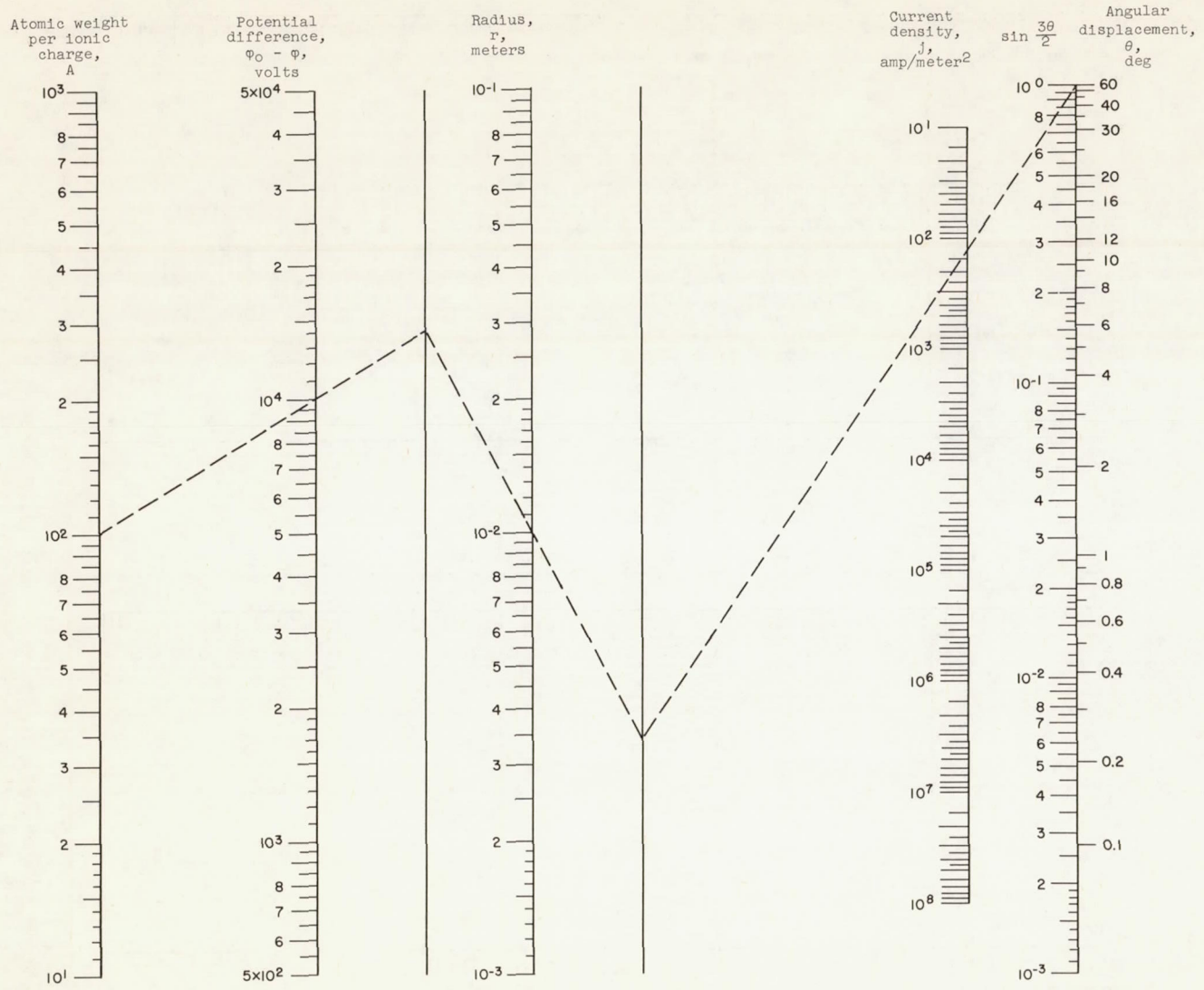

Figure 9. - Circular flow. $j = 1.23\times10^{-7}A^{-1/2}(\varphi_o - \varphi)^{3/2}\left(r \sin \frac{3\theta}{2}\right)^{-2}$. (See appendix C for rescaling.)

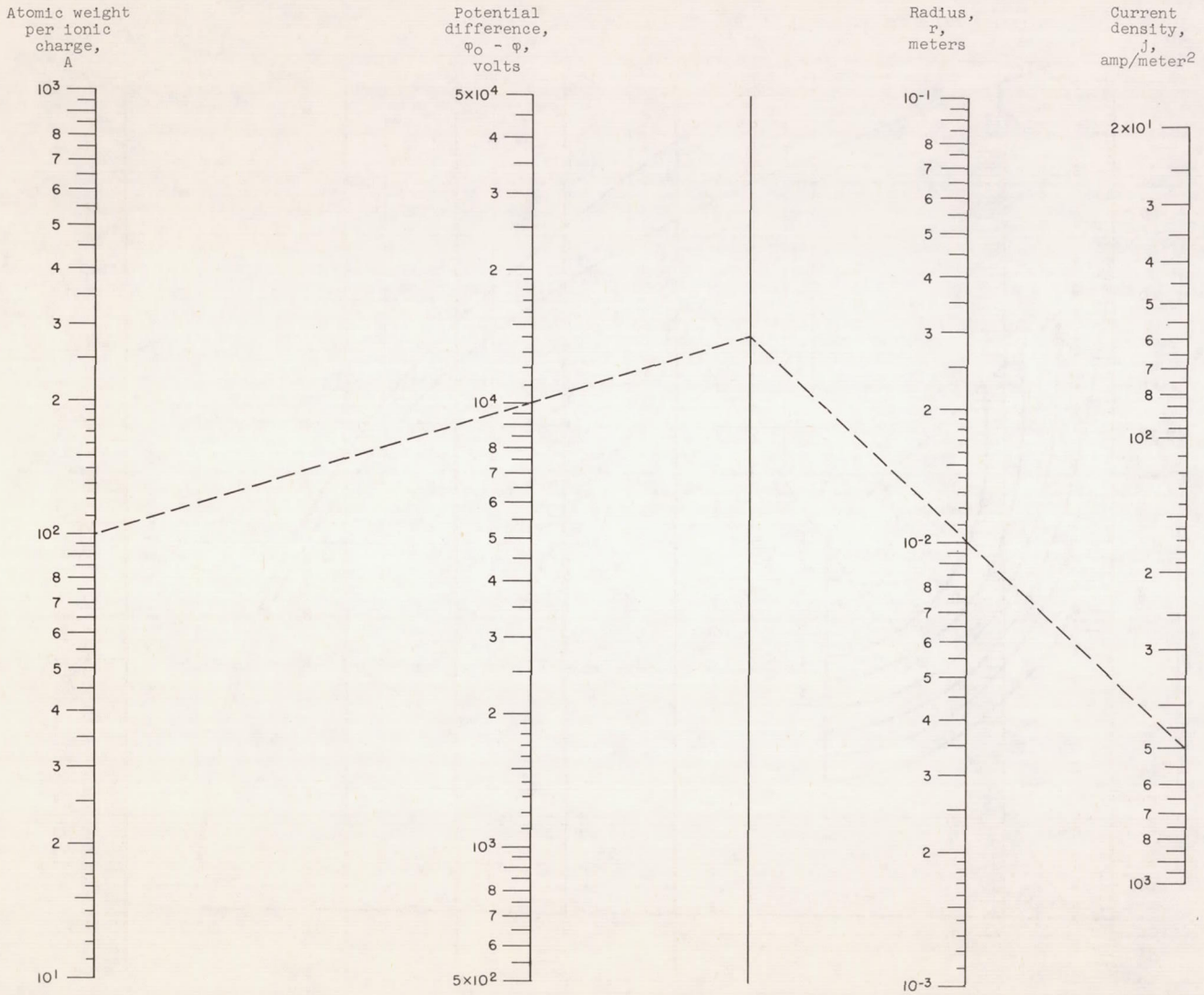

Figure 10. - Hyperbolic flow. $j = 4.92\times10^{-7}A^{-1/2}(\varphi_o - \varphi)^{3/2}r^{-2}$. (See appendix C for rescaling.)

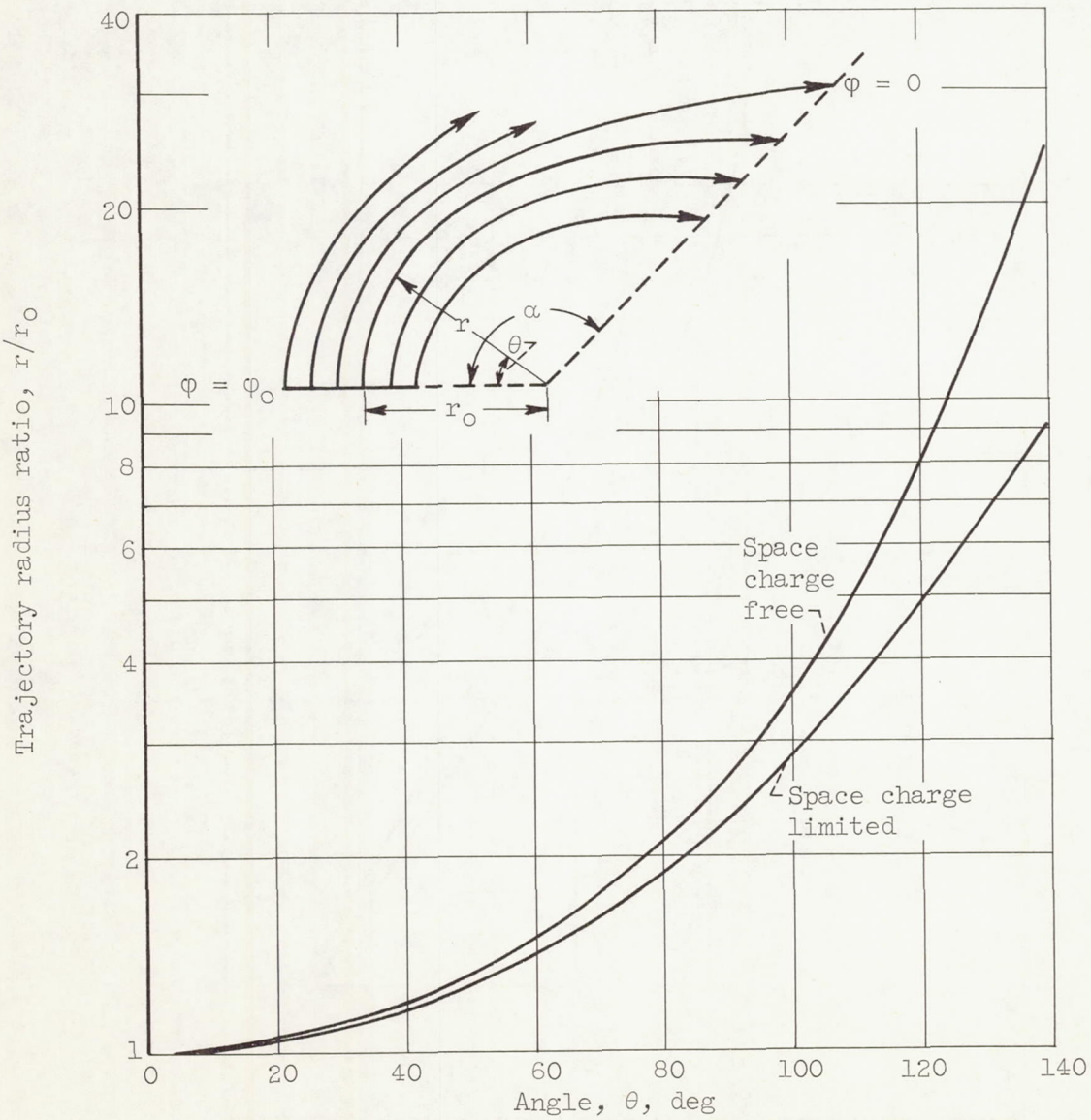

Figure 11. - General trajectory plot for flow between inclined planes (eqs. (41) and (48)).

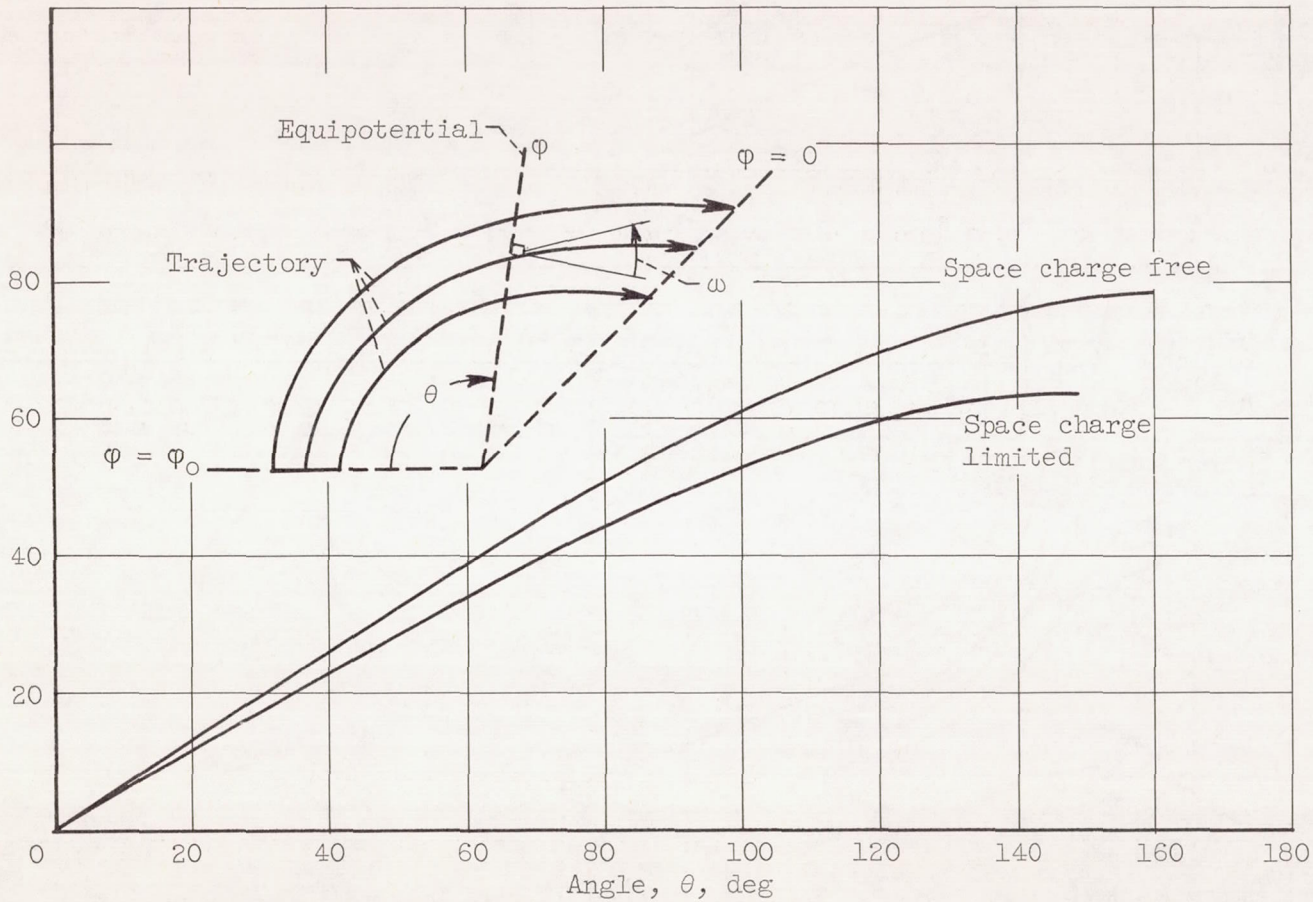

Figure 12. - Angle between trajectories and normals to equipotentials for inclined planes (eqs. (42) and (49)).

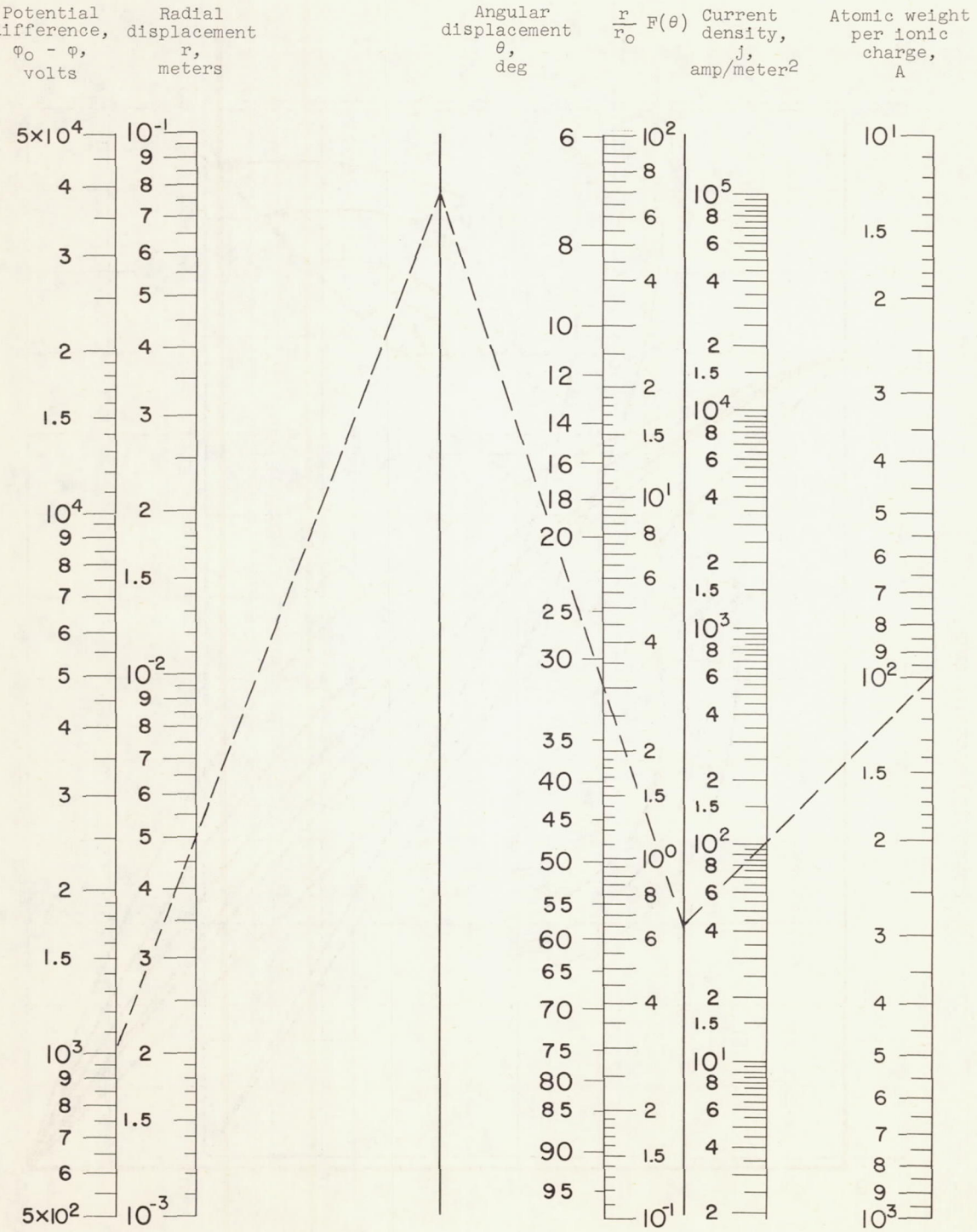

Figure 13. - Space-charge-limited flow between inclined planes.
$j = 5.467 \times 10^{-8} A^{-1/2} (\varphi_o - \varphi)^{3/2} r^{-2} \left[\frac{r}{r_o} F(\theta)\right]$.
(See appendix C for rescaling.)

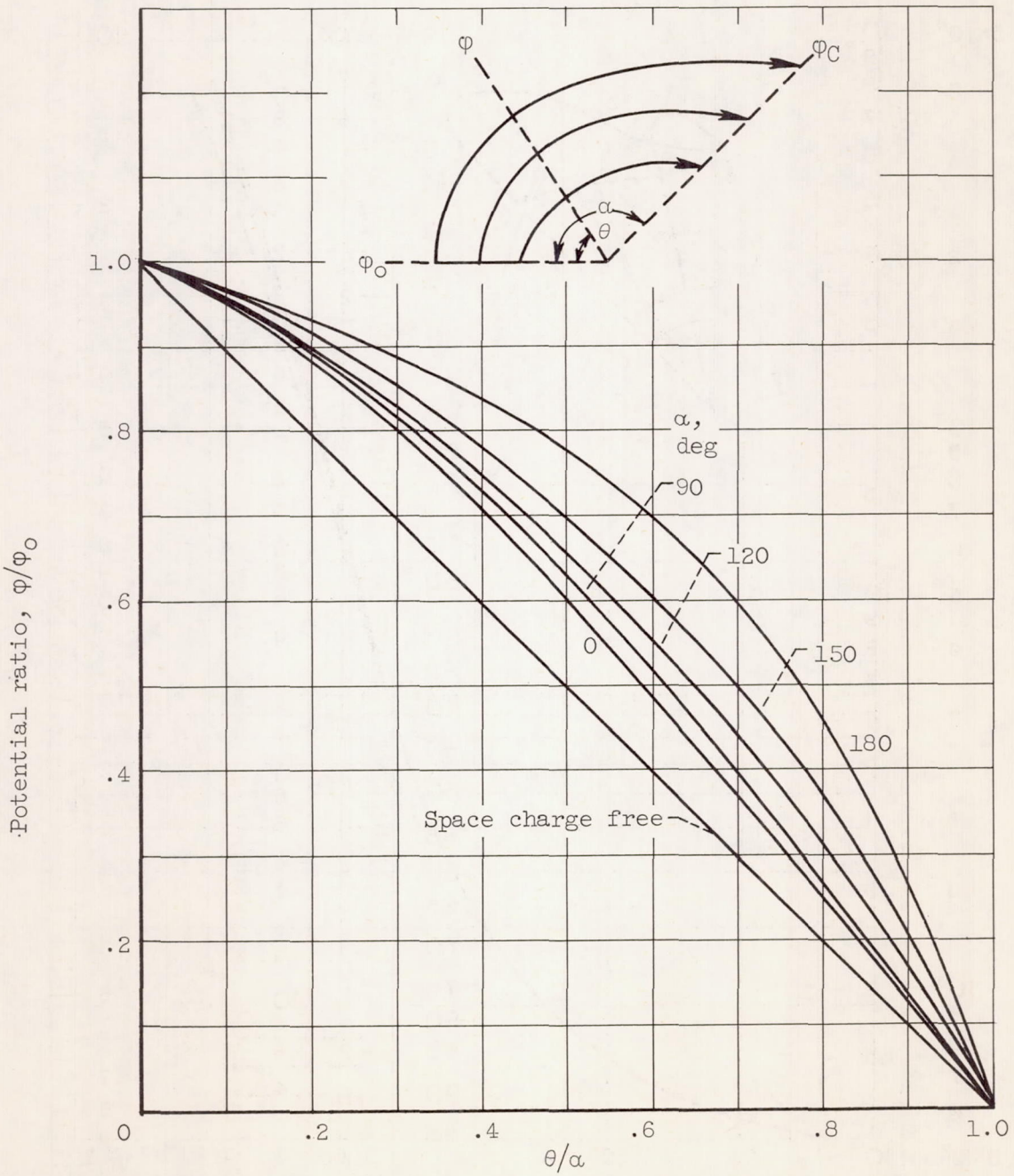

Figure 14. - Potential distribution between inclined plane electrodes (space-charge limited).

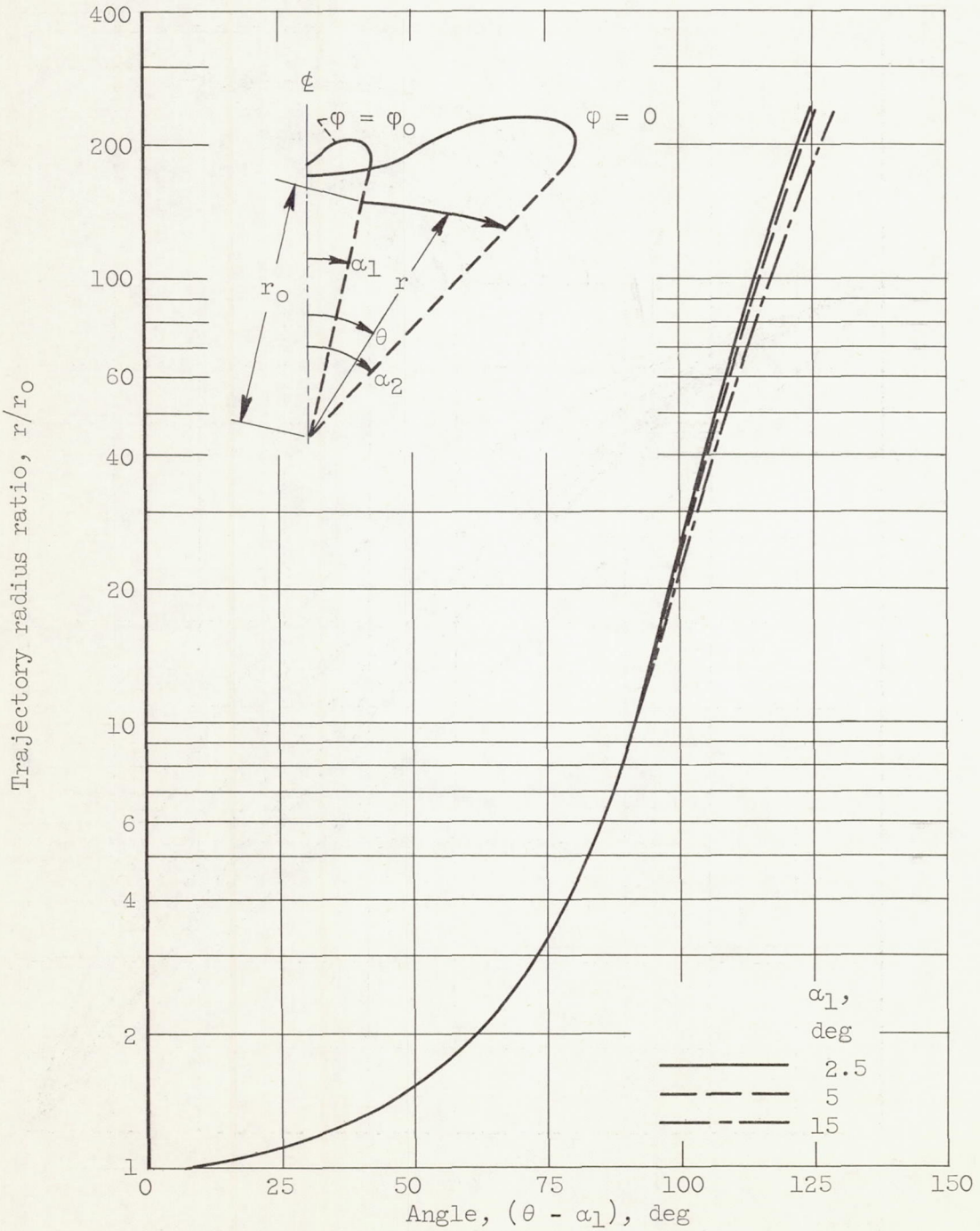

Figure 15. - General trajectory plot for flow between coaxial right circular cones (eq. (59)).

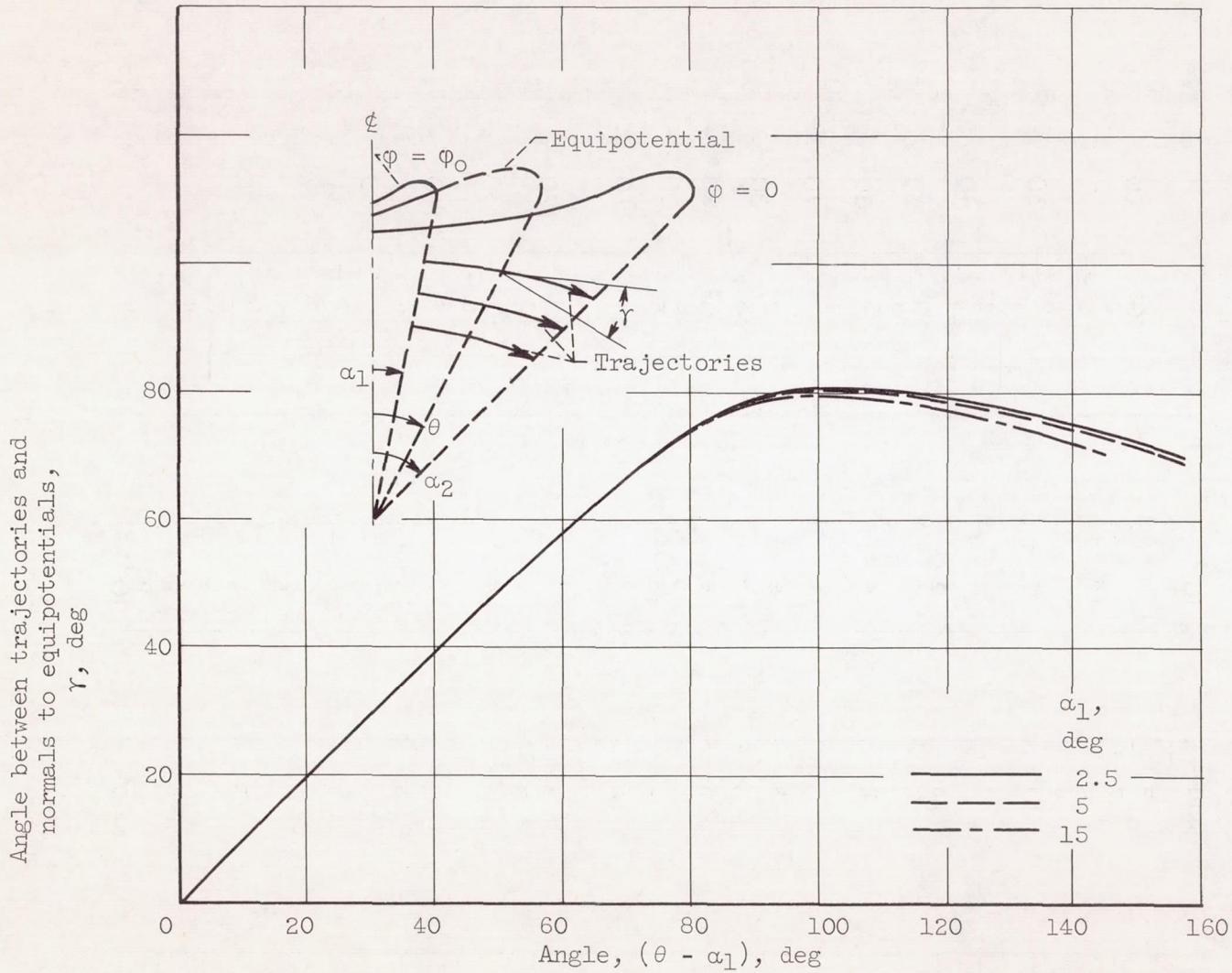

Figure 16. - Angle between trajectories and normals to equipotentials for coaxial right circular conical electrodes (eq. (60)).

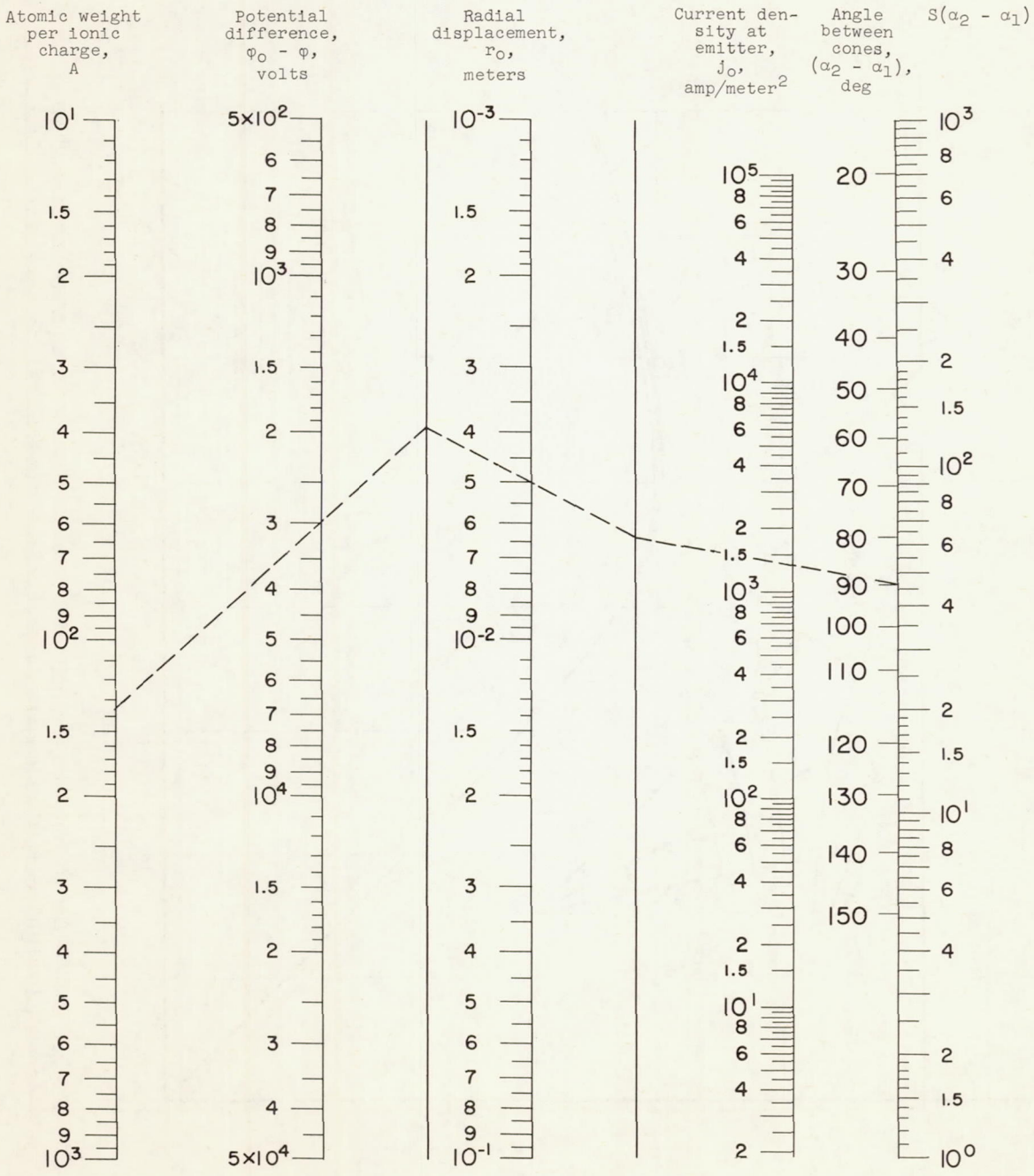

Figure 17. - Space-charge-limited flow between coaxial cones.
$j_o = 5.467 \times 10^{-8} A^{-1/2} (\varphi_o - \varphi)^{3/2} r_o^{-2} S(\alpha_2 - \alpha_1)$.
(See appendix C for rescaling.)

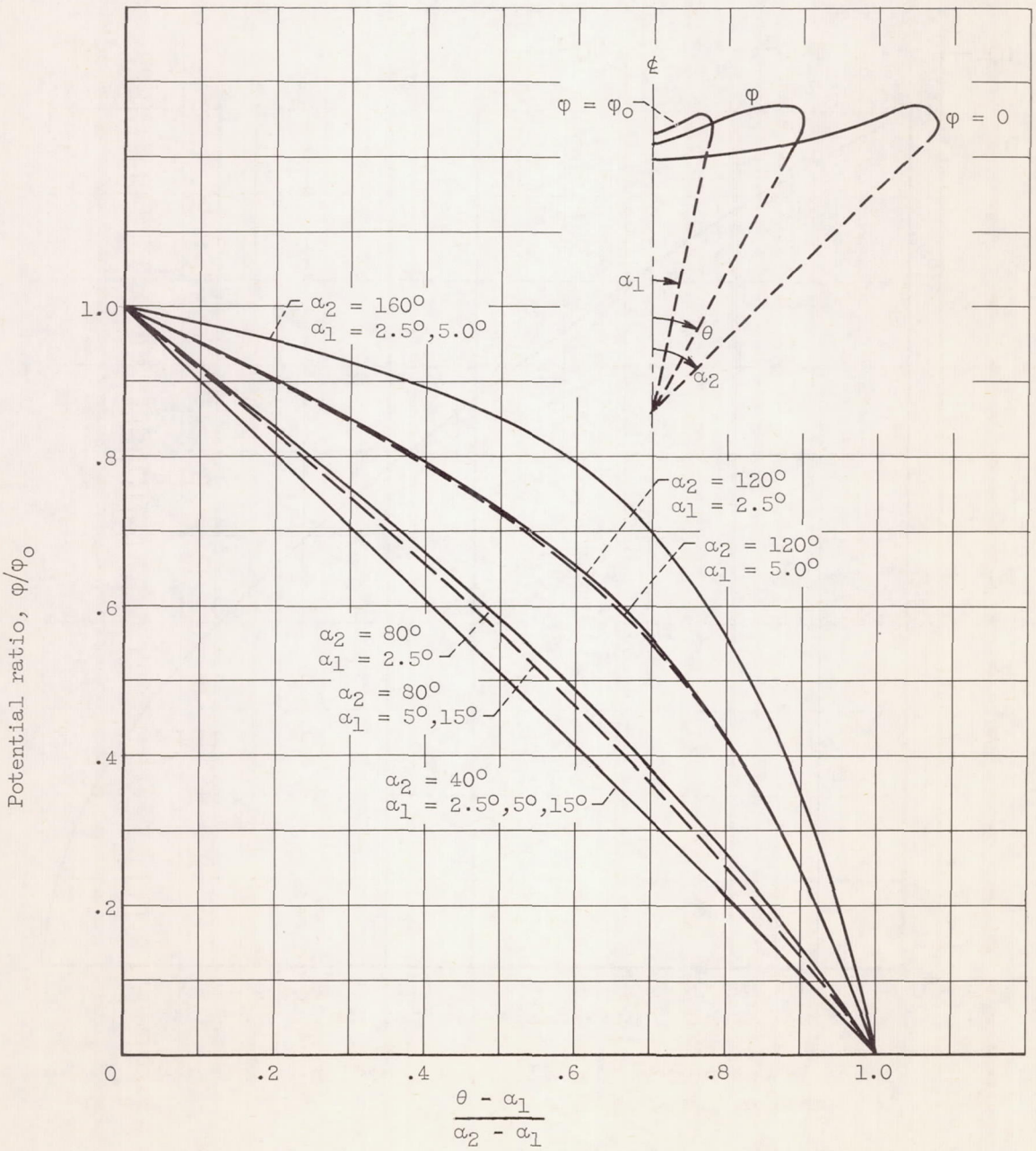

Figure 18. - Space-charge-limited potential distribution between coaxial cones.

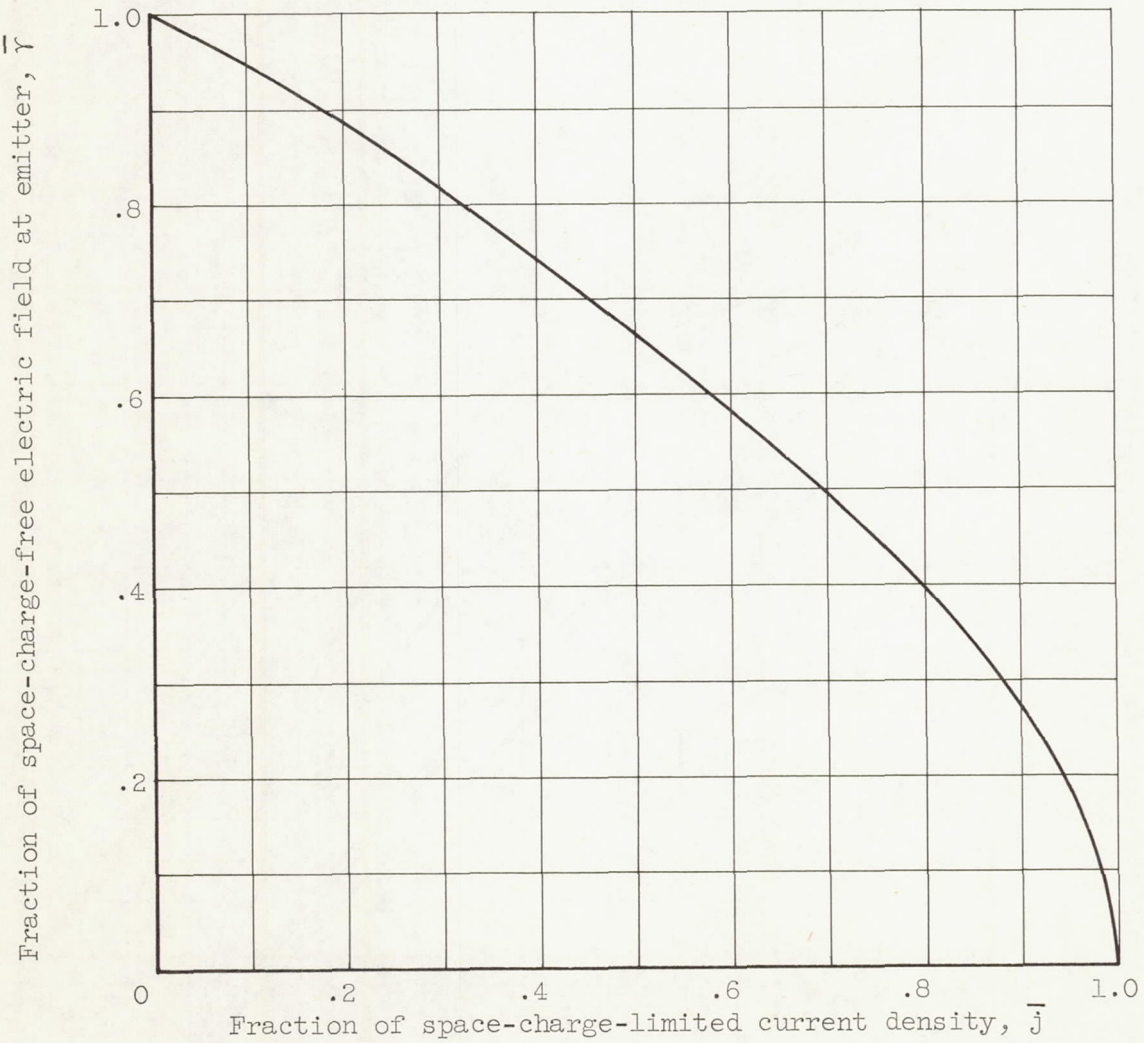

Figure 19. - Current density as a function of electric field at emitter (ref. 15).

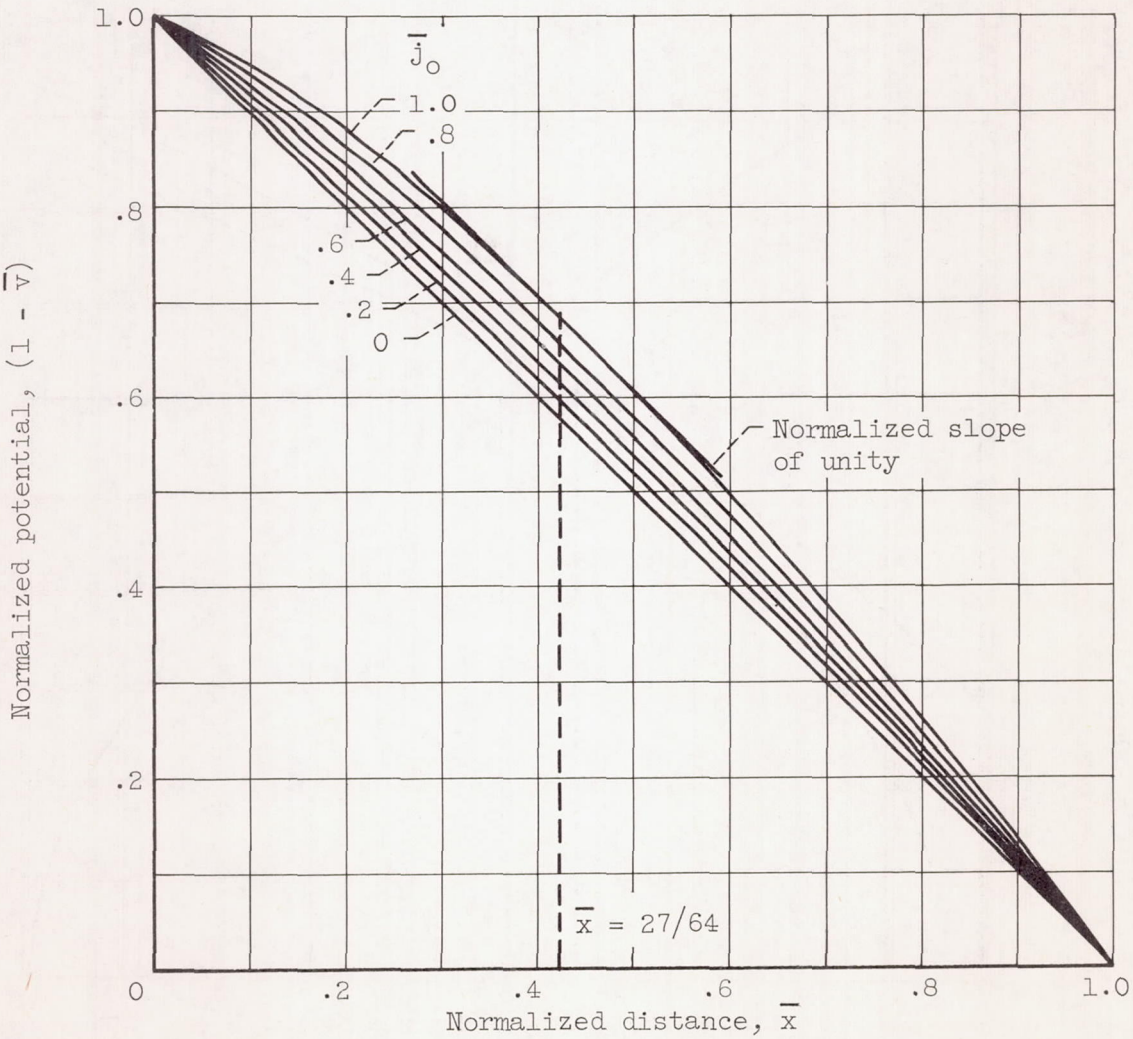

Figure 20. - Normalized potential distribution for partial space-charge flow (ref. 15).

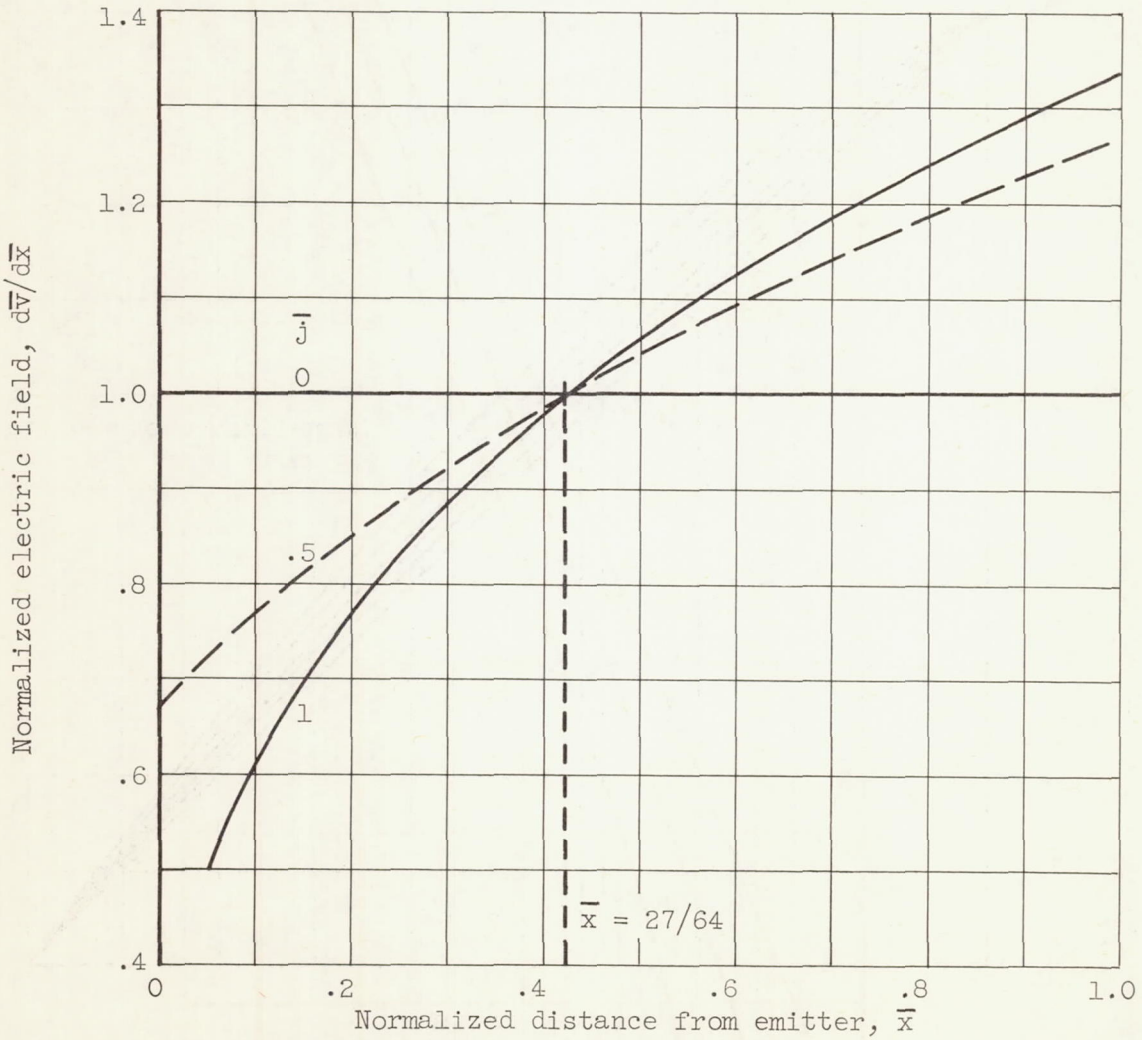

Figure 21. - Electric field in space between emitter and collector for several current densities (ref. 15).

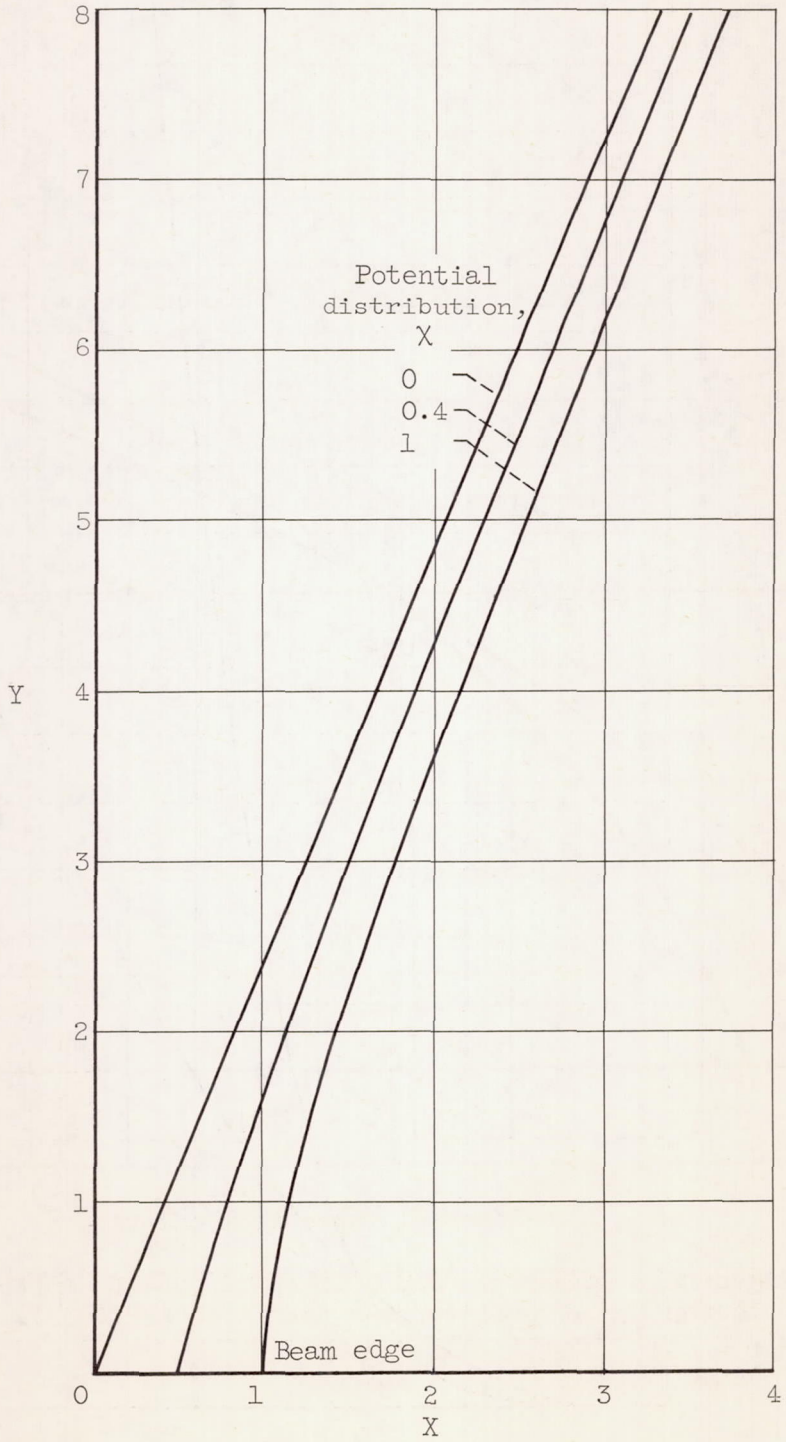

Figure 22. - Typical electrode shapes for a rectilinear slab ion beam.

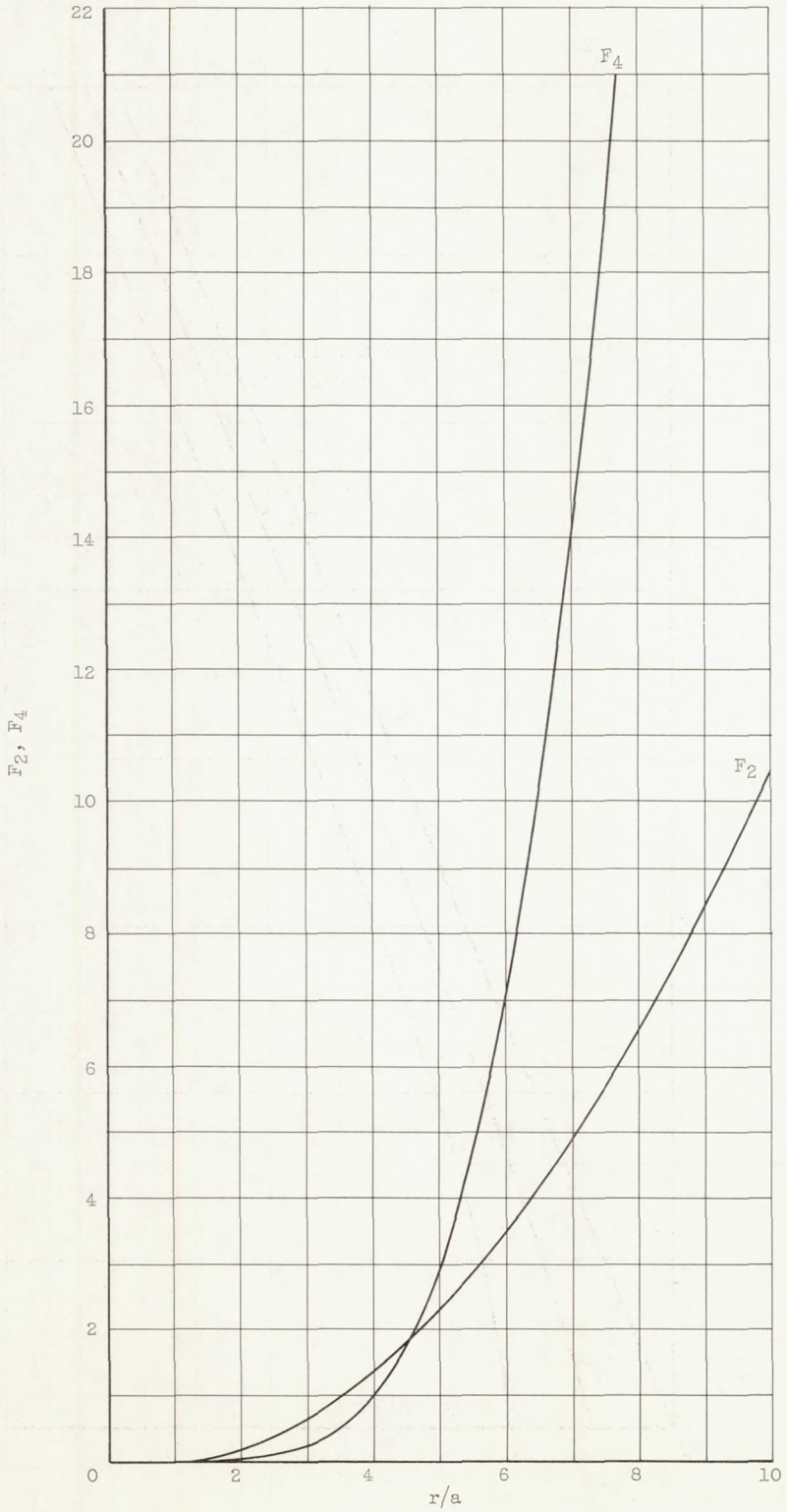

Figure 23. - Dominant terms in series expansion of potential function near edge of a rectilinear ion beam with circular cross section (eq. (79)).

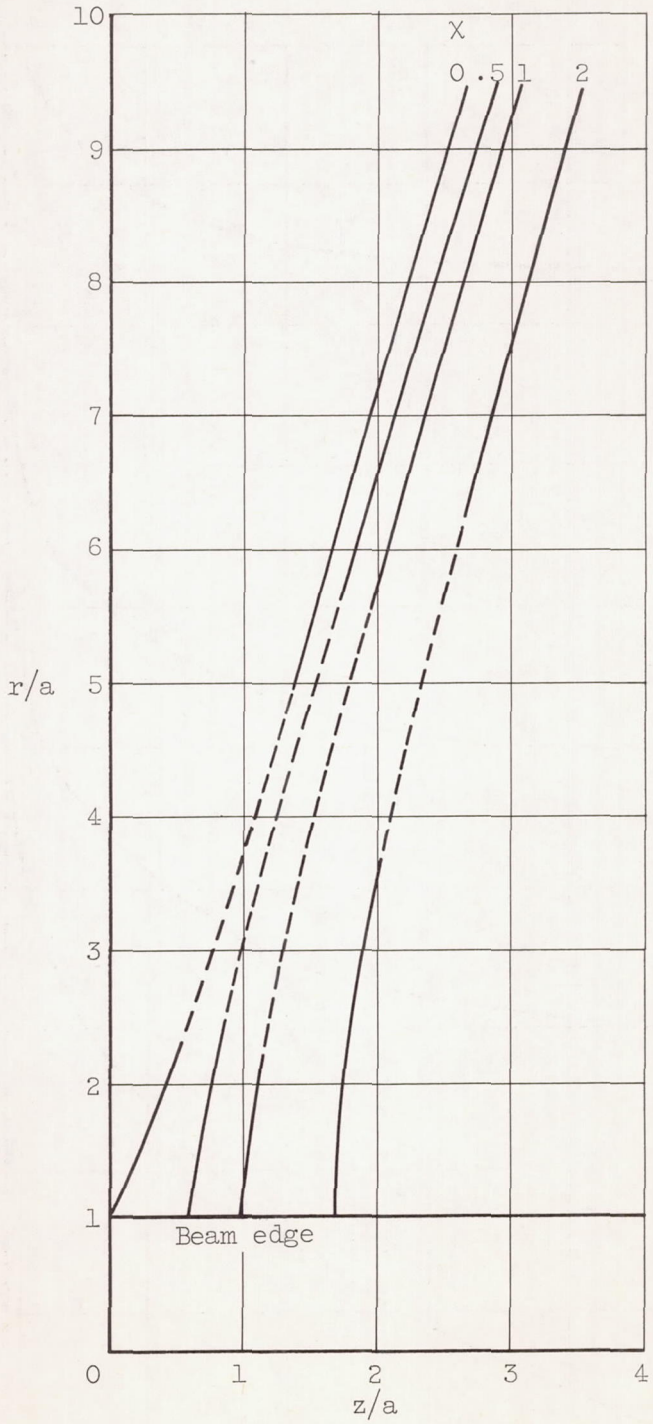

(a) Outer electrode shapes.

Figure 24. - Typical electrode shapes for a rectilinear ion beam with circular cross section.

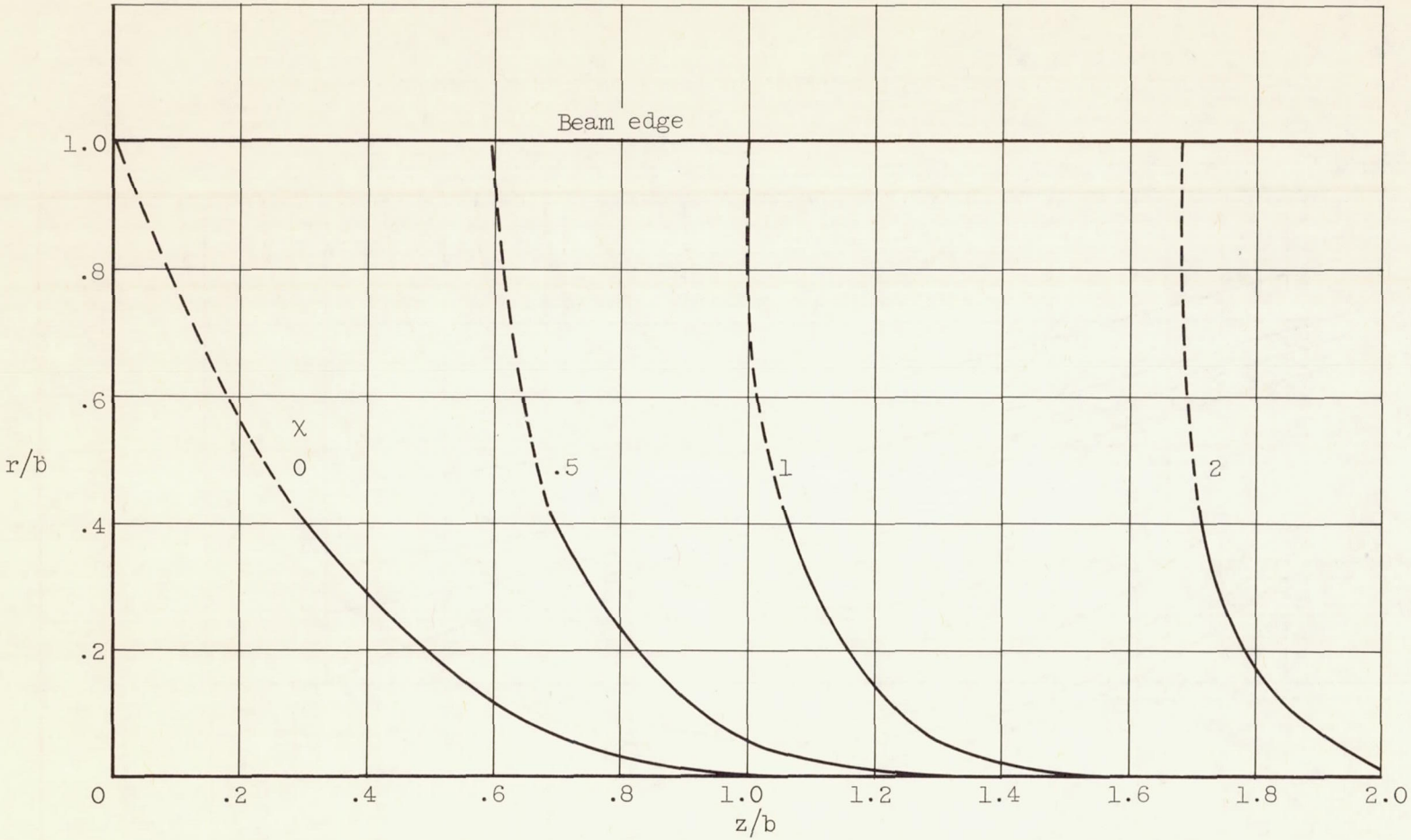

(b) Inner electrode shapes.

Figure 24. - Concluded. Typical electrode shapes for a rectilinear ion beam with circular cross section.

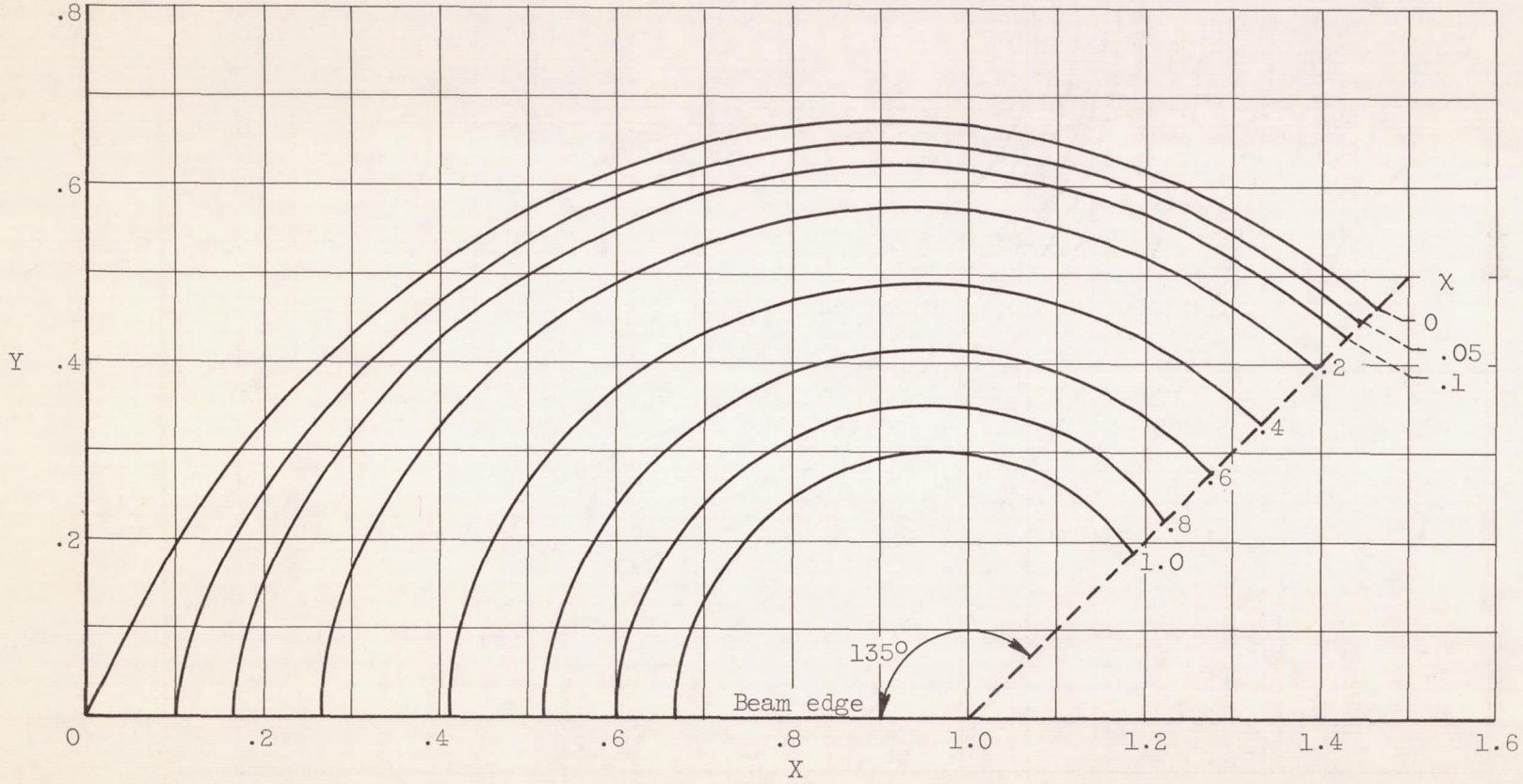

Figure 25. - Electrode shapes for converging cylindrical flow ($r/r_o < 1$).

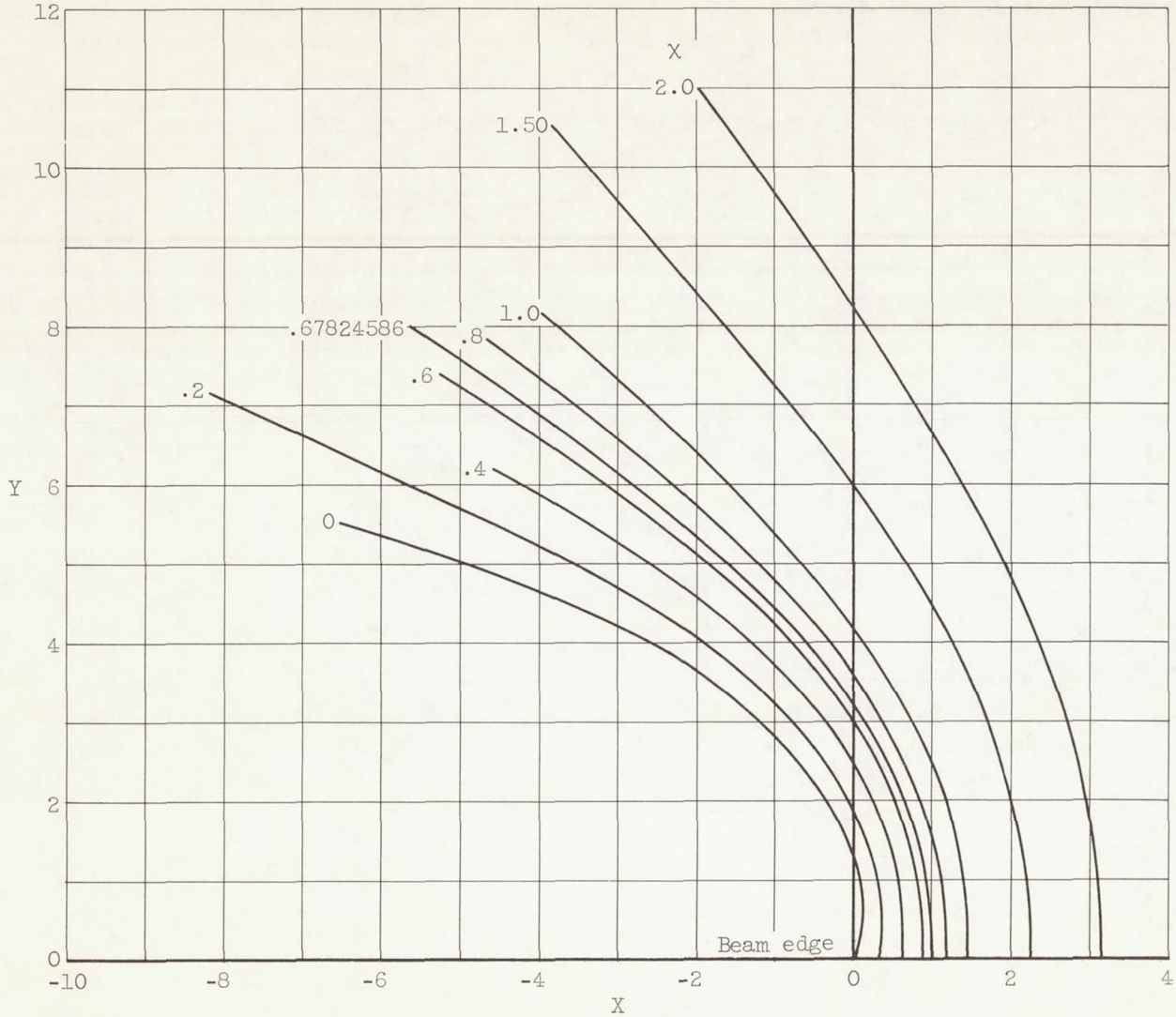

Figure 26. - Electrode shapes for diverging flow between coaxial cylinders ($r/r_o > 1$).

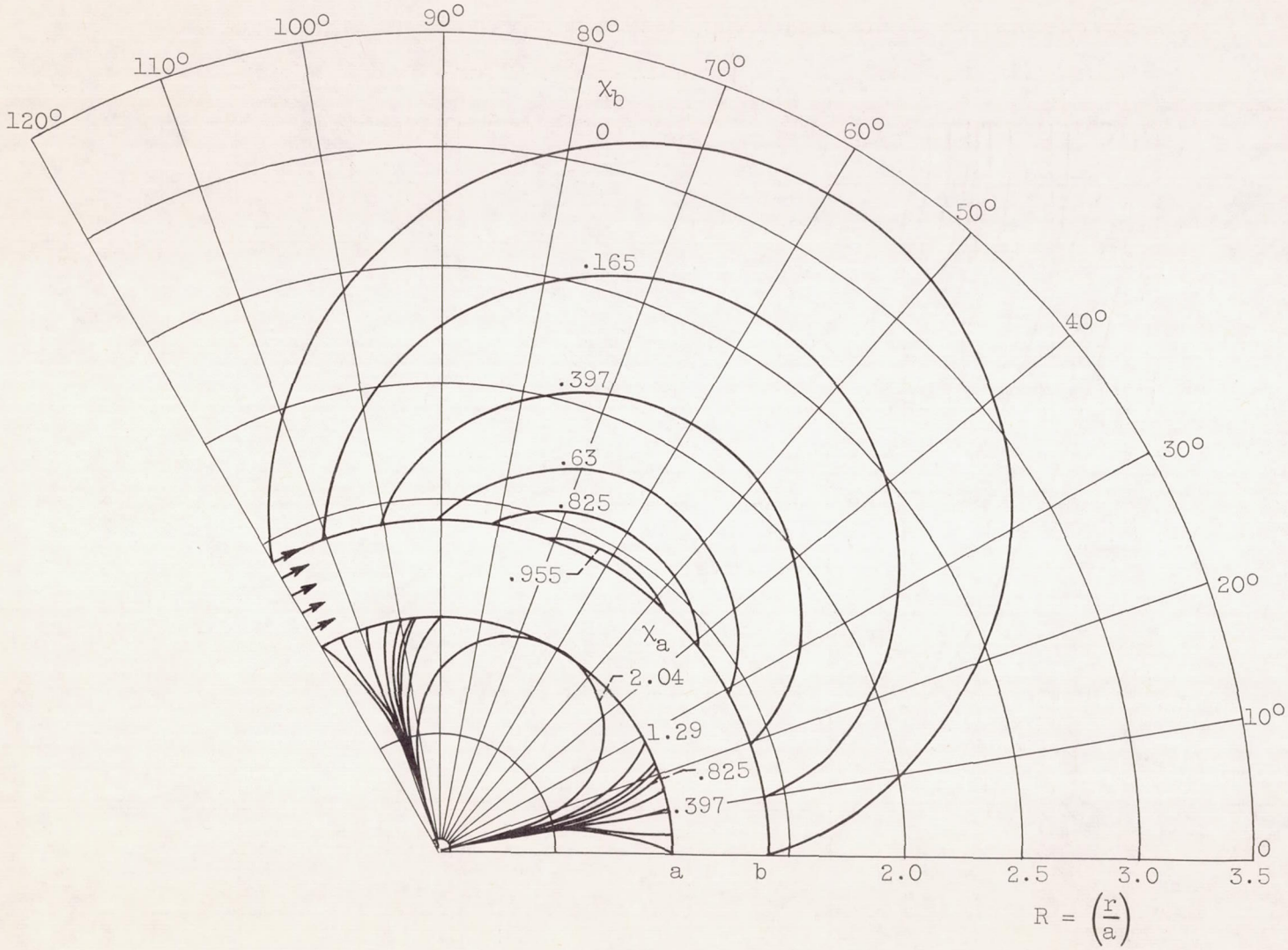

Figure 27. - Electrode shapes for circular flow. $\chi_b = \frac{\Phi b^2}{C_3} = \left(\sin \frac{3\theta}{2}\right)^{4/3}$; $\chi_a = \left(\frac{a}{b}\right)^2 \chi_b$.

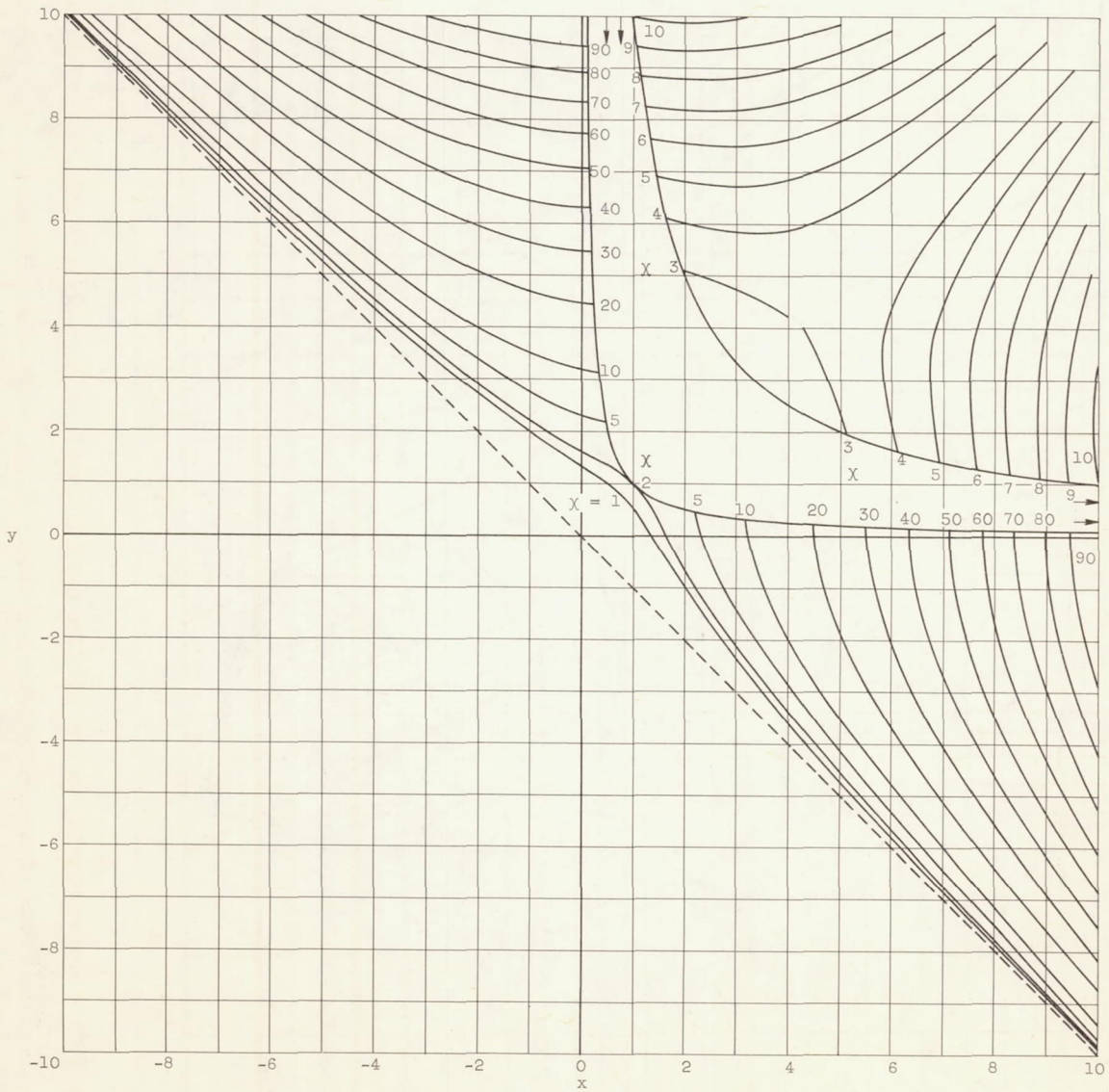

Figure 28. - Electrode shapes for hyperbolic flow.

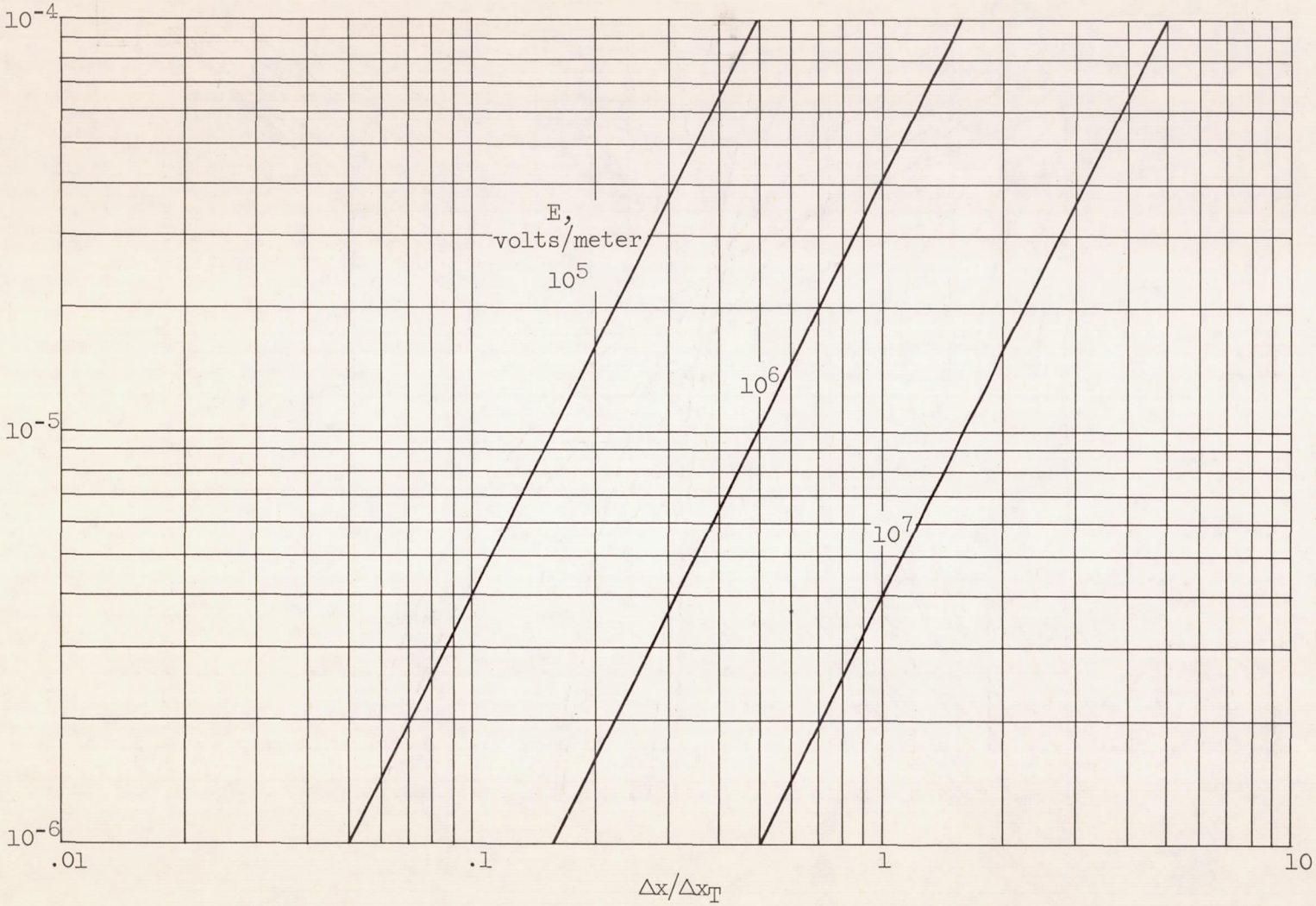

Figure 29. - Approximate ratio of ion beam spreading due to a surface irregularity to thermal spreading.

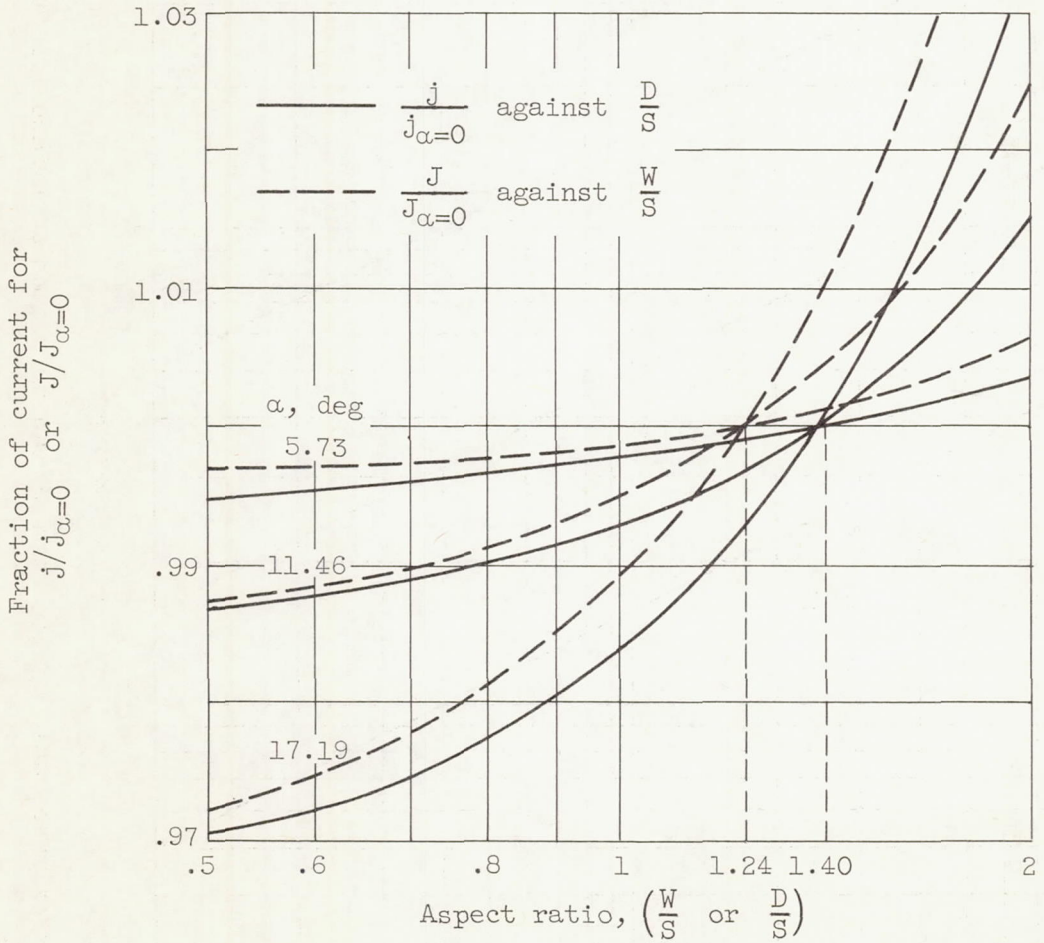

Figure 30. - Effect of electrode tilt on current density in a plane diode (ref. 10). (Rectangular emitter tilted about axis parallel to side and disk emitter.)

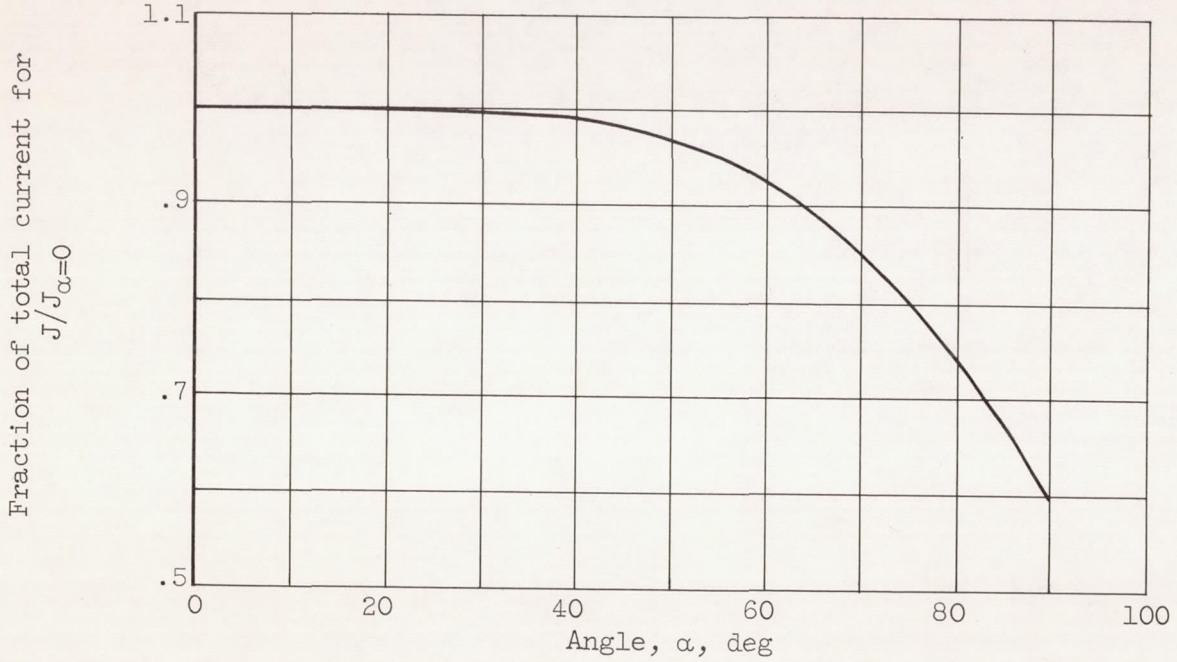

Figure 31. - Effect of electrode tilt on current density in a plane diode with disk emitter of optimum aspect ratio D/S = 1.42 (ref. 10).